AD-A135 135 NUMERICAL ANALYSIS OF DUSTY SUPERSONIC FLOW PAST BLUNT AXISYMMETRIC BODIE..(U) TORONTO UNIV DOWNSVIEW (ONTARIO) INST FOR AEROSPACE STUDIES H SUGIYAMA AUG 83 UTIAS-267 AFOSR-TR-83-0922 AFOSR-82-0096 F/G 20/4 NL

1/1

UNCLASSIFIED

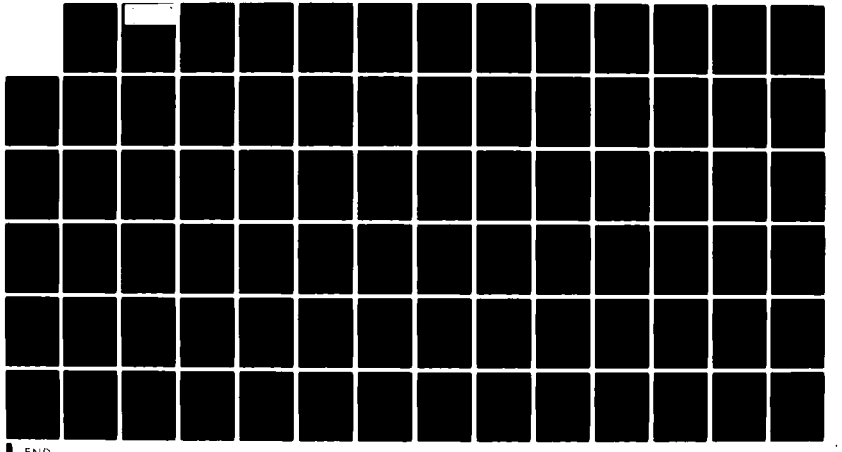

END
DATE FILMED
1-84
DTIC

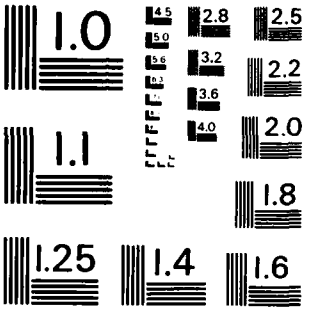

MICROCOPY RESOLUTION TEST CHART
NATIONAL BUREAU OF STANDARDS-1963-A

INSTITUTE
FOR
AEROSPACE STUDIES

UNIVERSITY OF TORONTO

NUMERICAL ANALYSIS OF DUSTY SUPERSONIC FLOW PAST BLUNT AXISYMMETRIC BODIES

BY

H. SUGIYAMA

AUGUST, 1983

UTIAS REPORT NO. 267
CN ISSN 0082-5255

13

REPORT DOCUMENTATION PAGE

READ INSTRUCTIONS BEFORE COMPLETING FORM

1. REPORT NUMBER: AFOSR-TR- 83-0922	2. GOVT ACCESSION NO.
3. RECIPIENT'S CATALOG NUMBER	
4. TITLE (and Subtitle): NUMERICAL ANALYSIS OF DUSTY SUPERSONIC FLOW PAST BLUNT AXISYMMETRIC BODIES	5. TYPE OF REPORT & PERIOD COVERED: Interim
6. PERFORMING ORG. REPORT NUMBER: UTIAS Report No. 267	
7. AUTHOR(s): H. SUGIYAMA	8. CONTRACT OR GRANT NUMBER(s): -AFOSR 82-0096
9. PERFORMING ORGANIZATION NAME AND ADDRESS: University of Toronto, Institute for Aerospace Studies, 4925 Dufferin St., Downsview, Ontario, Canada, M3H 5T6	10. PROGRAM ELEMENT, PROJECT, TASK AREA & WORK UNIT NUMBERS: 61102F 2307/A1
11. CONTROLLING OFFICE NAME AND ADDRESS: Air Force Office of Scientific Research /NA, Bldg. 410, Bolling Air Force Base, D C 20332, U.S.A.	12. REPORT DATE: August, 1983 13. NUMBER OF PAGES: 77
14. MONITORING AGENCY NAME & ADDRESS (if different from Controlling Office)	15. SECURITY CLASS. (of this report): UnCLassified 15a. DECLASSIFICATION DOWNGRADING SCHEDULE

16. DISTRIBUTION STATEMENT (of this Report)

Approved for public release; distribution unlimited.

17. DISTRIBUTION STATEMENT (of the abstract entered in Block 20, if different from Report)

18. SUPPLEMENTARY NOTES

19. KEY WORDS (Continue on reverse side if necessary and identify by block number)

1. Dusty-supersonic-hypersonic flow
2. Blunt-body flow
3. Pitot-tube flow
4. Numerical analysis

20. ABSTRACT (Continue on reverse side if necessary and identify by block number)

An inverse method was developed for treating gas-particle supersonic flow past axisymmetric blunt bodies. This method is based on two transformations (von Mises and an additional one), which are convenient for determining the shock-layer flow-fields and the body shapes.

In using the present method, the pure-gas flow-fields around spheres were first solved numerically for the freestream Mach numbers M_∞ = 10, 6, 4, 3, 2 and 1.5 These were found to be in very good agreement with the available

results of Van Dyke and Gordon. Then the gas-solid-particle flow in the shock layer around blunt bodies (nearly spheres) were solved for the freestream Mach numbers M_∞ = 10 and 1.5, with freestream loading ratios α = 0, 0.2, 0.5 and 1.0 and particle diameters $\bar{d}_p$ = 1, 2, 5 and 10 μm, respectively. The effects of M_∞, $\bar{d}_p$ and α on the shock-layer thickness and the body surface pressures are discussed. The variations of the flow properties along the stagnation and adjacent streamlines are also shown in some detail.

NUMERICAL ANALYSIS OF DUSTY SUPERSONIC FLOW PAST BLUNT AXISYMMETRIC BODIES

by

H. SUGIYAMA

Submitted December, 1982

August, 1983

UTIAS Report No. 267
CN ISSN 0082-5255

Acknowledgements

It is my pleasure to express my appreciation to Prof. I. I. Glass for his stimulating discussions, kind advice and a critical reading of the manuscript. Professor M. Honda, Institute of High Speed Mechanics, Tohoku University, Sendai, Japan, and Prof. K. Okuda, Muroran Institute of Technology, Muroran, Japan, deserve special thanks.

I also wish to thank Dr. J. J. Gottlieb, Dr. J. P. Sislian and Dr. W. S. Liu for their reading of my manuscript.

I am grateful to the Ministry of Education of Japan and the Muroran Institute of Technology for making possible my full-year's leave at UTIAS.

The financial assistance received from the Canadian Natural and Engineering Research Council, the U.S. Air Force through Grant [redacted]-AFOSR 82-0096 and the U.S. Army Research Office is acknowledged with thanks.

Summary

An inverse method was developed for treating gas-particle supersonic flow past axisymmetric blunt bodies. This method is based on two transformations (von Mises and an additional one), which are convenient for determining the shock-layer flow fields and the body shapes.

In using the present method, the pure gas flow fields around spheres were first solved numerically for the freestream Mach numbers M_∞ = 10, 6, 4, 3, 2 and 1.5. These were found to be in very good agreement with the available results of Van Dyke and Gordon. Then the gas-solid-particle flow in the shock layer around blunt bodies (nearly spheres) were solved for the freestream Mach numbers M_∞ = 10 and 1.5, with freestream loading ratios α_∞ = 0, 0.2, 0.5 and 1.0 and particle diameters $d_{p\infty}$ = 1, 2, 5 and 10 μm, respectively. The effects of M_∞, d_p and α on the shock-layer thickness and the body surface pressures are discussed. The variations of the flow properties along the stagnation and adjacent streamlines are also shown in some detail.

Contents

Notation

$\bar{a}_\infty$	freestream gas sound speed = $(\gamma \bar{R} \bar{T}_\infty)^{1/2}$, m/sec
B_b	bluntness of body shape
B_s	bluntness of shock-wave shape
C_D	drag coefficient of a particle
C_p	gas specific heat at constant pressure, $\bar{C}_p/\bar{C}_p = 1$
C_v	gas specific heat at constant volume, $\bar{C}_v/\bar{C}_p = 1/\gamma$
C_s	specific heat of solid-particle material, $\bar{C}_s/\bar{C}_p = \beta/\gamma$
$\bar{d}_p$	dimensional particle diameter, μm
d_p	particle diameter, $\bar{d}_p/\bar{R}_s$
$\bar{k}$	dimensional gas thermal conductivity, J/(m·sec·K)
k	gas thermal conductivity, $\bar{k}/(\bar{\rho}_\infty \bar{U}_\infty \bar{C}_p \bar{R}_s)$
$\bar{m}$	mass of a particle = $\bar{\rho}_s \cdot \pi/6 \cdot \bar{d}_p^3$, g
M_e	equilibrium freestream Mach number [see Eq. (5.14)]
M_∞	freestream Mach number, $\bar{U}_\infty/\bar{a}_\infty$
$\bar{n}$	number of particles in a unit volume, $1/cm^3$
n	$n = \bar{n} \cdot \bar{R}_s^3$
Nu	Nusselt number of a particle
P	gas pressure, $\bar{p}/\bar{\rho}_\infty \bar{U}_\infty^2$
P_{st}	stagnation pressure, $\bar{p}_{st}/\bar{\rho}_\infty \bar{U}_\infty^2$
$\bar{p}_\infty$	freestream gas pressure, kPa
Pr	gas Prandtl number
$\bar{R}$	gas constant, m^2/sec^2K
R_b	nose radius of body shape, $\bar{R}_b/\bar{R}_s$
$\bar{R}_s$	dimensional nose radius of shock wave shape, cm
R_s	nose radius of shock wave shape, $\bar{R}_s/\bar{R}_s = 1$
Re	particle Reynolds number, $\bar{\rho}\bar{w}\bar{d}_p/\bar{\mu}$
T	gas temperature, $\bar{T}/(\bar{U}_\infty^2/\bar{C}_p)$
T_p	particle temperature, $\bar{T}_p/(\bar{U}_\infty^2/\bar{C}_p)$
$\bar{T}_\infty$	freestream gas temperature, K
u	gas velocity component in x-direction, $\bar{u}/\bar{U}_\infty$
u_p	particle velocity component in x-direction, $\bar{u}_p/\bar{U}_\infty$
$\bar{U}_\infty$	freestream gas velocity = $M_\infty \cdot \bar{a}_\infty$, m/sec
v	gas velocity component in r-direction, $\bar{v}/\bar{U}_\infty$

v_p	particle velocity component in r-direction, $\bar{v}_p/\bar{U}_\infty$
V	transformed gas velocity, $V = v/Y$
V_p	transformed particle velocity, $V_p = v_p/Y$
w	relative velocity between gas and particle, $[(u-u_p)^2 + (v-v_p)^2]^{1/2}$
x, r	cylindrical coordinates (see Fig. 1), $x = \bar{x}/\bar{R}_s$, $r = \bar{r}/\bar{R}_s$
α	loading ratio in freestream = ratio of particle phase density to gas density in freestream, $\bar{\rho}_p/\bar{\rho}_\infty$
β	specific heat ratio of two phases, C_s/C_v
γ	gas specific heat ratio, C_p/C_v
γ_e	specific heat ratio of equilibrium gas-particle mixture [see Eq. (5.13)]
δ	impact angle [see Fig. 10(a)]
ϵ	density ratio across shock wave [see Eq. (5.11)]
Δ	shock stand-off distance, $\bar{\Delta}/\bar{R}_s$
$\Delta\eta$	integration step size in η-direction
$\Delta\xi$	step size in ξ-direction
ξ, η	coordinates defined by Eqs. (4.3) and (4.4)
$\bar{\mu}$	gas viscosity, poise = g/(cm·sec)
ρ	gas density, $\bar{\rho}/\bar{\rho}_\infty$
$\bar{\rho}_p$	dimensional density of particle phase = $\bar{n}\cdot\bar{m}$
$\bar{\rho}_s$	density of solid particle material, g/cm^3
$\bar{\rho}_\infty$	freestream gas density = $\bar{p}_\infty/\bar{R}\bar{T}_\infty$, g/cm^3
ψ, Y	coordinates defined by Eqs. (3.5) and (3.6)
ψ	gas phase stream function
ψ_p	particle phase stream function

Superscript

$(\bar{\ })$	dimensional quantity

Subscripts

b	body
p	particle
s	shock or solid particle
st	stagnation
∞	freestream

1. INTRODUCTION

High-speed gas flows including small solid or liquid particles have been studied by a number of authors [Refs. 1-6] in the last few years owing to important engineering applications relating to rocket-nozzle flow, shock waves in a dusty gas [Refs. 7, 8] and in supersonic flight [Refs. 9-13]. In such two-phase flows the gas-phase flow field will differ from its corresponding field in a pure gas owing to the gas-particle interaction through viscous drag and heat transfer.

The present report deals with supersonic gas particle flow past blunt bodies. Assuming that the mass ratio of the particle phase to the gas phase in the freestream, or the loading ratio in the freestream α, is small enough and that the particle phase does not affect the gas phase, Probstein and Fassio [Ref. 9], Waldman and Reinecke [Ref. 10], and Spurk and Gerber [Ref. 11] calculated the particle trajectories in the hypersonic shock layer. Their main interest was to find the *collection efficiency* defined as the ratio of the number of particles which strike the body to the number of particles which could strike it if their trajectories were straight and unaltered by the vehicle flow field.

Taking into account the interactions, i.e., the drag force and the heat exchange between the gas and the particles, Chang [Ref. 13] investigated dusty supersonic flow past blunt bodies using a direct method. He showed that the shock-layer flow is in nonequilibrium and investigated the effects of the loading ratio α on this flow. His main interest was to clarify the nonequilibrium phenomena in the two-phase flow within the shock layer, which is also the purpose of the present report.

In this report a numerical method for treating dusty supersonic flow past blunt bodies will be developed. This method is the so-called inverse method in which the shock shape is specified and the flow field and body shape is to be determined. First, the governing equations for dusty flow past axisymmetric bodies are derived in a cylindrical coordinate system (x, r). It is assumed that there are no collisions between the particles. The interactions between the gas and the particles considered are only the drag force and the heat exchange. Next, the governing equations are transformed into a (ψ, Y) coordinate system by using a von Mises transformation, where ψ is the stream function for the gas phase, and $Y = r$. To facilitate the integration of the governing equations in the shock layer, they are further transformed into a (ξ, η) coordinate system, which will be discussed subsequently. The advantages of the present method are: (1) body shapes are easily determined without any approximate calculations; (2) relatively low computer storage is required, since it is unnecessary to store all the flow field data within the shock layer; and (3) solutions are obtained quickly.

Although the advantages and disadvantages of the inverse method and the direct method (including the time-dependent method) for the blunt-body problem have been fully discussed in Refs. 14-19, it is worthwhile to summarize. The direct method is more important for practical-type problems than the inverse method. However, the inverse method is significant and useful for complex flow problems which have not been fully clarified, such as three-dimensional flows of a pure gas, and two or three-dimensional flows with relaxation processes. The inverse method is much easier for numerical calculations, gives a more detailed flow field, and provides better insight into the flow fields.

Using the present method, the dusty-gas shock layer flows around blunt bodies (nearly spheres) were solved numerically. For experimental purposes, glass microspheres in air were chosen as the dusty gas. To investigate the effects of the freestream Mach number M_∞, particle diameter $\bar{d}_p$, and freestream loading-ratio α on the shock layer of the dusty-gas flow, the following parameters were chosen:

$$M_\infty = 10,\ 1.5$$

$$\bar{d}_p = 1,\ 2,\ 5,\ 10\ \mu m$$

$$\alpha = 0,\ 0.2,\ 0.5,\ 1.0$$

Numerical results for a pure gas ($\alpha = 0$) were compared with those of Van Dyke and Gordon [Ref. 16] and very good agreement was obtained, thus lending confidence to the dusty-gas calculations.

It is worth noting that spalling, ablation and erosion of the glass particles were not considered in the present study.

2. GOVERNING EQUATIONS

To formulate the motion of the gas-particle flow in the shock layer, the following assumptions are made [Ref. 4]:

(1) The volume fraction of the particles is small so that the collisions between individual particles are neglected.

(2) The interactions between the gas and particles consist only of the drag force between the gas and particles and the heat exchange between them.

(3) The particles are assumed to be spheres of uniform size.

(4) The number of particles is large and the flow can be treated as a continuum.

In this report a superscript $(\bar{\ })$ over a quantity means a dimensional quantity, otherwise it is nondimensional. Let u and v be the x and r components of velocity (Fig. 1), ρ the density, p the pressure, and T the temperature of the gas, and u_p, v_p, ρ_p and T_p be the corresponding values of the particle phase. Here, $\rho_p = \bar{\rho}_p/\bar{\rho}_\infty = n\cdot\bar{m}/\bar{\rho}_\infty$, where n is the number of particles per unit volume and $\bar{m}$ is the mass of a particle. All lengths are nondimensionalized by the shock nose radius $\bar{R}_s$, velocities by the freestream velocity $\bar{U}_\infty$, densities by the freestream gas density $\bar{\rho}_\infty$, pressure by $\bar{\rho}_\infty \bar{U}_\infty^2$, and temperatures by $\bar{U}_\infty^2/\bar{c}_p$, where $\bar{c}_p$ is the gas specific heat at constant pressure. The other nondimensional quantities are listed in the Notation.

Under the above assumptions, the governing equations of the steady, axisymmetric, dusty-gas flow become (Refs. 4, 13):

For the gas phase,

Continuity:

$$\frac{\partial}{\partial x}(r\rho u) + \frac{\partial}{\partial r}(r\rho v) = 0 \tag{2.1}$$

Momentum:

$$\rho u\frac{\partial u}{\partial x} + \rho v\frac{\partial u}{\partial r} = -\frac{\partial p}{\partial x} + F_{px} \tag{2.2}$$

$$\rho u\frac{\partial v}{\partial x} + \rho v\frac{\partial v}{\partial r} = -\frac{\partial p}{\partial r} + F_{pr} \tag{2.3}$$

Energy:

$$\rho uc_p\frac{\partial T}{\partial x} + \rho vc_p\frac{\partial T}{\partial r} - u\frac{\partial p}{\partial x} - v\frac{\partial p}{\partial r}$$

$$= Q_p + (u_p-u)F_{px} + (v_p-v)F_{pr} \tag{2.4}$$

State:

$$p = \frac{\gamma-1}{\gamma}\rho T \tag{2.5}$$

and for the particle phase,

Continuity:

$$\frac{\partial}{\partial x}(r\rho_p u_p) + \frac{\partial}{\partial r}(r\rho_p v_p) = 0 \tag{2.6}$$

Momentum:

$$\rho_p u_p\frac{\partial u_p}{\partial x} + \rho_p v_p\frac{\partial u_p}{\partial r} = -F_{px} \tag{2.7}$$

$$\rho_p u_p\frac{\partial v_p}{\partial x} + \rho_p v_p\frac{\partial v_p}{\partial r} = -F_{pr} \tag{2.8}$$

Energy:

$$\rho_p u_p c_s\frac{\partial T_p}{\partial x} + \rho_p v_p c_s\frac{\partial T_p}{\partial r} = -Q_p \tag{2.9}$$

where c_s is the specific heat of the particles. F_{px} and F_{pr} are the components of the force exerted upon a unit volume of gas by the particles, and Q_p is the heat transferred from the particles. The terms $u_pF_{px} + v_pF_{pr}$ represent the work done by the particles passing through the gas. Equation (2.4) shows that the thermal energy of the gas is changed by both the heat exchange and the dissipation due to the particles moving relative to the gas. Equation (2.9) states that the thermal energy of the particles can be changed only by heat transfer. From Eqs. (2.2) and (2.3),

$$\rho\left(u\frac{\partial}{\partial x} + v\frac{\partial}{\partial r}\right)\left(\frac{u^2+v^2}{2}\right)$$

$$= -u\frac{\partial p}{\partial x} - v\frac{\partial p}{\partial r} + uF_{px} + vF_{pr} \tag{2.10}$$

Similarly, from Eqs. (2.7) and (2.8),

$$\rho_p\left(u_p\frac{\partial}{\partial x} + v_p\frac{\partial}{\partial r}\right)\left(\frac{u_p^2+v_p^2}{2}\right) = -u_pF_{px} - v_pF_{pr} \tag{2.11}$$

that is, the kinetic energy of the particles is only affected by the work done by the drag on the particles.

The drag force exerted by n-particles of diameter d_p in a unit volume ($=R_S^3$) of space moving through a perfect gas is given by

$$F_{px} = n\frac{1}{8}(\pi d_p^2)C_D\bar{\rho}w(u_p-u) \tag{2.12}$$

$$F_{pr} = n\frac{1}{8}(\pi d_p^2)C_D\bar{\rho}w(v_p-v) \tag{2.13}$$

where

$$w = [(u-u_p)^2 + (v-v_p)^2]^{1/2} \tag{2.14}$$

is the relative velocity between the gas and particles, and C_D is the drag coefficient. At present the nonstationary drag coefficient for a gas-particle flow is uncertain [Ref. 6], and is assumed as [Ref. 20]

$$C_D = 0.48 + 28/Re^{0.85} \tag{2.15}$$

where

$$Re = \bar{\rho}\bar{w}\bar{d}_p/\bar{\mu} \tag{2.16}$$

is the Reynolds number based on the diameter of the particle $\bar{d}_p$ and the relative velocity $\bar{w}$.

The heat transfer between the gas and particles is given by

$$Q_p = n\,Nu\,\pi d_p k(T_p-T) \tag{2.17}$$

where the Nusselt number is expressed as [Ref. 21]

$$Nu = 2.0 + 0.6\,Pr^{1/3}\,Re^{1/2} \tag{2.18}$$

where Pr is the Prandtl number,

$$Pr = \frac{\bar{\mu}\bar{c}_p}{\bar{k}} \tag{2.19}$$

and $\bar{k}$ is the gas thermal conductivity.

In the present analysis, the Prandtl number is taken at 0.75, the specific heat of the gas is held constant, the specific heat ratio of the two phases is taken as $\beta = c_s/c_v = 1.0$, and the power law for the viscosity-temperature variation is assumed as [Ref. 22]

$$\bar{\mu} = 1.71\times10^{-4}\times\left(\frac{\bar{T}}{273}\right)^{0.77}\ \text{poise} \tag{2.20}$$

It is worth noting that any other relation for

viscosity can be easily inserted without affecting other parts of the analysis.

3. EQUATION OF MOTION IN (ψ, Y) COORDINATE SYSTEM

Introduce the stream functions $\psi(x, r)$ for the gas phase and $\psi_p(x, r)$ for the particle phase as

$$\frac{\partial \psi}{\partial r} = r\rho u \tag{3.1}$$

$$\frac{\partial \psi}{\partial x} = -r\rho v \tag{3.2}$$

$$\frac{\partial \psi_p}{\partial r} = r\rho_p u_p \tag{3.3}$$

$$\frac{\partial \psi_p}{\partial x} = -r\rho_p v_p \tag{3.4}$$

which satisfy the continuity equations (2.1) and (2.6). Using the von Mises transformation [Ref. 23] to transform the governing equations in (x, r) coordinate system into those in a (ψ, Y) coordinate system, where Y = r, a set of transformation operators can be obtained as [Refs. 24, 25]

$$\frac{\partial}{\partial x} = \psi_x \frac{\partial}{\partial \psi} \tag{3.5}$$

$$\frac{\partial}{\partial r} = \frac{\partial}{\partial Y} + \psi_r \frac{\partial}{\partial \psi} \tag{3.6}$$

$$u \frac{\partial}{\partial x} + v \frac{\partial}{\partial r} = v \frac{\partial}{\partial Y} \tag{3.7}$$

From the inverse transformation,

$$\frac{\partial}{\partial Y} = \frac{\partial}{\partial r} + \frac{\partial x}{\partial Y} \frac{\partial}{\partial x} \tag{3.8}$$

$$\frac{\partial}{\partial \psi} = \frac{\partial x}{\partial \psi} \cdot \frac{\partial}{\partial x} \tag{3.9}$$

Comparing Eqs. (3.7) and (3.8) and Eqs. (3.5) and (3.9),

$$\frac{\partial x}{\partial Y} = \frac{u}{v} \tag{3.10}$$

$$\frac{\partial x}{\partial \psi} = -\frac{1}{r\rho v} \tag{3.11}$$

Using the above transformation operators, the governing equations (2.1)-(2.5) for the gas phase are transformed as follows:

$$\psi_x \frac{\partial u}{\partial \psi} + \psi_r \frac{\partial v}{\partial \psi} + \frac{\partial v}{\partial Y} + \frac{v}{\rho} \frac{\partial \rho}{\partial Y} + \frac{v}{Y} = 0 \tag{3.12}$$

$$\rho v \frac{\partial u}{\partial Y} = -\psi_x \frac{\partial p}{\partial \psi} + F_{px} \tag{3.13}$$

$$\rho v \frac{\partial v}{\partial Y} = -\frac{\partial p}{\partial Y} - \psi_r \frac{\partial p}{\partial \psi} + F_{pr} \tag{3.14}$$

$$\rho v c_p \frac{\partial T}{\partial Y} - v \frac{\partial p}{\partial Y} = Q_p + (u_p - u)F_{px} + (v_p - v)F_{pr} \tag{3.15}$$

$$p = \frac{\gamma - 1}{\gamma} \rho T \tag{3.16}$$

Similarly, the governing equations (2.6)-(2.9) for the particle phase are transformed to

$$\psi_x \frac{\partial u_p}{\partial \psi} + \frac{\partial v_p}{\partial Y} + \psi_r \frac{\partial v_p}{\partial \psi} + \frac{1}{\rho_p}(u_p \psi_x + v_p \psi_r)\frac{\partial \rho_p}{\partial \psi} + \frac{v_p}{\rho_p}\frac{\partial \rho_p}{\partial Y} + \frac{v_p}{Y} = 0 \tag{3.17}$$

$$\rho_p(u_p \psi_x + v_p \psi_r)\frac{\partial u_p}{\partial \psi} + \rho_p v_p \frac{\partial u_p}{\partial Y} = -F_{px} \tag{3.18}$$

$$\rho_p(u_p \psi_x + v_p \psi_r)\frac{\partial v_p}{\partial \psi} + \rho_p v_p \frac{\partial v_p}{\partial Y} = -F_{pr} \tag{3.19}$$

$$\rho_p(u_p \psi_x + v_p \psi_r)C_s \frac{\partial T_p}{\partial \psi} + \rho_p v_p C_s \frac{\partial T_p}{\partial Y} = -Q_p \tag{3.20}$$

4. EQUATIONS OF MOTION IN (ξ, η) COORDINATE SYSTEM

The shock-layer gas-particle flow is now analysed by the inverse method, that is, the shock wave is prescribed and the body surface is then determined.

For the stream functions ahead of the shock wave, choose

$$\psi = \frac{r^2}{2} \tag{4.1}$$

$$\psi_p = \frac{r^2}{2} \tag{4.2}$$

To facilitate the integration of the governing equations in the shock layer, introduce further the following independent variables [Ref. 24]:

$$\xi = \frac{Y^2}{2} \tag{4.3}$$

$$\eta = \frac{2\psi}{Y^2} \tag{4.4}$$

In this (ξ, η) coordinate system, the shock wave surface and the body surface correspond to $\eta = 1$ and 0, respectively. From the transformation equations (4.3) and (4.4), a set of transformation operators are obtained:

$$\frac{1}{Y}\frac{\partial}{\partial Y} = \frac{\partial}{\partial \xi} - \frac{\eta}{\xi}\frac{\partial}{\partial \eta} \tag{4.5}$$

$$\frac{\partial}{\partial \psi} = \frac{1}{\xi}\frac{\partial}{\partial \eta} \tag{4.6}$$

Considering $v \propto Y$, $v_p \propto Y$ near $Y = 0$, transform the dependent variables v and v_p to V and V_p as

$$V = \frac{v}{Y} \tag{4.7}$$

$$V_p = \frac{v_p}{Y} \tag{4.8}$$

Then the governing equations (3.12)-(3.20) become, for the gas phase,

$$\frac{\partial u}{\partial t} - 2\pi \frac{\partial x}{\partial t}\frac{\partial V}{\partial t} + \frac{\gamma}{2}\frac{\partial \rho}{\partial t} = \frac{\rho}{\rho}\left\{\frac{1}{V}\frac{\partial v}{\partial t} + \frac{1}{\rho}\frac{\partial \rho}{\partial t}\right\} + \frac{1}{\rho} \tag{4.9}$$

$$\frac{\partial u}{\partial t} + \frac{\partial p}{\partial t} = \frac{\partial u}{\partial t} - \frac{F_{px}}{2\rho V} \tag{4.10}$$

$$\frac{\partial V}{\partial t} - \frac{\partial x}{\partial t}\frac{\partial p}{\partial t} = \frac{\partial V}{\partial t} + \frac{1}{2\rho V}\frac{\partial p}{\partial t} + \frac{V}{2} - \frac{F_{pr}}{2\pi}\frac{1}{2\rho V} \tag{4.11}$$

$$c_p\frac{\partial T}{\partial t} - \frac{1}{\rho}\frac{\partial p}{\partial t} = c_p\frac{\partial T}{\partial t} - \frac{1}{\rho}\frac{\partial p}{\partial t} - \frac{Q_p}{2\rho V} - \frac{u_p-u}{2\rho V}F_{px} - \frac{v_p-v}{2\rho V}F_{pr} \tag{4.12}$$

$$\frac{1}{p}\frac{\partial p}{\partial t} - \frac{1}{\rho}\frac{\partial \rho}{\partial t} - \frac{1}{T}\frac{\partial T}{\partial t} = 0 \tag{4.13}$$

and for the particle phase,

$$\frac{\partial u_p}{\partial t} - 2\pi\frac{\partial x}{\partial t}\frac{\partial V_p}{\partial t} + \frac{1}{\rho_p}\left\{u_p - 2\pi V_p\frac{\partial x}{\partial t}\right\}\frac{\partial \rho_p}{\partial t} = \frac{\rho}{\rho}\left\{\frac{1}{V}\frac{\partial V_p}{\partial t} + \frac{V_p}{V}\frac{1}{\rho_p}\frac{\partial \rho_p}{\partial t}\right\} + \frac{1}{\rho}\frac{V_p}{V} \tag{4.14}$$

$$\rho_p\left\{u_p - 2\pi V_p\frac{\partial x}{\partial t}\right\}\frac{\partial u_p}{\partial t} = \frac{\rho_p V_p}{\rho V}\frac{\partial u_p}{\partial t} + \frac{F_{px}}{2\rho V} \tag{4.15}$$

$$\rho_p\left\{u_p - 2\pi V_p\frac{\partial x}{\partial t}\right\}\frac{\partial V_p}{\partial t} = \frac{\rho_p V_p}{\rho V}\frac{\partial V_p}{\partial t} + \frac{\rho_p V_p}{\rho V}\frac{V_p}{2} + \frac{F_{pr}}{2\pi}\frac{1}{2\rho V} \tag{4.16}$$

$$\rho_p\left\{u_p - 2\pi V_p\frac{\partial x}{\partial t}\right\}c_s\frac{\partial T_p}{\partial t} = \frac{\rho_p V_p}{\rho V}c_s\frac{\partial T_p}{\partial t} + \frac{Q_p}{2\rho V} \tag{4.17}$$

Equation (3.11) becomes

$$\frac{\partial x}{\partial t} = -\frac{1}{2\rho V} \tag{4.18}$$

In deriving the above equations, the following relations were used:

$$\frac{\psi_x}{\rho} = -2\rho V \tag{4.19}$$

$$\frac{\psi_r Y - Y^2\rho}{\rho} = 2(\rho u - \rho) = 4\pi\rho V\frac{\partial x}{\partial t} \tag{4.20}$$

For the ten unknown variables, u, V, ρ, T, p, u_p, V_p, ρ_p, T_p and x, the ten equations (4.9)-(4.18) provide a solution through numerical integration.

5. INITIAL CONDITIONS

The initial conditions immediately behind the shock wave for the gas are the usual jump conditions (Rankine-Hugoniot relations), and for the dust particles use the frozen conditions, that is, the particle flow quantities immediately behind the shock wave are the same as those immediately ahead of the shock wave.

Let

$$x = s(r) \tag{5.1}$$

be the equation of the shock-wave shape. Then the flow quantities behind the shock wave are given by

$$u = 1 - \frac{1-\cdot}{N^2} \tag{5.2}$$

$$V = \frac{1-\cdot}{N^2}\cdot\frac{s_r}{r} \tag{5.3}$$

$$p = \frac{1}{\gamma M_\infty^2} + \frac{1-\cdot}{N^2} \tag{5.4}$$

$$\cdot = \frac{1}{\cdot} \tag{5.5}$$

$$T = \frac{\gamma}{\gamma-1}\frac{p}{\rho} \tag{5.6}$$

for the gas, and

$$u_p = 1 \tag{5.7}$$

$$V_p = 0 \tag{5.8}$$

$$\rho_p = \cdot \tag{5.9}$$

$$T_p = \frac{\gamma}{\gamma-1}\frac{1}{M_\infty^2} \tag{5.10}$$

for the particles, where

$$\cdot = \frac{\gamma-1}{\gamma+1} + \frac{2}{\gamma+1}\frac{N^2}{M_\infty^2} \tag{5.11}$$

$$N^2 = 1 + s_r^2 \tag{5.12}$$

and γ is the specific heat ratio of the gas, and $M_\infty = U_\infty/\bar{a}_\infty$ is the freestream Mach number.

It is worth noting that the specific heat ratio of the equilibrium gas-particle mixture γ_e and the equilibrium Mach number ahead of the shock wave M_e are given by [Ref. 6]

$$\gamma_e = \frac{\gamma+\alpha\cdot\beta}{1+\alpha\cdot\beta} \tag{5.13}$$

$$M_e = M_\infty \sqrt{\frac{(1+\alpha)(1+\alpha\beta)}{1+\alpha\beta/\gamma}} \qquad (5.14)$$

where α is the loading ratio, and $\beta = c_s/c_v$ is the ratio of the specific heats of the two phases.

6. NUMERICAL PROCEDURE

The governing equations (4.9)-(4.18) are numerically integrated from a point immediately behind the shock wave ($\eta = 1$) to the body surface ($\eta = 0$) by a forward (i.e., downstream) integration method [Ref. 16].

The numerical procedure is summarized as follows:

1. Calculate the initial values $f^{(m)}$ at $\eta = 1$ from Eqs. (5.2)-(5.10), where $f^{(m)}$ means any flow quantity.
2. Calculate ξ derivatives $f_\xi^{(m)}$ by numerical differentiation (here a 5-point Lagrange relation was used).
3. Calculate $f_\eta^{(m)}$ from the governing equations (4.9)-(4.18).
4. Extrapolate $f^{(m+1)}$ linearly to the next smaller value of η:

$$f^{(m+1)} = f^{(m)} - \Delta\eta \cdot f_\eta^{(m)} \qquad (6.1)$$

5. Calculate ξ derivatives $f_\xi^{(m+1)}$ as in step 2.
6. Calculate $f_\eta^{(m+1)}$ as in step 3.
7. Extrapolate again $f^{(m+1)}$ using average value of f_η:

$$f^{(m+1)} = f^{(m)} - \frac{\Delta\eta}{2}\left\{f_\eta^{(m)} + f_\eta^{(m+1)}\right\} \qquad (6.2)$$

8. Repeat steps 2 to 7 for this new value of η, and continue until $\eta = 0$.

As the freestream Mach number M_∞ reaches a low value, the numerical calculations become difficult owing to numerical instability at the outer calculation points (end instability). In this case, the end stability is eliminated by dropping the outermost 2 or 3 points at each step.

The mesh sizes $\Delta\xi$, $\Delta\eta$ used were $\Delta\xi = 0.005$, 0.01 and $\Delta\eta = 0.1$, 0.2. The numerical calculations were done on an IBM 1130 computer at UTIAS, and the calculation time was about 1 to 3 seconds for each case.

7. NUMERICAL RESULTS AND DISCUSSIONS

7.1 Pure-Gas Case

To check the adequacy of the present numerical results, the flow field around a sphere in a pure gas (i.e., no solid particles) was solved and compared with those of Van Dyke and Gordon [Ref. 16].

Any shock wave ahead of a smooth, blunt body may be described by [Refs. 15, 16]

$$\bar{r}^2 = 2\bar{R}_s\bar{x} - B_s\bar{x}^2 \qquad (7.1a)$$

or

$$r^2 = 2x - B_s x^2 \qquad (7.1b)$$

where $\bar{R}_s$ is the nose radius, B_s is the bluntness of the shock shape, and $r = \bar{r}/\bar{R}_s$, $x = \bar{x}/\bar{R}_s$. The bluntness B_s is a convenient parameter that characterizes the eccentricity of the conic section. It is worth noting that $B_s < 0$ generates a hyperbola, $B_s = 0$ generates a parabola, and $B_s > 0$ generates an ellipse, and $B_s = 1$ results in the special case of a sphere. Table 1 shows the values of B_s taken from Ref. 16. In addition, other quantities such as shock standoff distance Δ, nose radius R_b and bluntness B_b are also tabulated and will be discussed subsequently.

The body shape corresponding to a given shock shape may be approximated by [Refs. 16-19]

$$\bar{r}^2 = 2\bar{R}_b(\bar{x}-\bar{\Delta}) - B_b(\bar{x}-\bar{\Delta})^2 \qquad (7.2a)$$

or

$$r^2 = 2R_b(x-\Delta) - B_b(x-\Delta)^2 \qquad (7.2b)$$

where $R_b = \bar{R}_b/\bar{R}_s$ is the nondimensional nose radius, B_b the bluntness of the body, and $\Delta = \bar{\Delta}/\bar{R}_s$ the nondimensional standoff distance. The process used to determine R_b and B_b is the same as that of Refs. 16 and 17, that is, the quantity

$$\frac{r^2}{2(x-\Delta)} = R_b - \frac{B_b}{2}(x-\Delta) \qquad (7.2c)$$

is plotted versus $(x-\Delta)$, and the points are approximated by a straight line. Then, the vertical intercept of the line is R_b, and its slope is $-\frac{1}{2}B_b$.

Figures 2(a)-(d) show the shock waves, sonic lines and streamlines for a sphere at freestream Mach numbers $M_\infty = 10$, 3, 2 and 1.5, respectively. The abscissa $x = \bar{x}/\bar{R}_s$ and the ordinate $r = \bar{r}/\bar{R}_s$ are nondimensional distances, as noted previously. For comparison, Van Dyke and Gordon's numerical results [Ref. 16] are shown. The present calculated body shapes agree very well with those of Ref. 16 for the high freestream Mach number $M_\infty = 10$, and the agreement is also good for the low freestream Mach numbers $M_\infty = 3$, 2 and 1.5. The present calculated sonic line shapes almost coincide with those of Ref. 16 except for the case of $M_\infty = 1.5$. It may be noted that the present sonic-line shape for $M_\infty = 1.5$ resembles that of Ref. 27. The flow patterns of the shock layer around a sphere are well-defined from the present calculated streamlines.

In Figs. 3(a) and (b) appear the relations between the quantities $r^2/2(x-\Delta)$ and $(x-\Delta)$ for the calculated bodies. From these figures R_b and B_b are determined as shown in Table 1. It is seen that the present nose radii R_b coincide with those of Van Dyke and Gordon [Ref. 16] within 1.5%, and the present bluntness of the body $B_b = 1$, i.e., the calculated body shapes are spheres.

The shock standoff distances Δ are also listed in Table 1. The present results agree very well with those of Ref. 16 for high freestream Mach numbers $M_\infty = 10$, 6 and 4, and also agree quite well with those of Ref. 16 for low freestream Mach numbers $M_\infty = 3$, 2 and 1.5 within 2.5%.

Table 2 shows the stagnation pressure on the bodies. The exact values shown in Table 2 are calculated from the following equation [Ref. 26]:

$$p_{st} = \frac{\bar{p}_{st}}{\bar{\rho}_\infty \bar{U}_\infty^2} = \frac{1}{\gamma M_\infty^2} \left\{ \frac{(\gamma+1)M_\infty^2}{2} \right\}^{\frac{\gamma}{\gamma-1}} \cdot \left\{ \frac{\gamma+1}{2\gamma M_\infty^2 - (\gamma-1)} \right\}^{\frac{\gamma}{\gamma-1}} \qquad (7.3)$$

The present results coincide with the exact values within 1%.

The pressure distributions on the bodies (spheres) are shown in Figs. 4(a)-(d) for M_∞ = 10, 3, 2 and 1.5, respectively. The present results agree very well with those of Van Dyke and Gordon [Ref. 16] in the stagnation region for all freestream Mach numbers. But the difference between the present results and those of Ref. 16 appear near sonic lines on the bodies at the low freestream Mach numbers M_∞ = 3, 2 and 1.5. It may be worth noting that Hamilton [Ref. 19] has pointed out that the results of Ref. 16 underpredict the pressure near the sonic line on the body at low freestream Mach numbers.

7.2 Dusty-Gas Case

The following numerical examples concern the flow of gas-solid particles past blunt bodies (near spheres). Since the inverse method is used, the freestream-flow conditions and the shock waves described by Eq. (7.1) are assumed first and then the numerical method is used to find the shock-layer gas-particle flows and the body shapes.

Air (γ = 1.4, gas constant $\bar{R}$ = 287 m^2/s^2K) and glass spheres ($\bar{\rho}_s$ = 2.5 g/cm^3) are used for the gas-solid particle flow. The temperature and the pressure of the air ahead of the shock wave are $\bar{T}_\infty$ = 300 K, $\bar{p}_\infty$ = 101.3 KPa, and the reference length is $\bar{R}_s$ = 1 cm for all the calculations.

To investigate the effects of the freestream Mach number M_∞, the freestream loading ratio α and the particle diameter $\bar{d}_p$ on the shock layer gas-particle flow, the following range of parameters were used:

$$M_\infty = 10,\ 1.5$$

$$\alpha = 0,\ 0.2,\ 0.5,\ 1.0$$

$$\bar{d}_p = 1,\ 2,\ 5,\ 10\ \mu m$$

The number of solid particles in the freestream flow ahead of the shock wave appear in Table 3.

7.2.1 Results for M_∞ = 10

Although the results for M_∞ = 10 are only of academic interest because of the assumptions made concerning gas properties at high temperature and the resulting particle drag and heat transfer coefficients, these calculations were performed in order to show the trends of the shock-layer gas-particle flows. As noted previously, the Prandtl number was taken at 0.75, the specific heat of the gas was held constant, and the viscosity power law, Eq. (2.20), and the drag coefficient, Eq. (2.15), remained unchanged.

Figures 5(a)-(d) show the assumed shock waves and calculated body shapes for M_∞ = 10 and $\bar{d}_p$ = 1, 2, 5 and 10 μm, respectively. The loading ratios α ahead of the shock wave were α = 0, 0.2, 0.5 and 1.0. The abscissa and ordinate are nondimensionalized by the shock nose radius $\bar{R}_s$ = 1 cm. It is seen that, when $\bar{d}_p$ = 1 μm, the shock layer thickness decreases as α increases from 0 to 0.5 [Fig. 5(a)]. (When α = 1.0, a body shape was not obtained because of numerical instability near the body surface.) This tendency is similar to the results of Ref. 13 for an aerosol-gas mixture. However, when $\bar{d}_p$ = 2, 5 and 10 μm, the shock layer thicknesses increase, that is, the shock standoff distance increases with α. The reason will be considered later, since the shock stand-off distance is closely associated with the variation of the gas-flow quantities within the shock layer.

Figures 6(a)-(d) show the relations between the quantities $r^2/2(x-\bar{x})$ and $(x-\bar{x})$ of the calculated bodies. From these figures, the nose radius R_b and the bluntness of the body B_b were calculated, which are shown in Tables 4(a)-(d). It is seen that, for example, when $\bar{d}_p$ = 1 μm, R_b increases with increasing α, and B_b differs slightly from unity with increasing α. It may be noted that B_s = 1.0 means a true sphere, and B_s = 0.93 means a prolate sphere.

Figures 7(a)-(d) show the variations of the velocities and the temperatures of the gas and particles along the stagnation streamlines for $\bar{d}_p$ = 1, 2, 5 and 10 μm, respectively. Similarly, Figs. 8(a)-(d) show the variation of the gas and particle densities and gas pressures along the stagnation streamlines. As noted previously, the particle density $\rho_p = \bar{\rho}_p/\bar{\rho}_\infty = m \cdot n/\bar{\rho}_\infty$, and it changes within the shock-layer flow field.

The results for $\bar{d}_p$ = 1 μm will now be discussed in detail. Figure 7(a) shows that the gas velocity u decreases gradually along the stagnation streamline and becomes zero at the body surface. However, the particle velocity u_p decreases much more rapidly as a result of the drag interaction of the particles with the gas. The particles reach almost the same velocity as the gas near the body surface. In other words, the particle and gas velocities are in dynamic equilibrium near the body surface.

Figure 7(a) also shows that the gas temperature T increases along a stagnation streamline until it reaches a maximum, and then decreases as the loading ratio ahead of the shock α increases from 0.2 to 1.0. This variation of the gas temperature is explained as follows. As noted previously [Eq. (2.4)], the gas temperature T is changed owing to both the work done by the particles on the gas $(u_p-u)F_{px}$ and the heat transfer from the gas to the particles Q_p. Just behind the shock wave, the difference between the gas and particle velocities is so large that the heat generated by the work done by the particles $(u_p-u)F_{px}$ dominates the heat loss Q_p, and as a result the gas temperature T increases behind the shock wave at first. Near the body surface, the velocity difference (u_p-u) becomes small, and $(u_p-u)F_{px}$ becomes small. However, the increase in ρ_p results in a larger heat loss from the gas to the particles. Consequently, the heat loss Q_p dominates the work done $(u_p-u)F_{px}$, and the gas temperature T decreases near the body surface. When the heat generated by the work done

by the particle on the gas is equal to the heat loss to the particle phase, the gas temperature reaches a maximum. This variation of gas temperature is similar to that obtained in Ref. 13.

It should be noted that the gas stagnation temperature on the body increases with increasing α owing to the decrease in kinetic energy of the particles. The particle temperature T_p increases monotonically because of the heat transfer from the gas phase, but it does not reach the gas temperature T. The gas and particle temperatures are always in nonequilibrium.

Figure 8(a) shows that the gas density ρ for $\alpha = 0$ decreases along the stagnation streamline at first and then it increases near the body surface. However, the density of the particle phase ρ_p increases gradually at first and then increases more rapidly near the body surface as α increases from 0.2 to 1.0. The gas pressure p increases along a stagnation streamline owing to the decrease of the gas and particle velocities.

The results for $\bar{d}_p$ = 2 μm [Fig. 8(b)] are significantly different than for $\bar{d}_p$ = 1 μm. In this case, the particle velocity u_p does not reach the gas velocity u near the body surface [Fig. 7(b)], and a substantial difference between the gas and particle velocities (u_p-u) always exists. Heat is always generated in the gas phase owing to the work done by the particles. On the other hand, the particle temperature T_p does not increase very much. That is, the heat loss from the gas to the particles is slight. Consequently, the gas temperature T always increases along the stagnation streamline. When α = 0.5 and 1.0, the gas temperature T reaches more than 10,000 K near the body surface. In these cases, one has to consider real-gas effects, and evaporation and melting of the particles. Consequently, the range of α for which the present analysis is applicable is $\alpha \leq 0.5$.

Figure 8(b) shows that the density of the gas ρ decreases along a stagnation streamline owing to the increase in gas temperature as α increases from 0.2 to 1.0. The gas pressure p and the density of the particle phase ρ_p increase along a stagnation streamline as α increases.

As mentioned previously, when $\bar{d}_p$ = 2, 5 and 10 μm, the shock standoff distance increases with increasing α [Figs. 5(b), (c), (d)]. This phenomenon can now be explained as follows: the gas density ρ along stagnation and adjacent streamlines decreases owing to the increase in gas temperature as α increases. On the other hand, the shock location is determined by the continuity condition of equal gas mass flow. Consequently, the shock standoff distance increases as α increases.

The results for $\bar{d}_p$ = 5 and 10 μm appear in Figs. 7(c), (d) and 8(c), (d). As the particle diameter d_p increases, the rates of decrease of u_p and increase of T_p along a stagnation streamline decrease. In other words, the particle flow behaves almost like a frozen flow as $\bar{d}_p$ increases. In the case of $\bar{d}_p$ = 5 and 10 μm, the variation of the other flow quantities u, T, p, ρ and ρ_p along a stagnation streamline are qualitatively the same as for $\bar{d}_p$ = 2 μm

Figures 9(a)-(d) show the pressure distributions on the body surfaces for $\bar{d}_p$ = 1, 2, 5 and 10 μm, respectively. In each case, the pressure increases with the loading ratio α, ahead of the shock wave. However, for α = 0, the agreement with the pressure distribution observed in Ref. 16 is very good.

Figures 10(a)-(d) show the gas and particle streamlines near the stagnation regions in the shock layers. When $\bar{d}_p$ = 1 μm, the particle paths are straight just behind the shock wave, and continue to deflect as they approach the body surface and collide at small impact angle γ as shown in Fig. 10(a). As $\bar{d}_p$ increases from 2 to 10 μm, the particle deflection decreases and they tend to move in a straight path towards the body surface where they collide with large impact angles.

After the particles collide with the body surface, they may break up or reflect or stick to the body surface. However, at present, it is not known how the particles behave after colliding. This analysis may be valid if the particles break after colliding into much smaller ones to form a thin dusty layer or if they stick to the body surface.

7.2.2 Results for M_∞ = 1.5

Figures 11(a)-(d) show the assumed shock shapes and calculated body shapes for M_∞ = 1.5 and $\bar{d}_p$ = 1, 2, 5 and 10 μm, respectively. In the case of M_∞ = 1.5, the shock standoff distances decrease with the loading ratio α ahead of the shock wave for all particle diameters $\bar{d}_p$. The greatest effect on the shock standoff distance occurs for the smallest particle diameter $\bar{d}_p$ = 1 μm. The reason is that when $\bar{d}_p$ = 1 μm, the gas density ρ increases most significantly along the stagnation streamline and adjacent streamlines owing to the gas and particle interaction as α increases [see Fig. 14(a)]. Consequently, the shock standoff distance decreases as α increases. As the particle diameter $\bar{d}_p$ increases from 2 to 10 μm, the effect of α on the shock standoff distance becomes weak. When $\bar{d}_p$ = 10 μm, the effect of α is indistinguishable from that of a pure-gas flow.

In Figs. 12(a)-(d), the quantities $r^2/2(x-\bar{x})$ are plotted versus $(x-\bar{x})$. In these cases, the calculated points near a sonic point deviate considerably from a straight line. Tables 5(a)-(d) show the shock standoff distance $\bar{x}$, nose radius R_b and bluntness B_b of the calculated bodies for dusty-gas flows. It is seen that, for all particle diameters $\bar{d}_p$, the nose radius R_b increases as α increases and the bluntness B_b becomes smaller than unity, i.e., the calculated body shapes become a prolate sphere as α increases.

Figures 13(a)-(d) and 14(a)-(d) show the variations of velocity, temperature and density for gas and particles along a stagnation streamline. From Fig. 13(a), we can see that in the case of M_∞ = 1.5 and $\bar{d}_p$ = 1 μm, the particle temperature T_p and gas temperature T almost achieve equilibrium near the stagnation point. However, the particle and gas velocities do not achieve equilibrium near the stagnation point. This tendency is just the reverse of the M_∞ = 10 case for $\bar{d}_p$ = 1 μm [see Fig. 7(a)]. It is worth noting that the variations

of the flow quantities along the stagnation streamlines resemble the known dusty-air solutions behind a normal shock wave [Refs. 4, 6, 28, 29]. As the particle diameters $\bar{d}_p$ increase from 2 to 10 μm, the particles tend to keep their initial values of u_p and T_p as if the particles do not influence the gas flow.

The gas pressure p and the gas and particle phase densities ρ and ρ_p increase along the stagnation streamlines as χ increases. These tendencies become weak as $\bar{d}_p$ increases.

Figures 15(a)-(d) show the pressure distributions on the body surfaces. As χ increases and $\bar{d}_p$ decreases, the pressures on the body surfaces become larger. These effects are similar to the case of $M_\infty = 10$.

Figures 16(a)-(d) show the gas and particle streamlines near the stagnation regions in the shock layers. When $\bar{d}_p = 1$ μm, the particle streamlines deflect significantly near the body surface as shown in Fig. 16(a). As the particle diameter $\bar{d}_p$ increases from 2 to 10 μm, the particle deflection decreases and it proceeds almost in a straight line to collide with the surface [Fig. 16(d)]. This particle behaviour is similar to the case of $M_\infty = 10$.

8. CONCLUSIONS

An inverse method was developed to study dusty supersonic flow past axisymmetric blunt bodies. The analysis was based on the assumptions that there are no collisions between the individual particles and that the interactions between the gas and the particles are only through drag and heat transfer. The governing equations for axisymmetric gas-particle flow were described in a cylindrical (x,r)-coordinate system. Then by using the von Mises transformation, the governing equations were again transformed into a (ψ, Y)-coordinate system, where ψ is the gas stream function, and $Y = r$. To facilitate the integration of the governing equations in the shock layer, they were further transformed into a (ξ, η)-coordinate system by using transformation equations (4.3) and (4.4). The advantages of the present method are: (1) body shapes are easily determined without any approximate calculation; (2) the computer memory required is not large; (3) the computer calculation time is very short, so that it is possible to extend this method to a direct method by using an iterative procedure.

In using the present method, the pure-gas flow fields around spheres were first solved numerically for the freestream Mach number range $1.5 \leq M_\infty \leq 10$. These were found to be in very good agreement with the results of Van Dyke and Gordon [Ref. 16].

Based on the assumptions that the Prandtl number Pr = 0.75, the specific heat of the gas is constant, the specific heat ratio of the two phases is unity, and the gas viscosity and drag coefficient were described by Eqs. (2.20) and (2.15), the supersonic gas-solid particle flows past near-spherical bodies were then solved for freestream Mach numbers $M_\infty = 1.5$ and 10, with freestream loading ratio $\chi = 0$, 0.2, 0.5 and 1.0, and particle diameters $\bar{d}_p = 1$, 2, 5 and 10 μm, respectively. The numerical results can be summarized as follows:

Shock standoff distance Δ

(a) For $M_\infty = 1.5$: the shock standoff distance Δ decreases with increasing χ for all particle diameters $\bar{d}_p$. As $\bar{d}_p$ increases, the effect of the freestream loading ratio χ on Δ becomes weak.

(b) For $M_\infty = 10$: the shock standoff distance Δ decreases with increasing χ for $\bar{d}_p = 1$ μm. However, when $\bar{d}_p = 2$, 5 and 10 μm, Δ increases with increasing χ, because of the decrease of the gas density ρ in the shock layer.

Variation of gas and particle velocities and temperatures along a stagnation streamline

(a) For $M_\infty = 1.5$: when $\bar{d}_p = 1$ μm, the gas and particle temperatures T and T_p almost achieve equilibrium near the stagnation point on the body. However, the gas and particle velocities u and u_p do not achieve equilibrium near the stagnation point. As $\bar{d}_p$ increases, the particles tend to keep their initial values of u_p and T_p.

(b) For $M_\infty = 10$: when $\bar{d}_p = 1$ μm, the particle and gas velocities u and u_p are in equilibrium near the stagnation point on the body. However, the gas and particle temperatures T and T_p are not in equilibrium. This tendency is just the reverse of the $M_\infty = 1.5$ case. When $\bar{d}_p = 2$, 5 and 10 μm, u_p does not reach the value of u near the body surface.

Variation of gas pressure p and gas and particle phase densities ρ and ρ_p along a stagnation streamline

(a) For $M_\infty = 1.5$: for all particle diameters $\bar{d}_p$, the gas pressure p and the gas and particle phase densities ρ and ρ_p always increase along a stagnation strreamline as χ increases.

(b) For $M_\infty = 10$: when $\bar{d}_p = 1$ μm, the gas density ρ decreases slightly along a stagnation streamline at first and then it increases near the body surface. However, when $\bar{d}_p = 2$, 5 and 10 μm, the density of the gas ρ decreases along a stagnation streamline owing to the gas temperature increase as χ increases. The density of the particle phase ρ_p and the gas pressure p increase along a stagnation streamline.

Body-surface pressure p_b

For both $M_\infty = 1.5$ and 10, the body surface pressure P_b increases as χ increases. This tendency is significant as $\bar{d}_p$ becomes smaller.

Behaviour of particle streamlines

For both $M_\infty = 1.5$ and 10, when $\bar{d}_p = 1$ μm, the particle streamlines deflect significantly near the body surface. As the particle diameter $\bar{d}_p$ increases, the particle deflection decreases and it proceeds almost in a straight line to collide with the body surface.

Within the limitations of the assumptions noted above, the present numerical results provide an understanding of dusty supersonic flow past blunt bodies.

REFERENCES

1. Soo, S. L., "Fluid Dynamics of Multiphase Systems", Blaisdell, Waltham, 1967.

2. Rudinger, G., "Relaxation in Gas-Particle Flow", in P. P. Wegener, "Nonequilibrium Flows", Vol. 1, Part 1, Marcel Dekker, New York, 1969, pp. 119-161.

3. Wallis, G. B., "One-Dimensional Two-Phase Flow", McGraw-Hill, New York, 1969.

4. Marble, F. E., "Dynamics of Dusty Gases", Annual Review of Fluid Mechanics, Vol. 2, 1970, pp. 397-446.

5. Boothroyd, R. G., "Flowing Gas-Solids Suspensions", Chapman and Hall, London, 1971.

6. Rudinger, G., "Fundamentals of Gas-Particle Flow", Elsevier, Amsterdam, 1980.

7. Miura, H., Glass, I. I., "On a Dusty-Gas Shock Tube", UTIAS Report No. 250, 1981 (see also Proc. Roy. Soc. A 382, 1982, pp. 373-388).

8. Miura, H., Glass, I. I., "On the Passage of a Shock Wave Through a Dusty-Gas Layer", UTIAS Report No. 252, 1982.

9. Probstein, R. F., Fassio, F., "Dusty Hypersonic Flows", AIAA J., Vol. 8, 1970, pp. 772-779.

10. Waldman, G. D., Reinecke, W. G., "Particle Trajectories, Heating, and Break up in Hypersonic Shock Layers", AIAA J., Vol. 9, 1971, pp. 1040-1048.

11. Spurk, J. H., Gerber, N., "Dust Collection Efficiency for Power Law Bodies in Hypersonic Flight", AIAA J., Vol. 10, 1972, pp. 755-761.

12. Peddieson, J., "Gas-Particle Flow Past Bodies with Attached Shock Waves", AIAA J., Vol. 13, 1975, pp. 939-941.

13. Chang, S. S-H., "Nonequilibrium Phenomena in Dusty Supersonic Flow Past Blunt Bodies of Revolution", The Physics of Fluids, Vol. 18, 1975, pp. 446-452.

14. Hayes, W. D., Probstein, R. F., "Hypersonic Flow Theory", Vol. 1-Inviscid Flows, Academic Press, New York and London, 1966.

15. Van Dyke, M. D., "The Supersonic Blunt-Body Problem – Review and Extension", Journal of Aero/Space Sci., Vol. 25, 1958, pp. 485-496.

16. Van Dyke, M. D., Gordon, H. D., "Supersonic Flow Past a Family of Blunt Axisymmetric Bodies", NASA TR R-1, 1959.

17. Fuller, F. B., "Numerical Solutions for Supersonic Flow of an Ideal Gas Around Blunt Two-Dimensional Bodies", NASA TN D-791, 1961.

18. Tomax, H., Inouye, M., "Numerical Anslysis of Flow Properties About Blunt Bodies Moving at Supersonic Speeds in an Equilibrium Gas", NASA TR R-204, 1964.

19. Hamilton, H. H. II, "Solution of Axisymmetric and Two-Dimensional Inviscid Flow Over Blunt Bodies by the Method of Lines", NASA Technical Paper 1154, 1978.

20. Gilbert, M., Davis, L., Altman, D., "Velocity Lag of Particles in Linearly Accelerated Combustion Gases", Jet Propulsion, Vol. 25, 1955, p. 26.

21. Knudsen, J. G., Katz, D. L., "Fluid Dynamics and Heat Transfer", McGraw-Hill, New York, 1958.

22. Chapman, S., Cowling, T. G., "The Mathematical Theory of Non-Uniform Gases", Cambridge Univ. Press, 1961.

23. von Mises, R., "Bemerkungen zur Hydrodynamik", ZAMM 7, 1927, pp. 425-431.

24. Honda, M., Sugiyama, H., "Analysis of Asymmetric Supersonic Flow", Mem. Inst. High Speed Mech., Tohoku Univ., Vol. 36, No. 348, 1975 (in Japanese).

25. Sugiyama, H., "A Numerical Method for Supersonic Conical Flow Without Axial Symmetry", Bulletin of the JSME, Vol. 20, No. 144, 1977, pp. 711-717.

26. Liepmann, H. W., Roshko, A., "Elements of Gasdynamics", John Wiley and Sons, Inc., New York, 1957.

27. Belotserkovskiy, O. M., Ed., "Supersonic Gas Flow Around Blunt Bodies - Theoretical and Experimental Investigation", NASA TT F-453, 1967.

28. Kriebel, A. R., "Analysis of Normal Shock Waves in Particle Laden Gas", Trans. ASME, Jour. of Basic Engineering, Vol. 86, 1964, pp. 655-665.

29. Rudinger, G., "Some Properties of Shcok Relaxation in Gas Flows Carrying Small Particles", The Physics of Fluids, Vol. 7, 1964, pp. 658-663.

Table 1

Shock Standoff Distance Δ, Nose Radius R_b and Bluntness B_b

of the Calculated Bodies (Spheres)

for Pure Gas, $\gamma = 1.4$

M_∞	B_s	$\Delta = \bar{\Delta}/\bar{R}_s$		$R_b = \bar{R}_b/\bar{R}_s$		$\bar{\Delta}/\bar{R}_b$		B_b	
		Present Method	Van Dyke & Gordon	Present Method	Van Dyke & Gordon	Present Method	Van Dyke & Gordon	Present Method	Van Dyke & Gordon
10	0.49	0.103	0.102	0.746	0.754	0.138	0.135	1.01	-
6	0.47	0.109	0.109	0.724	0.732	0.151	0.148	1.01	-
4	0.38	0.121	0.120	0.681	0.690	0.178	0.174	0.98	-
3	0.25	0.137	0.135	0.626	0.634	0.219	0.213	0.93	-
2	-0.06	0.174	0.170	0.499	0.500	0.349	0.340	1.02	-
1.5	-0.71	0.206	0.201	0.350	0.350	0.589	0.574	0.98	-

Table 2

Stagnation Pressure p_{st} on the Blunt Bodies

for Pure Gas, $\gamma = 1.4$

M_∞	1.5	2	3	4	6	10
Present Result	1.095	1.016	0.963	0.945	0.933	0.927
Van Dyke & Gordon	1.081	1.007	0.957	0.940	0.928	0.923
Exact Value	1.084	1.007	0.957	0.941	0.929	0.923

Table 3

Number of Solid Particles (Glass Spheres)

in Freestream Flow

$\bar{d}_p$ (μm) \ α	0.1 (cm^{-3})	0.2 (cm^{-3})	0.5 (cm^{-3})	1.0 (cm^{-3})
1	8.98×10^{7}	1.80×10^{8}	4.49×10^{8}	8.98×10^{8}
2	1.12×10^{7}	2.25×10^{7}	5.62×10^{7}	1.12×10^{8}
5	7.18×10^{5}	1.44×10^{6}	3.59×10^{6}	7.18×10^{6}
10	8.98×10^{4}	1.80×10^{5}	4.49×10^{5}	8.98×10^{5}

Table 4

Shock Standoff Distance Δ, Nose Radius R_b and Bluntness B_b of Calculated Bodies for Dusty-Gas Flows

$M_\infty = 10$, $\bar{T}_\infty = 300$ K, $\bar{p}_\infty = 101.3$ KPa, $\bar{R}_s = 1$ cm

(a) $\bar{d}_p = 1$ μm

α	$\Delta = \bar{\Delta}/\bar{R}_s$	$R_b = \bar{R}_b/\bar{R}_s$	$\bar{\Delta}/\bar{R}_b$	B_b
0	0.103	0.746	0.138	1.01
0.2	0.103	0.755	0.136	0.98
0.5	0.102	0.764	0.134	0.93

(b) $\bar{d}_p = 2$ μm

α	$\Delta = \bar{\Delta}/\bar{R}_s$	$R_b = \bar{R}_b/\bar{R}_s$	$\bar{\Delta}/\bar{R}_b$	B_b
0.2	0.106	0.744	0.143	0.98
0.5	0.110	0.742	0.148	0.91
1.0	0.115	0.742	0.155	0.89

(c) $\bar{d}_p = 5$ μm

α	$\Delta = \bar{\Delta}/\bar{R}_s$	$R_b = \bar{R}_b/\bar{R}_s$	$\bar{\Delta}/\bar{R}_b$	B_b
0.2	0.105	0.743	0.141	1.00
0.5	0.108	0.740	0.146	0.95
1.0	0.112	0.735	0.152	0.95

(d) $\bar{d}_p = 10$ μm

α	$\Delta = \bar{\Delta}/\bar{R}_s$	$R_b = \bar{R}_b/\bar{R}_s$	$\bar{\Delta}/\bar{R}_b$	B_b
0.2	0.104	0.745	0.139	1.01
0.5	0.106	0.742	0.142	0.91
1.0	0.108	0.738	0.147	0.99

Table 5

Shock Standoff Distance Δ, Nose Radius R_b and Bluntness B_b of Calculated Bodies for Dusty-Gas Flows

$M_\infty = 1.5$, $\bar{T}_\infty = 300$ K, $\bar{p}_\infty = 101.3$ KPa, $\bar{R}_s = 1$ cm

(a) $\bar{d}_p = 1$ μm

λ	$\Delta = \bar{\Delta}/\bar{R}_s$	$R_b = \bar{R}_b/\bar{R}_s$	$\bar{\Delta}/\bar{R}_b$	B_b
0	0.206	0.350	0.589	0.98
0.2	0.198	0.386	0.513	1.04
0.5	0.186	0.428	0.434	0.93
1.0	0.166	0.500	0.332	0.67

(b) $\bar{d}_p = 2$ μm

λ	$\Delta = \bar{\Delta}/\bar{R}_s$	$R_b = \bar{R}_b/\bar{R}_s$	$\bar{\Delta}/\bar{R}_b$	B_b
0.2	0.203	0.365	0.556	0.95
0.5	0.198	0.387	0.512	0.98
1.0	0.190	0.420	0.453	0.95

(c) $\bar{d}_p = 5$ μm

λ	$\Delta = \bar{\Delta}/\bar{R}_s$	$R_b = \bar{R}_b/\bar{R}_s$	$\bar{\Delta}/\bar{R}_b$	B_b
0.2	0.205	0.355	0.578	0.93
0.5	0.204	0.360	0.558	0.92
1.0	0.202	0.369	0.548	0.91

(d) $\bar{d}_p = 10$ μm

λ	$\Delta = \bar{\Delta}/\bar{R}_s$	$R_b = \bar{R}_b/\bar{R}_s$	$\bar{\Delta}/\bar{R}_b$	B_b
0.2	0.206	0.353	0.583	0.95
0.5	0.205	0.355	0.578	0.97
1.0	0.205	0.357	0.573	0.89

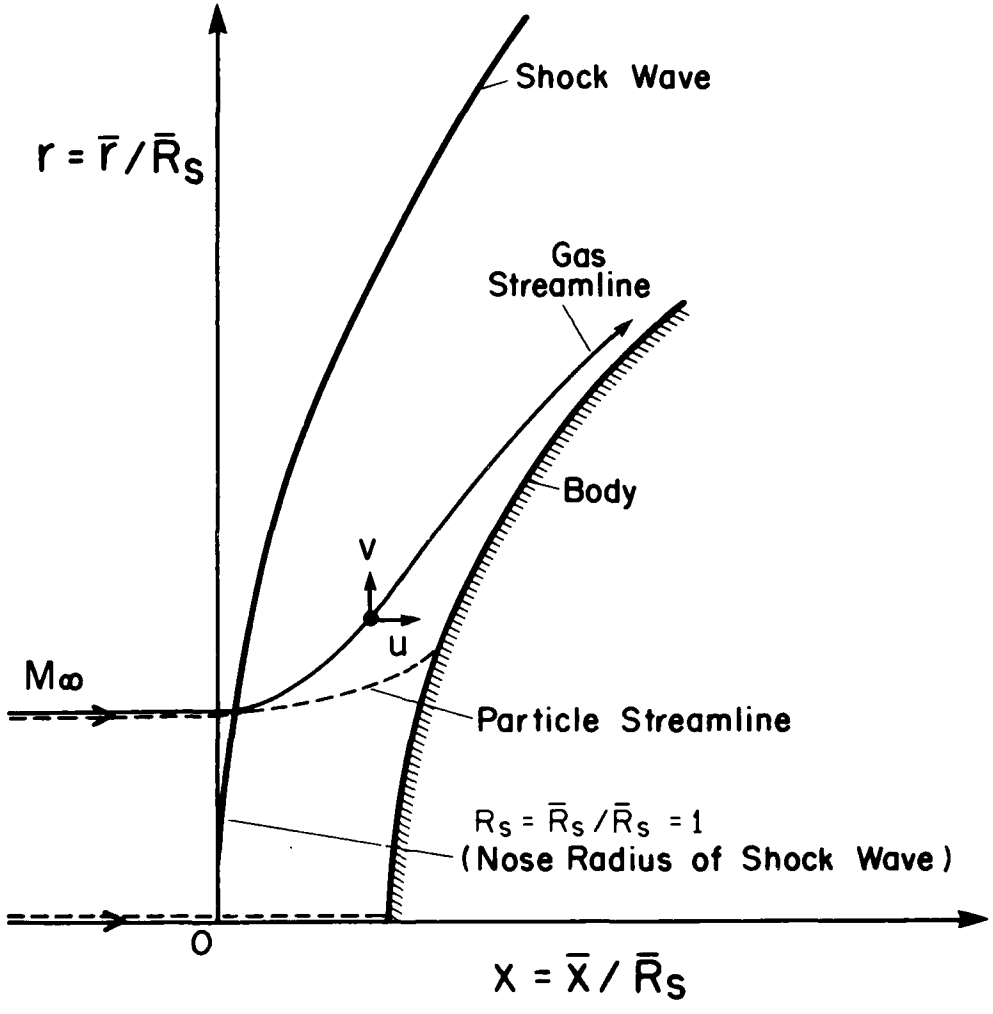

FIG. 1 CYLINDRICAL COORDINATE SYSTEM.

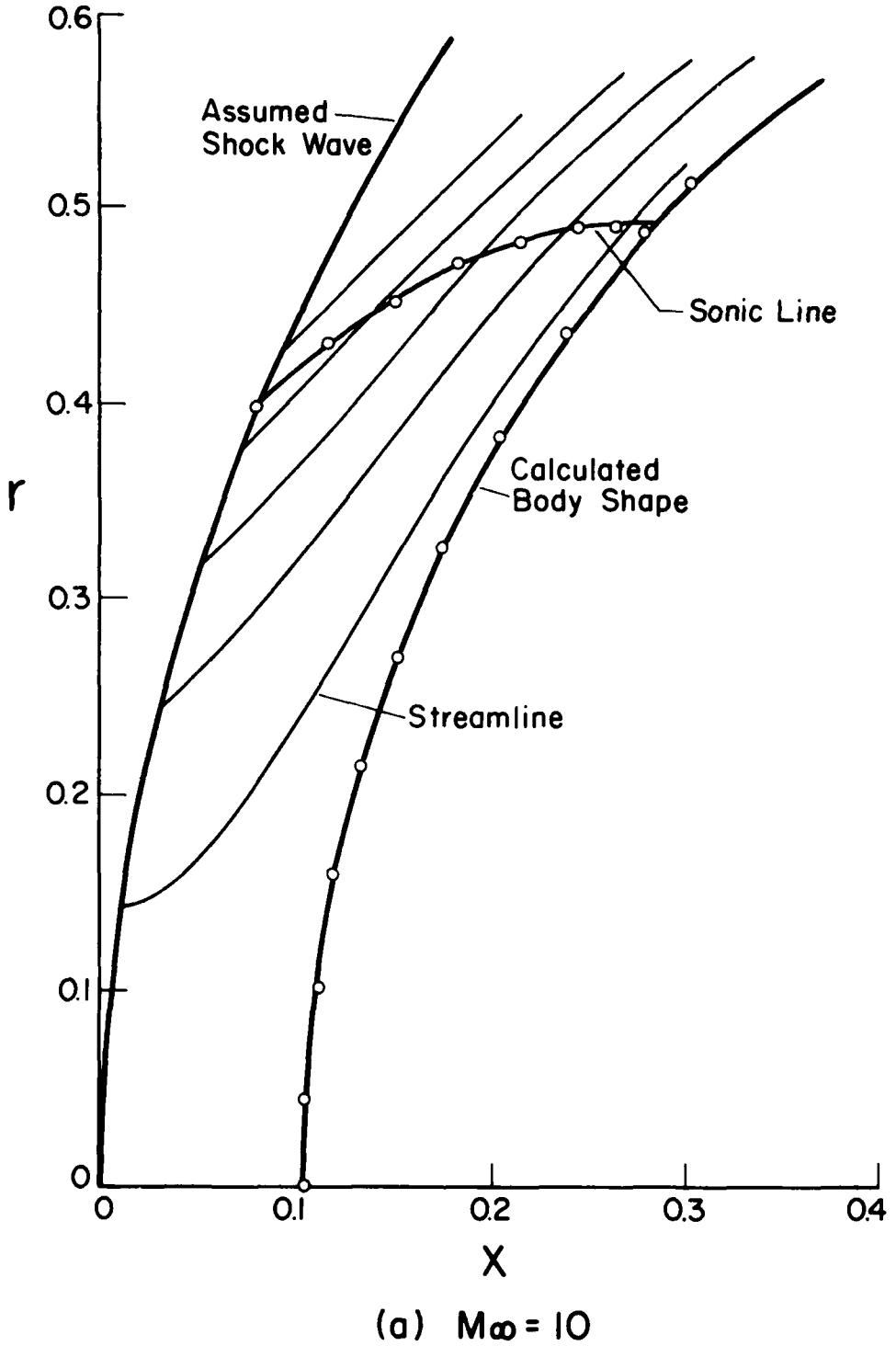

FIG. 2 SHOCK WAVE, SONIC LINE AND STREAMLINES FOR A SPHERE FOR PURE GAS, $\gamma = 1.4$. ○ VAN DYKE & GORDON [REF. 16].

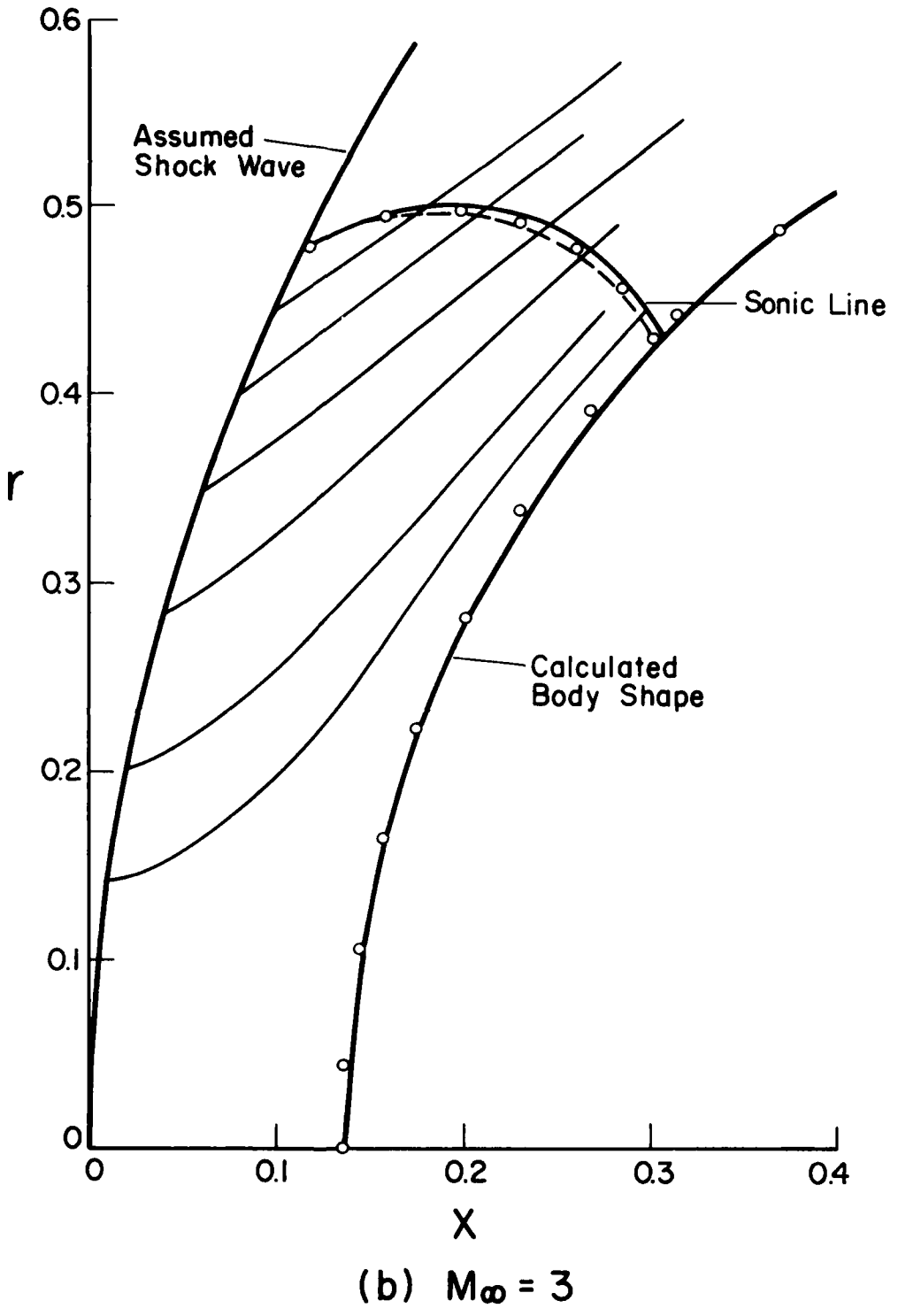

FIG. 2 - CONTINUED
SHOCK WAVE, SONIC LINE AND STREAMLINES FOR A SPHERE FOR PURE GAS, $\gamma = 1.4$. ° VAN DYKE & GORDON [REF. 16].

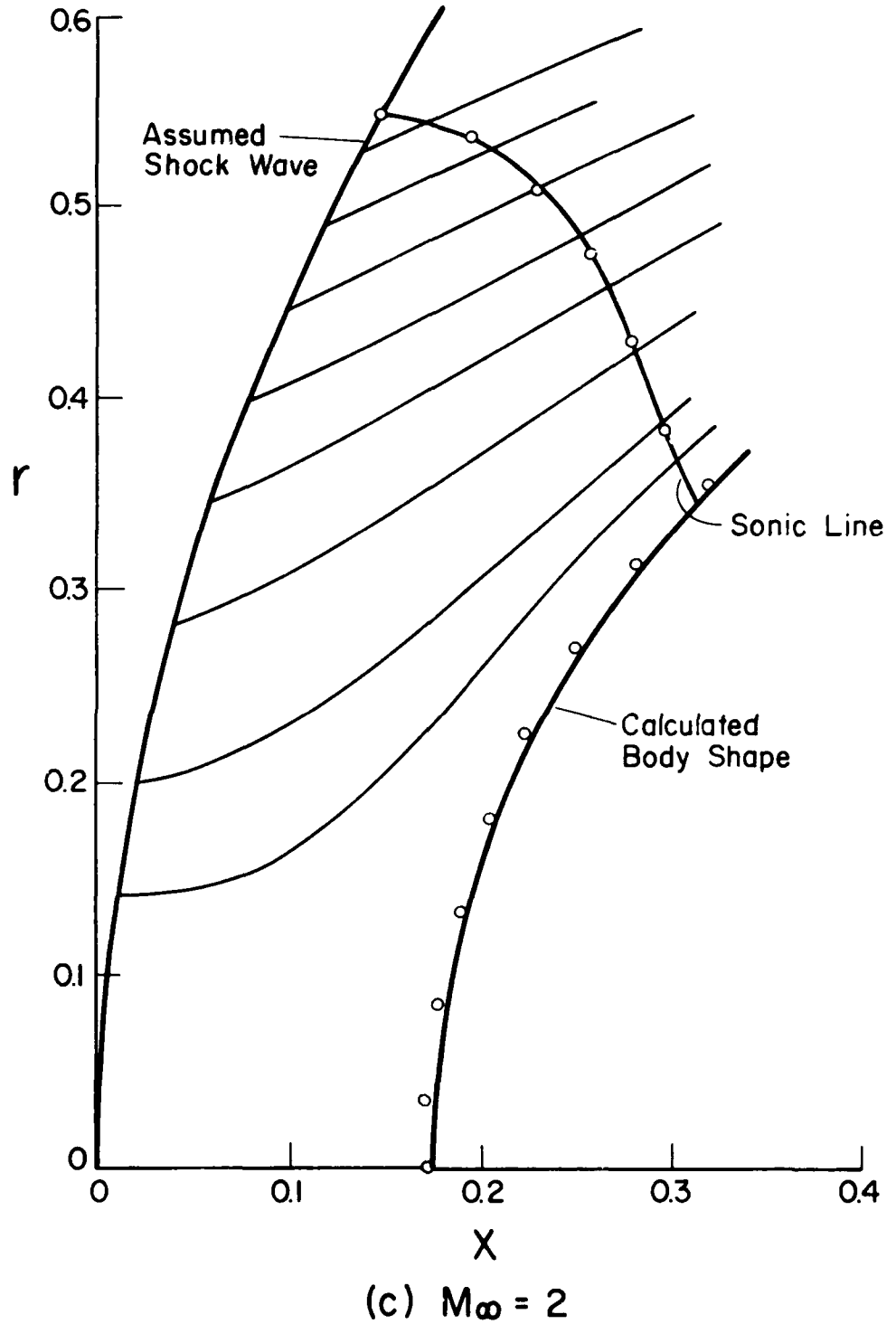

(c) $M_\infty = 2$

FIG. 2 - CONTINUED
SHOCK WAVE, SONIC LINE AND STREAMLINES FOR A SPHERE FOR PURE GAS, $\gamma = 1.4$. ○ VAN DYKE & GORDON [REF. 16].

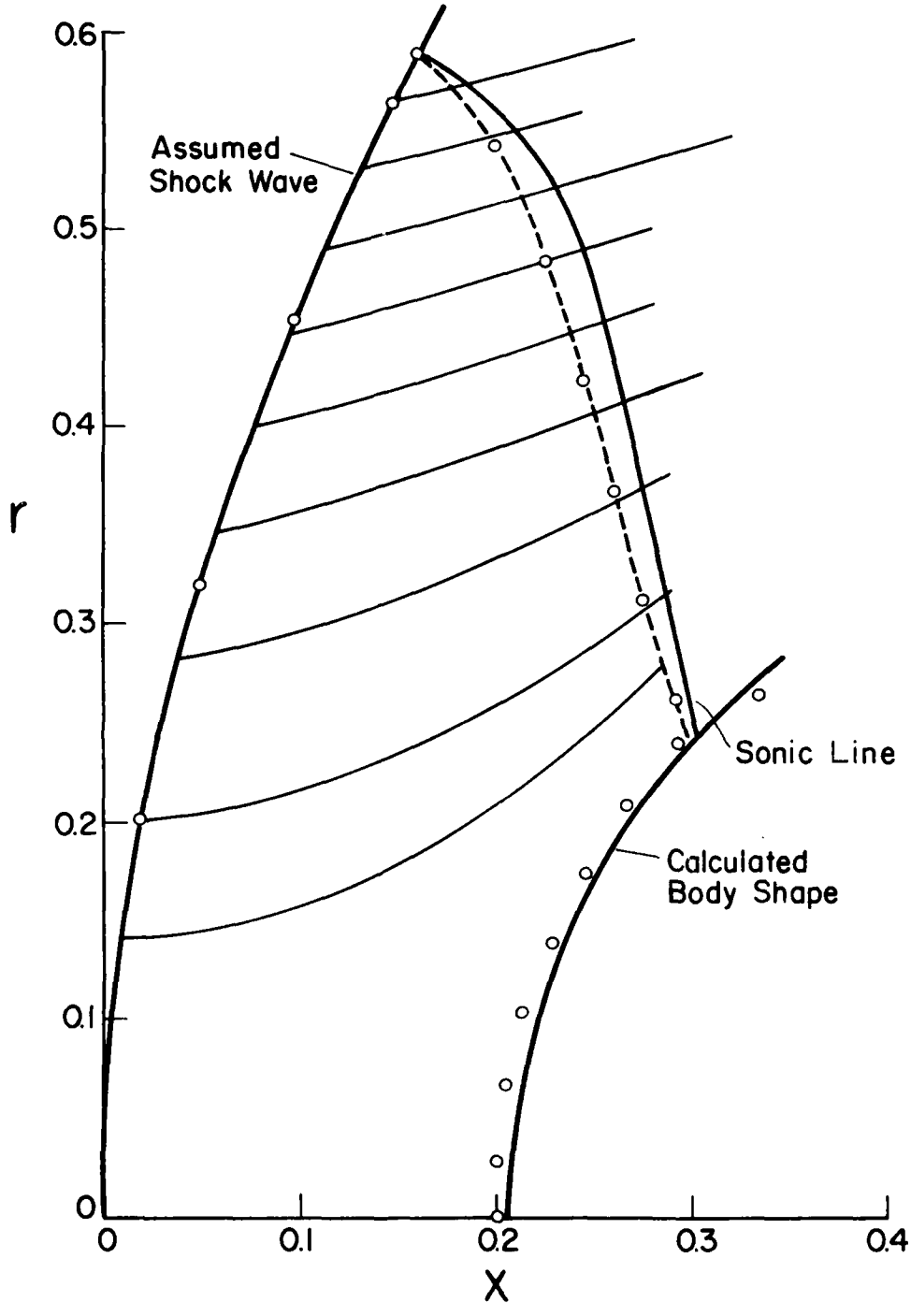

(d) $M_\infty = 1.5$

FIG. 2 - CONCLUDED
SHOCK WAVE, SONIC LINE AND STREAMLINES FOR A SPHERE FOR PURE GAS, $\gamma = 1.4$. ° VAN DYKE & GORDON [REF. 16].

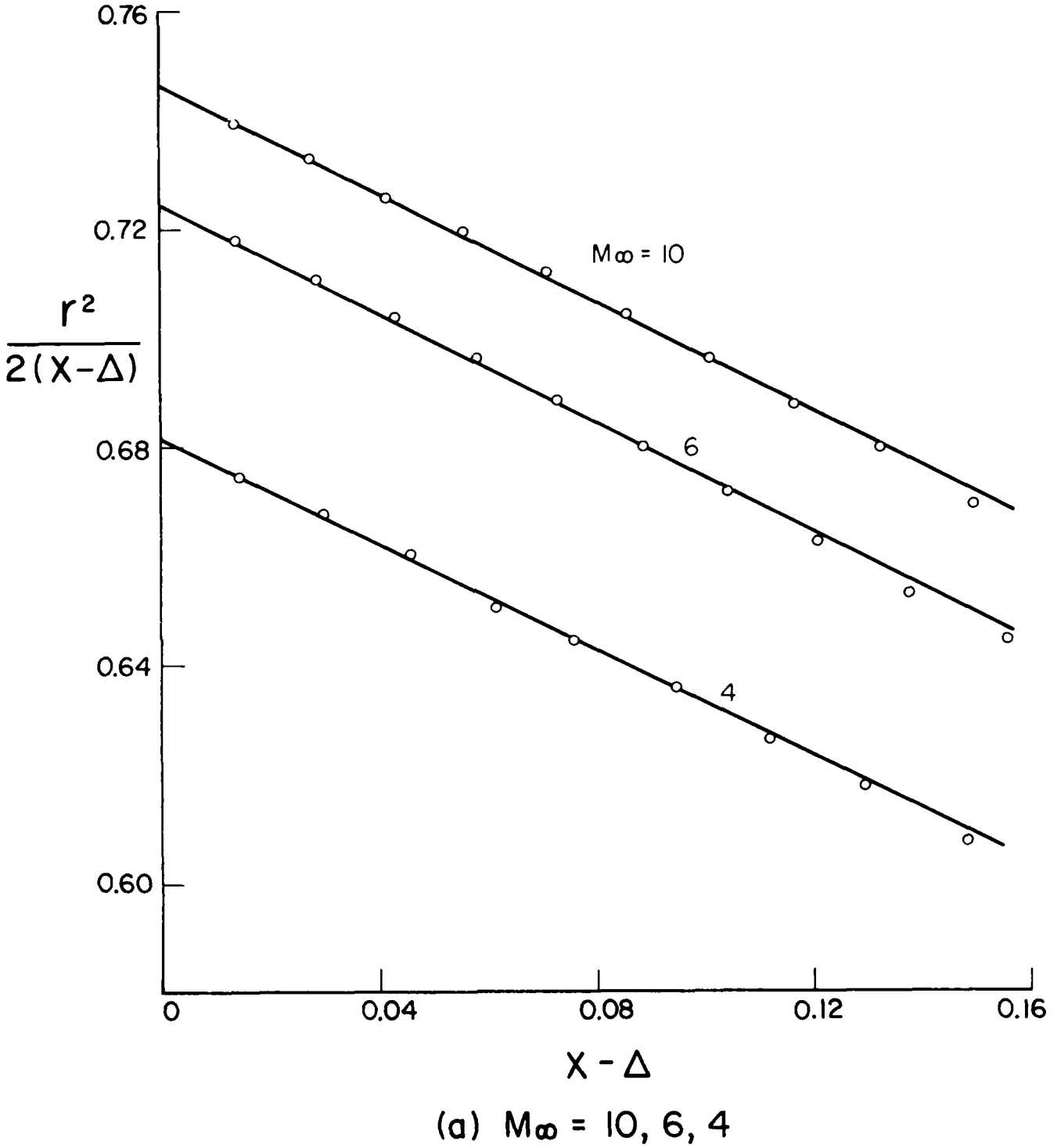

FIG. 3 RELATION BETWEEN $r^2/2(x-\Delta)$ AND $(x-\Delta)$ FOR CALCULATED BODY SHAPES. o CALCULATED POINTS.

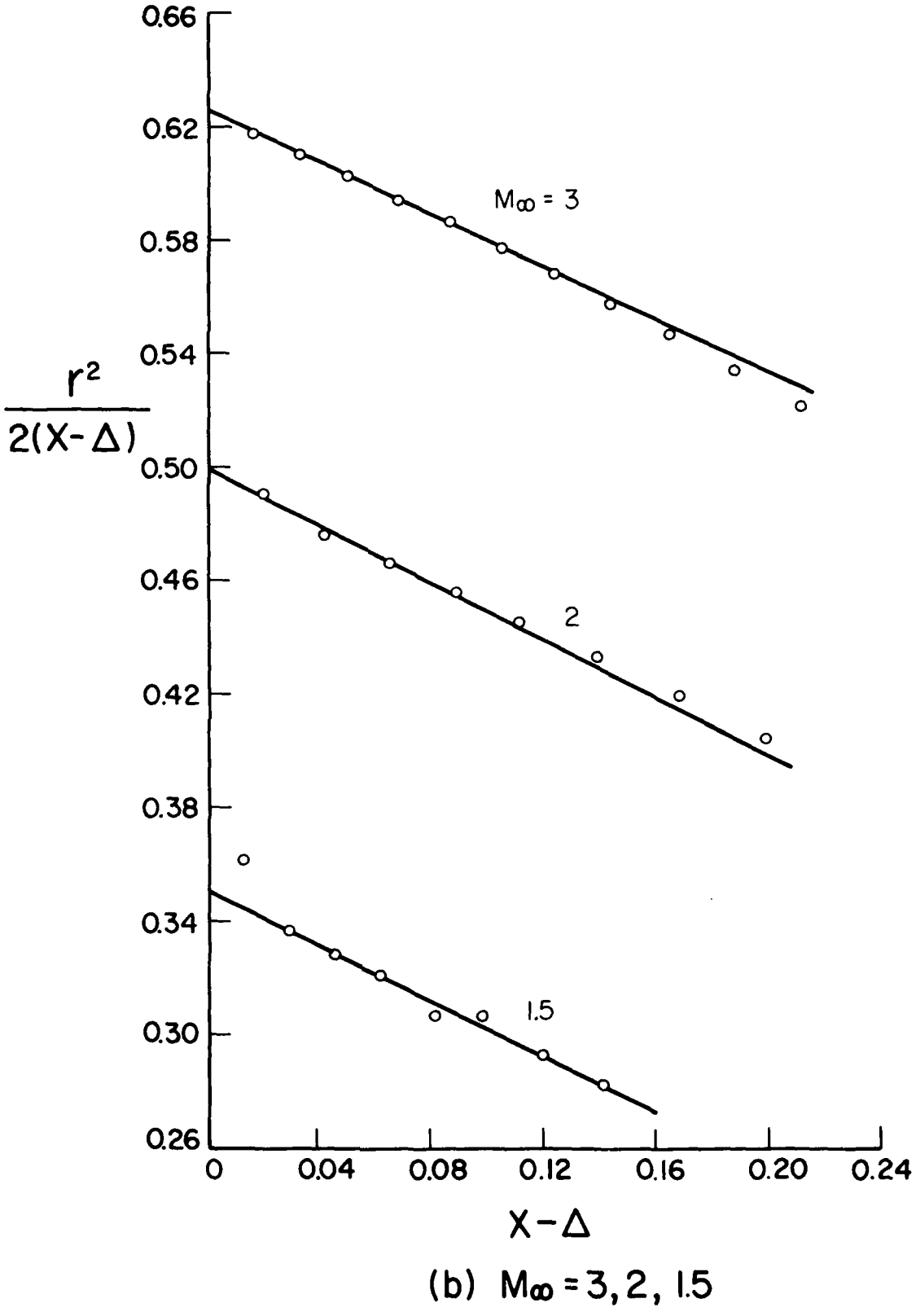

FIG. 3 - CONCLUDED
RELATION BETWEEN $r^2/(2(x-\Delta)$ AND $(x-\Delta)$ FOR CALCULATED BODY SHAPES. o CALCULATED POINTS.

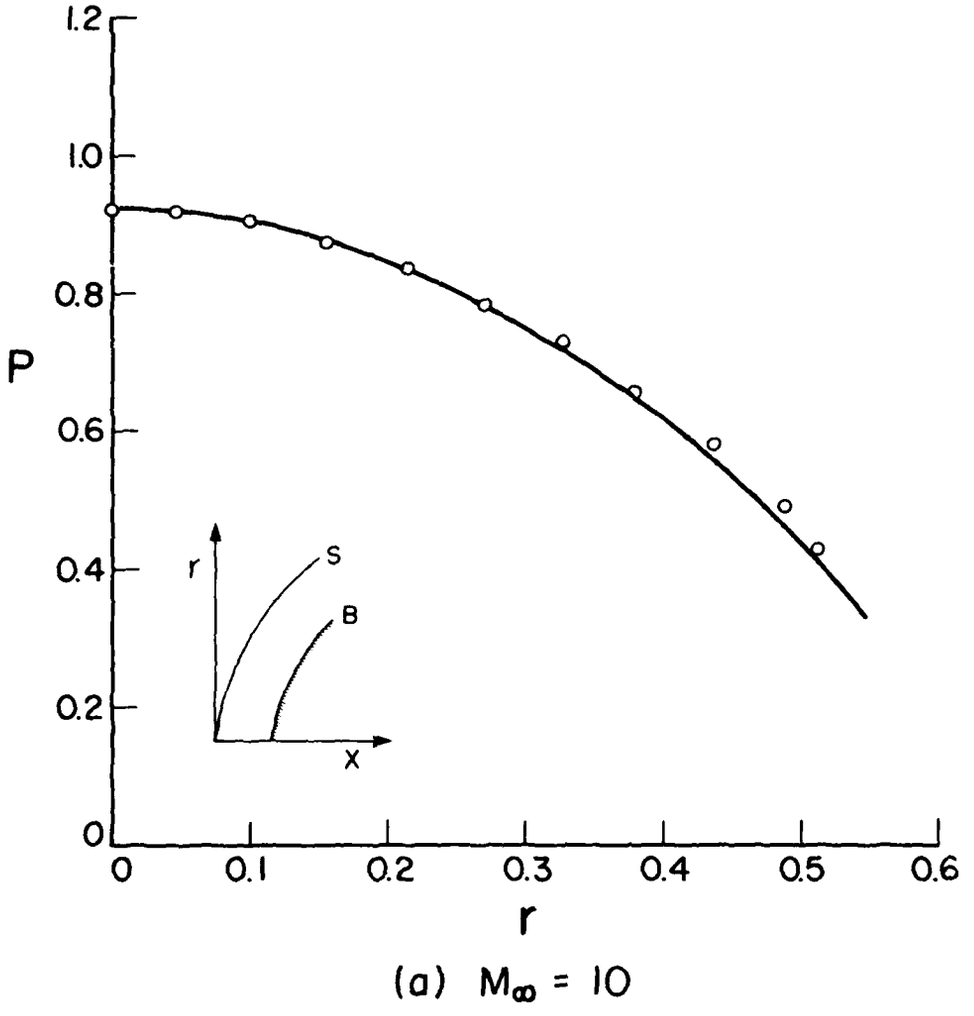

FIG. 4 PRESSURE DISTRIBUTION ON THE BODY (SPHERE) SURFACE FOR PURE GAS, $\gamma = 1.4$. ° VAN DYKE & GORDON [REF. 16].

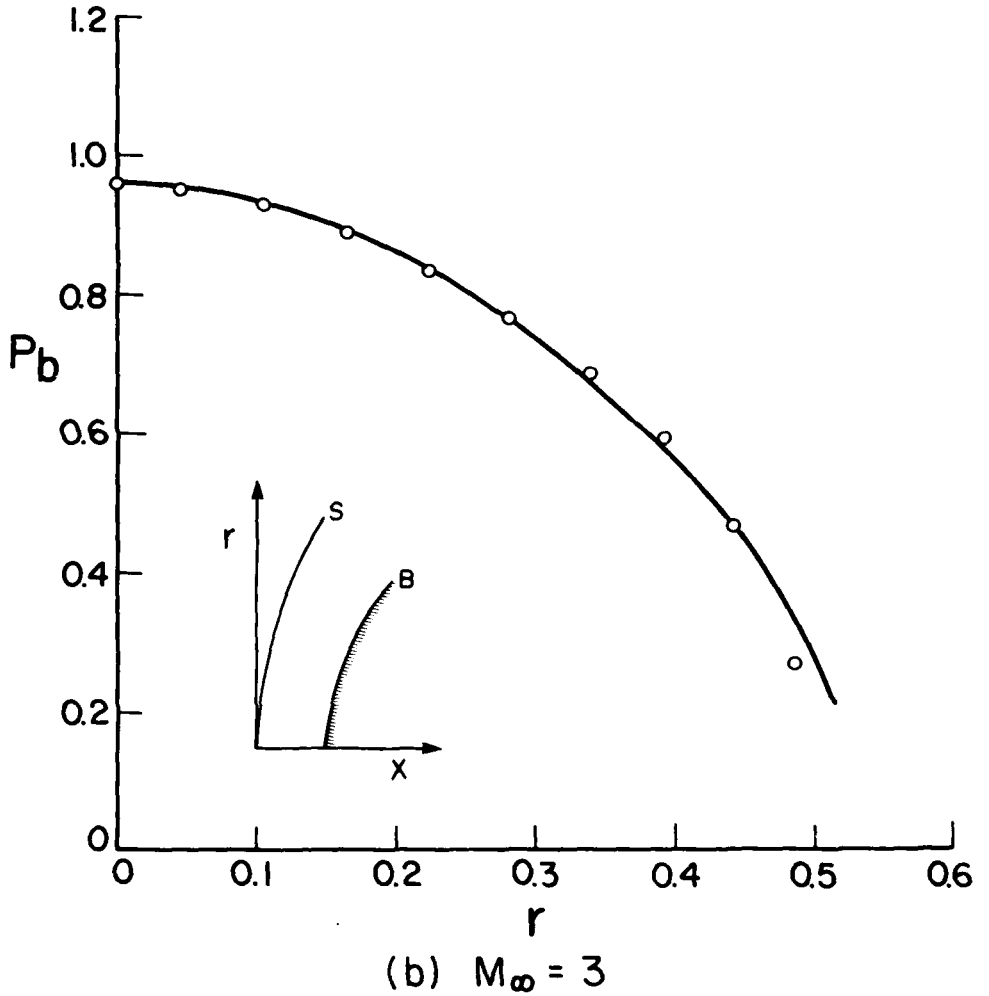

FIG. 4 - CONTINUED
PRESSURE DISTRIBUTION ON THE BODY (SPHERE) SURFACE
FOR PURE GAS, $\gamma = 1.4$. o VAN DYKE & GORDON [REF. 16].

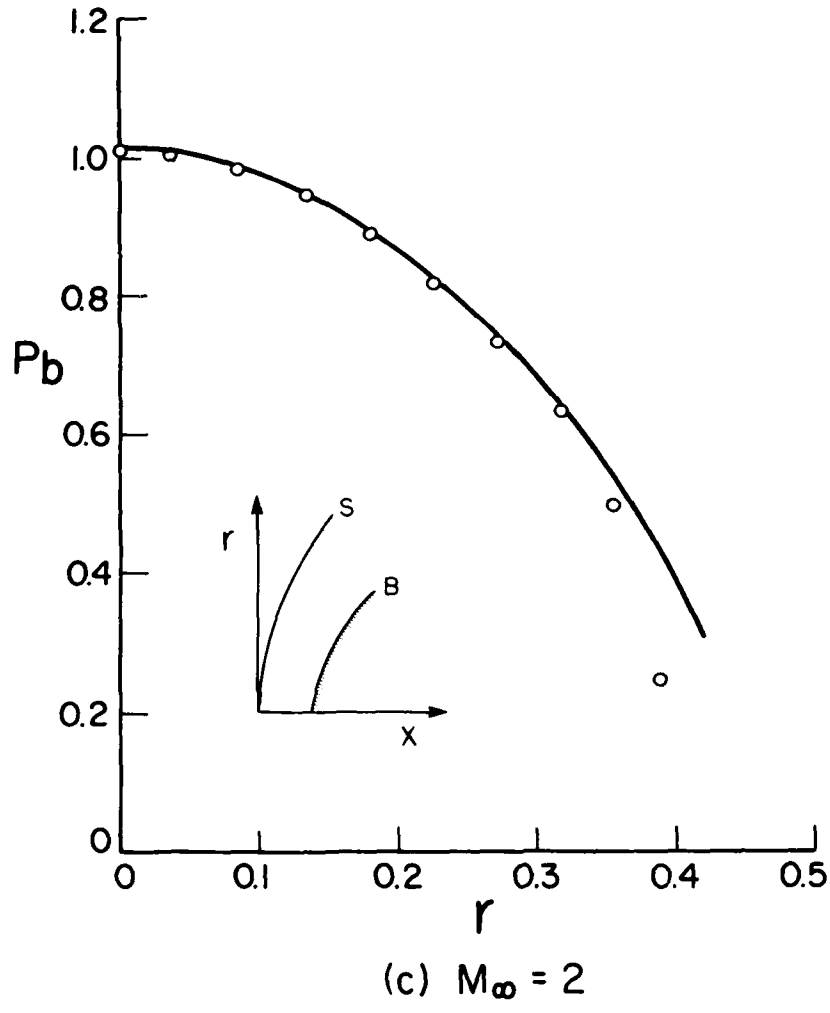

FIG. 4 - CONTINUED
PRESSURE DISTRIBUTION IN THE BODY (SPHERE) SURFACE
FOR PURE GAS, $\gamma = 1.4$. o VAN DYKE & GORDON [REF. 16].

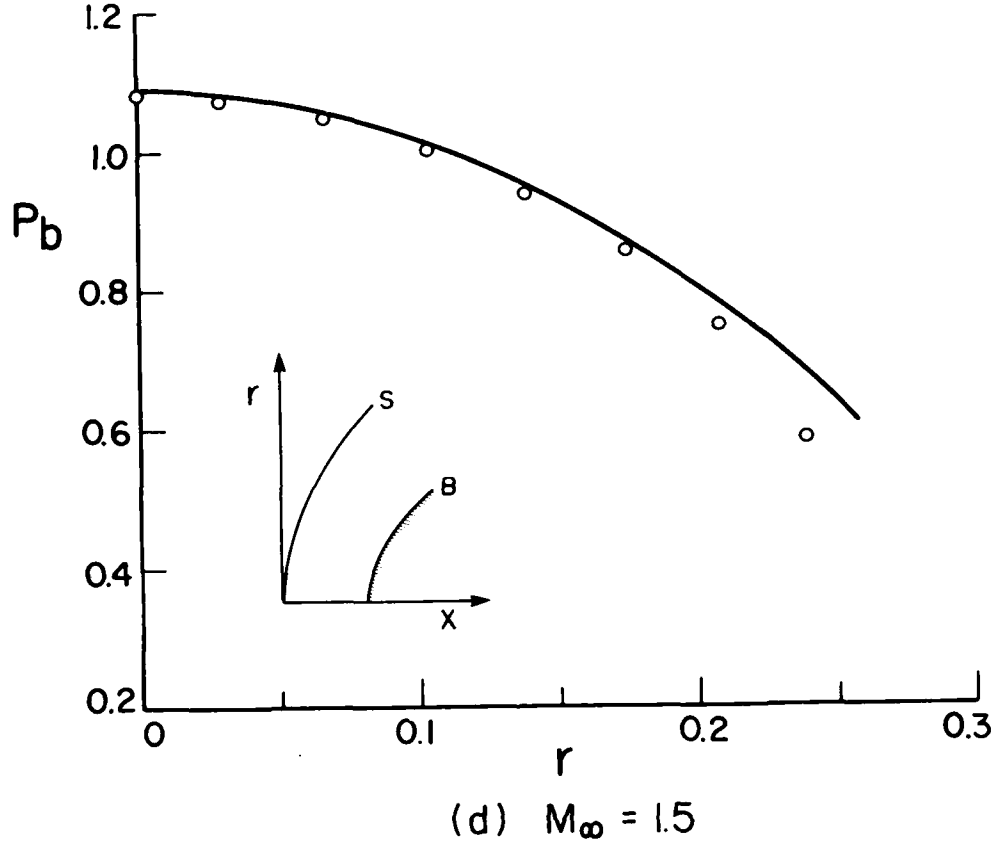

FIG. 4 - CONCLUDED
PRESSURE DISTRIBUTION ON THE BODY (SPHERE) SURFACE
FOR PURE GAS, $\gamma = 1.4$. o VAN DYKE & GORDON [REF. 16].

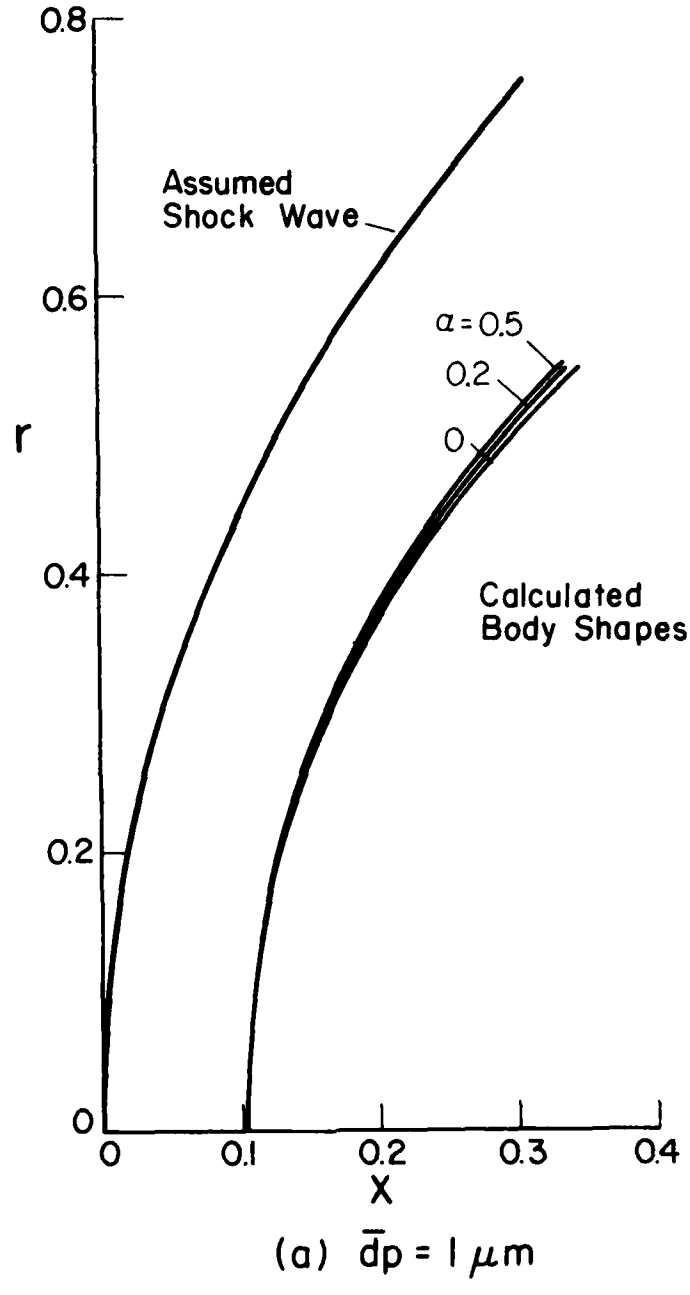

FIG. 5 ASSUMED SHOCK WAVE AND CALCULATED BODY SHAPES FOR $M_\infty = 10$, $\bar{T}_\infty = 300$ K, $\bar{p}_\infty = 101.3$ KPa AND $\bar{R}_S = 1$ CM.

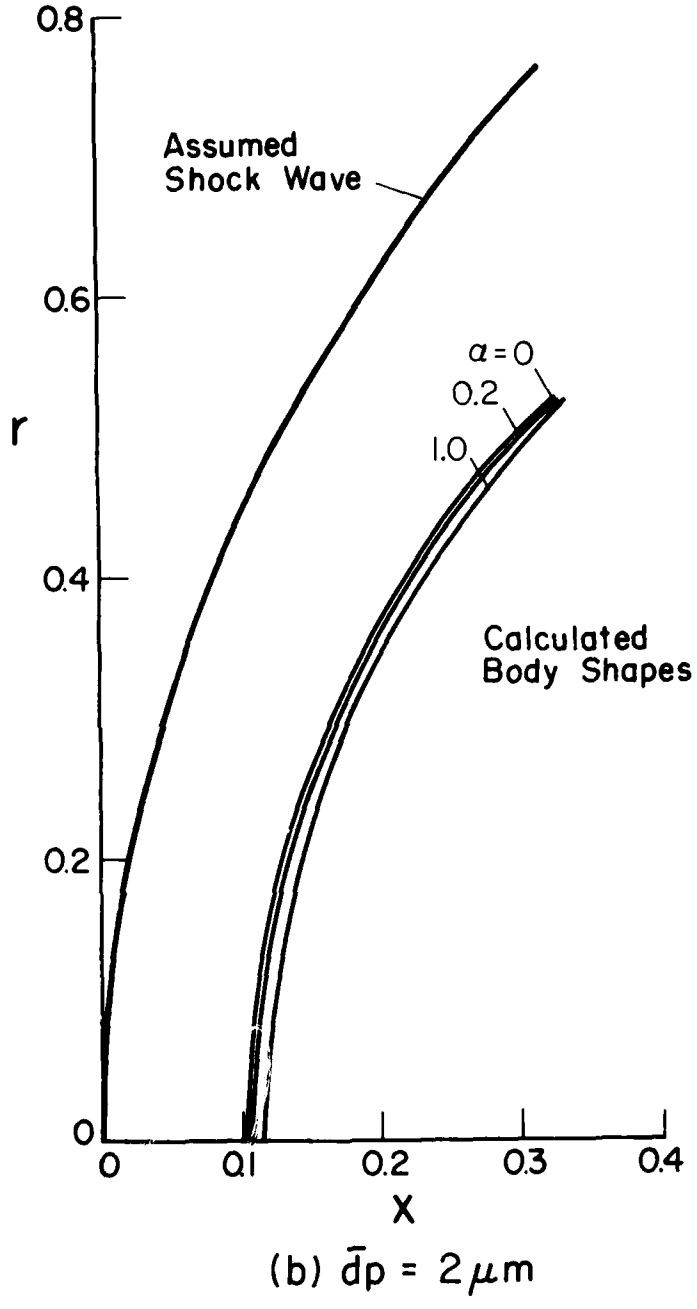

FIG. 5 - CONTINUED
ASSUMED SHOCK WAVE AND CALCULATED BODY SHAPES FOR $M_\infty = 10$, $\bar{T}_\infty = 300$ K, $\bar{p}_\infty = 101.3$ KPa AND $\bar{R}_S = 1$ CM.

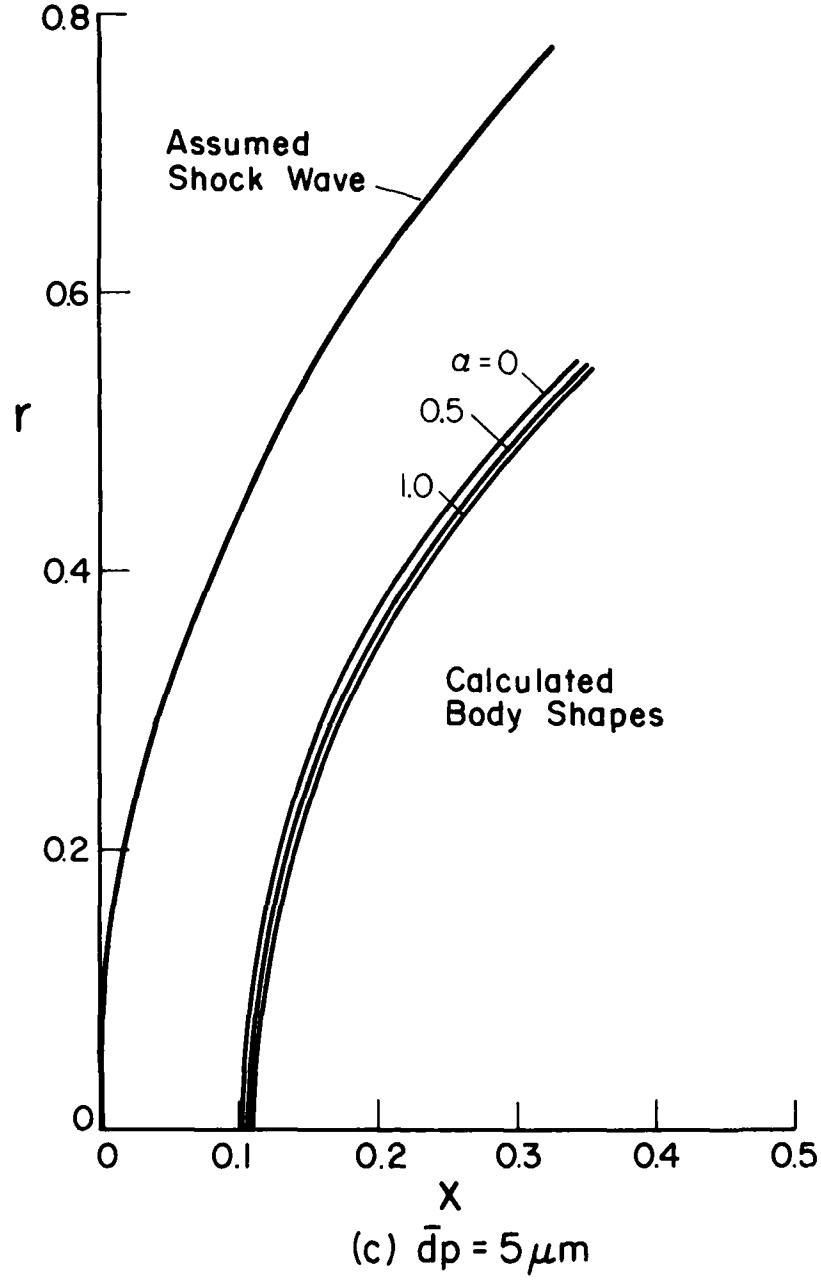

FIG. 5 - CONTINUED
ASSUMED SHOCK WAVE AND CALCULATED BODY SHAPES FOR M_∞ = 10, $\bar{T}_\infty$ = 300 K, $\bar{p}_\infty$ = 101.3 KPa AND $\bar{R}_S$ = 1 CM.

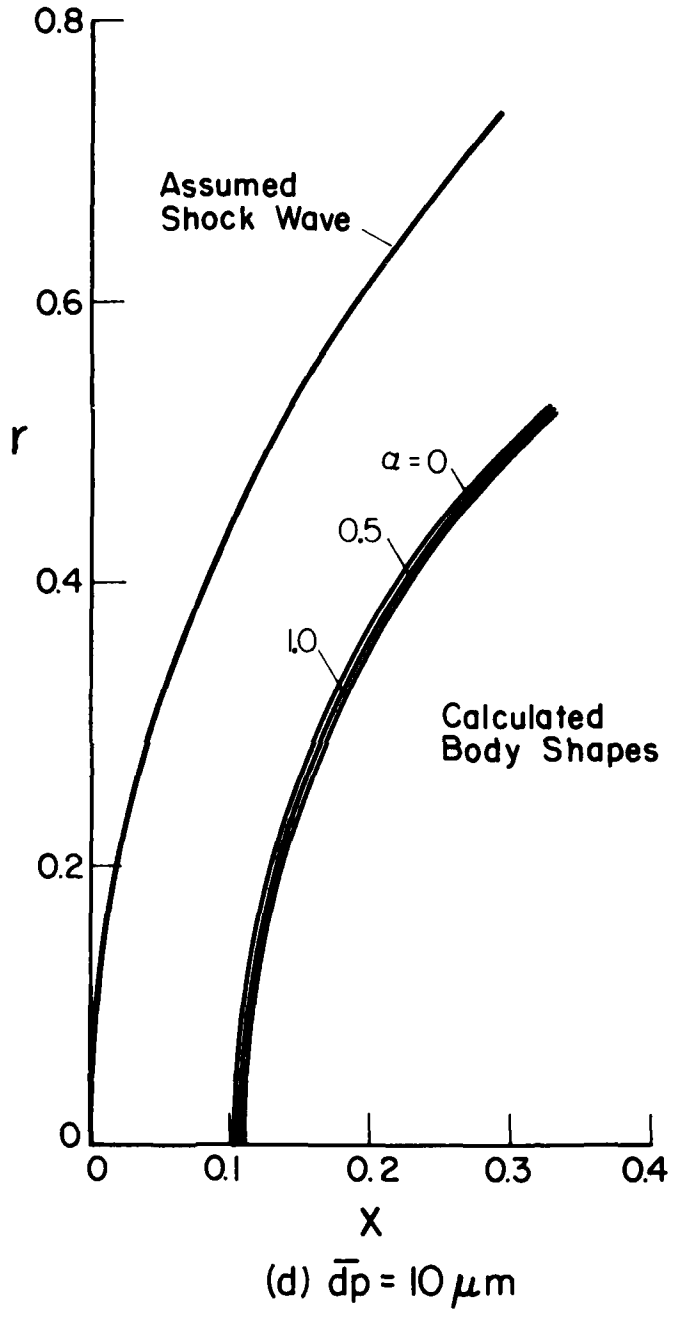

FIG. 5 - CONCLUDED
ASSUMED SHOCK WAVE AND CALCULATED BODY SHAPES FOR M_∞ = 10, $\bar{T}_\infty$ = 300 K, $\bar{p}_\infty$ = 101.3 KPa AND $\bar{R}_S$ = 1 CM.

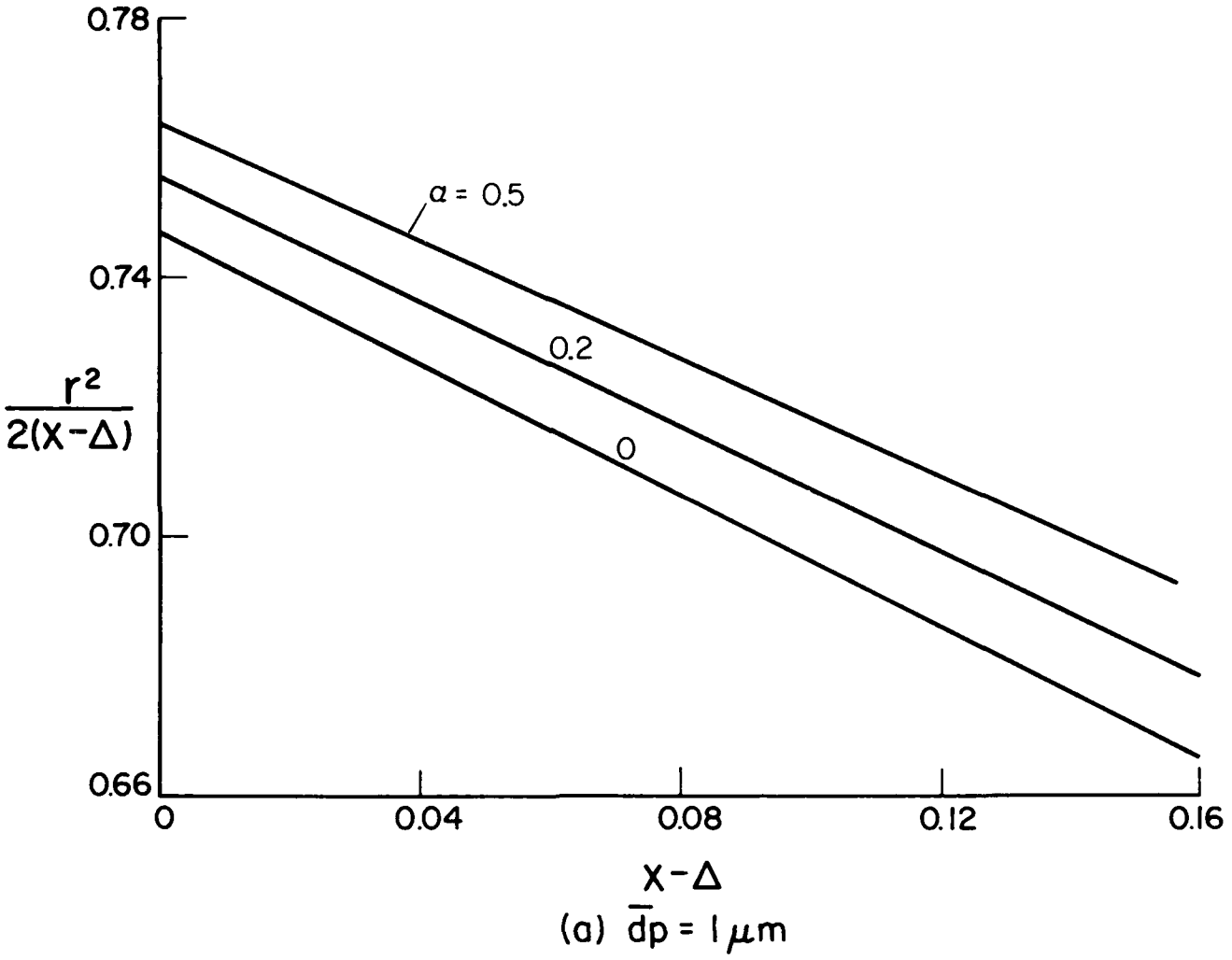

FIG. 6 RELATIONS BETWEEN $r^2/2(x-\Delta)$ AND $(x-\Delta)$ FOR CALCULATED BODIES FOR $M_\infty = 10$, $\bar{T}_\infty = 300$ K, $\bar{p}_\infty = 101.3$ KPa AND $\bar{R}_S = 1$ CM.

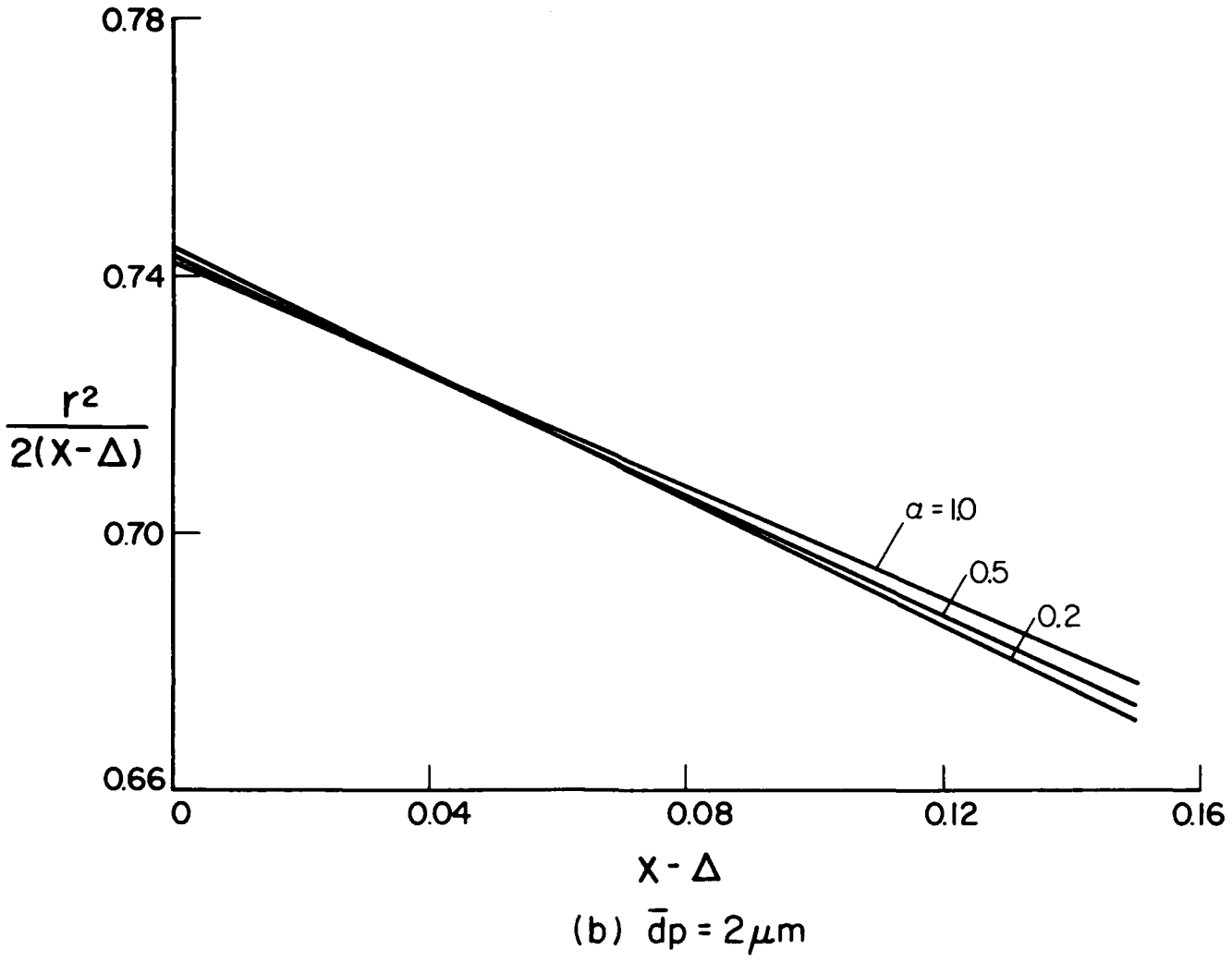

FIG. 6 - CONTINUED
RELATIONS BETWEEN $r^2/2(x-\Delta)$ AND $(x-\Delta)$ FOR CALCULATED BODIES FOR $M_\infty = 10$, $\bar{T}_\infty = 300$ K, $p_\infty = 101.3$ KPa AND $\bar{R}_S = 1$ CM.

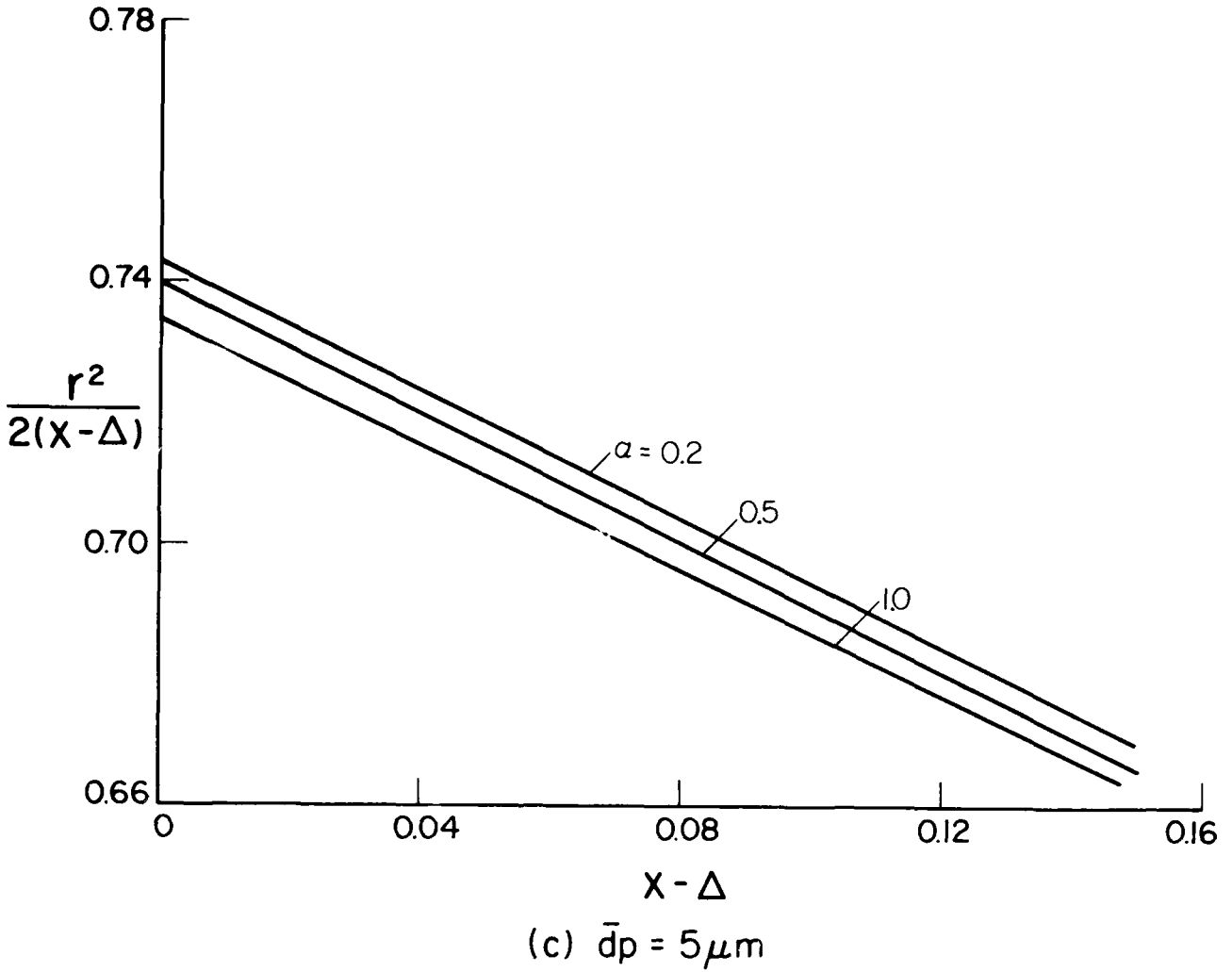

FIG. 6 - CONTINUED
RELATIONS BETWEEN $r^2/2(x-\Delta)$ AND $(x-\Delta)$ FOR CALCULATED BODIES FOR $M_\infty = 10$, $\bar{T}_\infty = 300$ K, $\bar{p}_\infty = 101.3$ KPa AND $\bar{R}_S = 1$ CM.

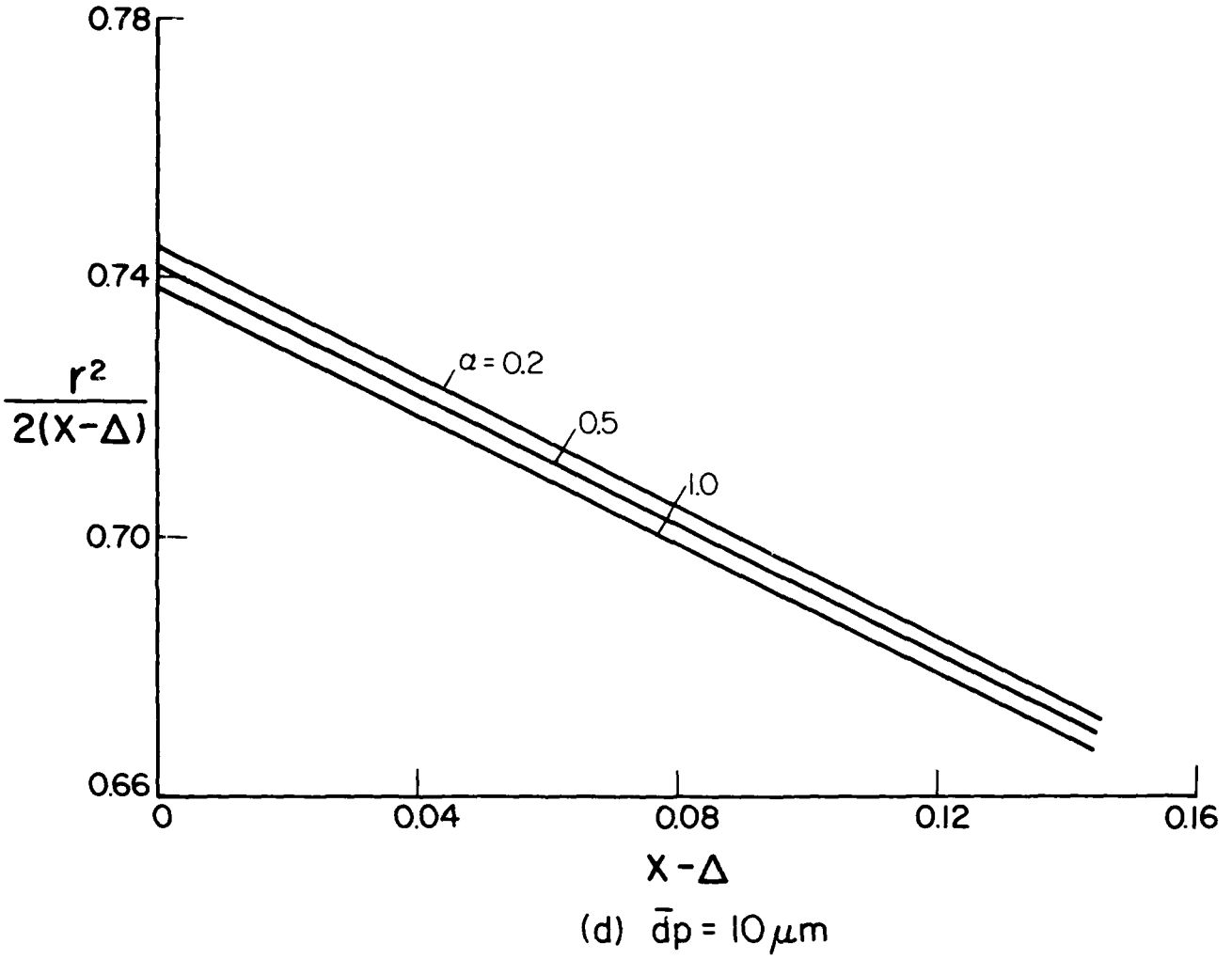

FIG. - CONCLUDED
RELATIONS BETWEEN $r^2/2(x-\Delta)$ AND $(x-\Delta)$ FOR CALCULATED BODIES FOR $M_\infty = 10$, $\bar{T}_\infty = 300$ K, $\bar{p}_\infty = 101.3$ KPa AND $\bar{R}_e = 1$ CM.

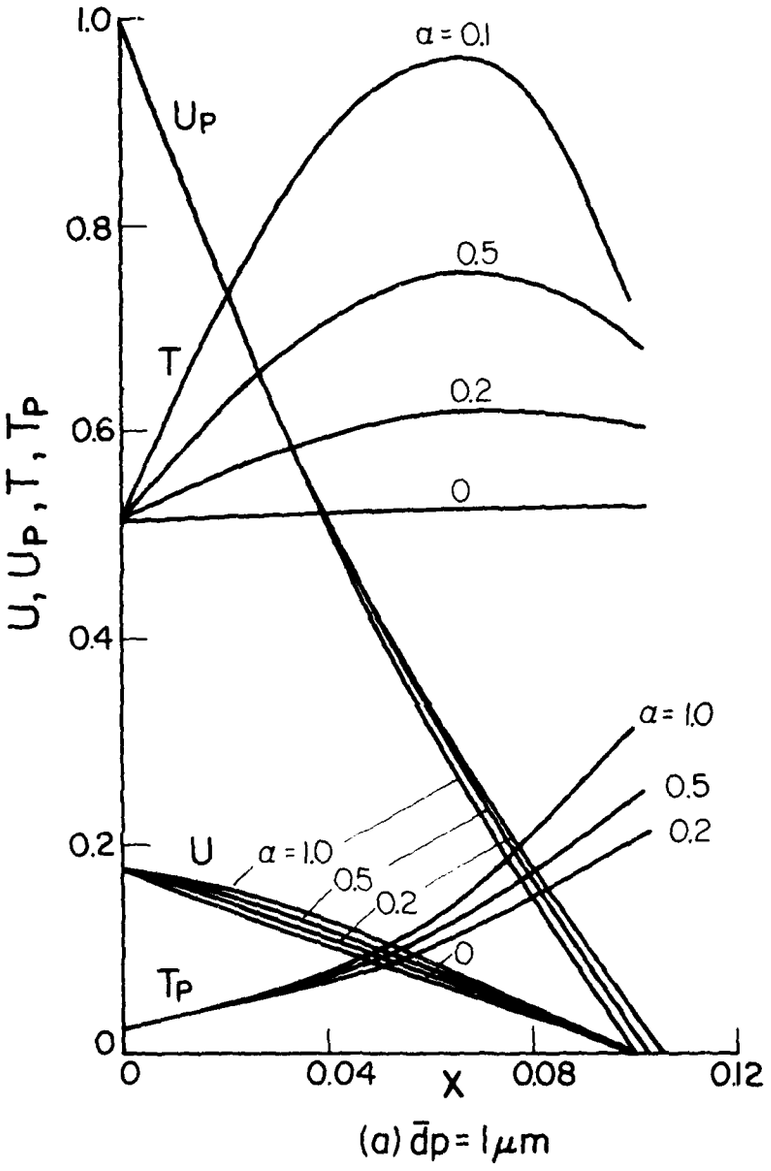

FIG. 7 VARIATION OF GAS AND PARTICLE VELOCITY AND TEMPERATURE WITH LOADING RATIO α ALONG STAGNATION STREAMLINES FOR $M_\infty = 10$, $\bar{T}_\infty = 300$ K, $\bar{p}_\infty = 101.3$ KPa AND $\bar{R}_S = 1$ CM.

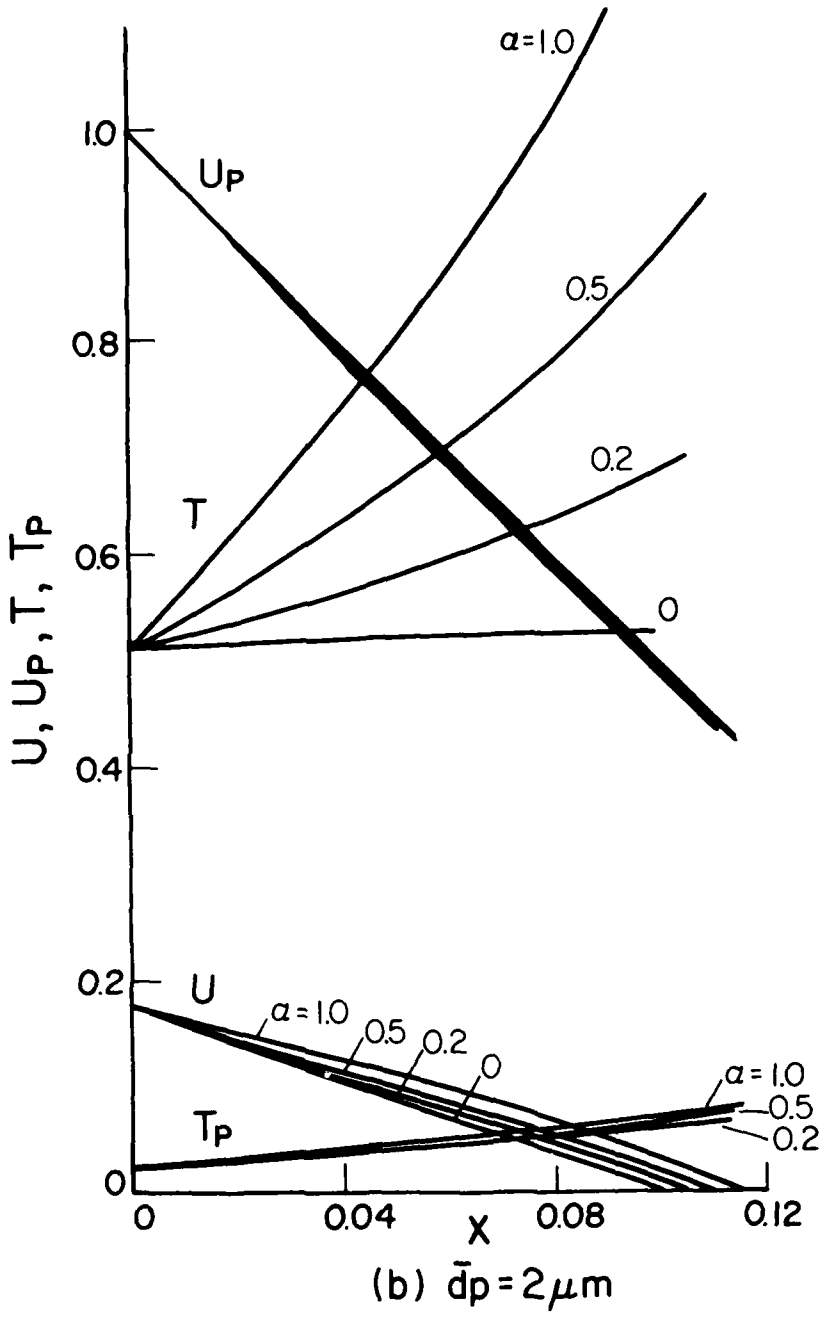

FIG. 7 - CONTINUED
VARIATION OF GAS AND PARTICLE VELOCITY AND TEMPERATURE WITH LOADING RATIO α ALONG STAGNATION STREAMLINES FOR M_∞ = 10, $\bar{T}_\infty$ = 300 K, $\bar{p}_\infty$ = 101.3 KPa AND $\bar{R}_S$ = 1 CM.

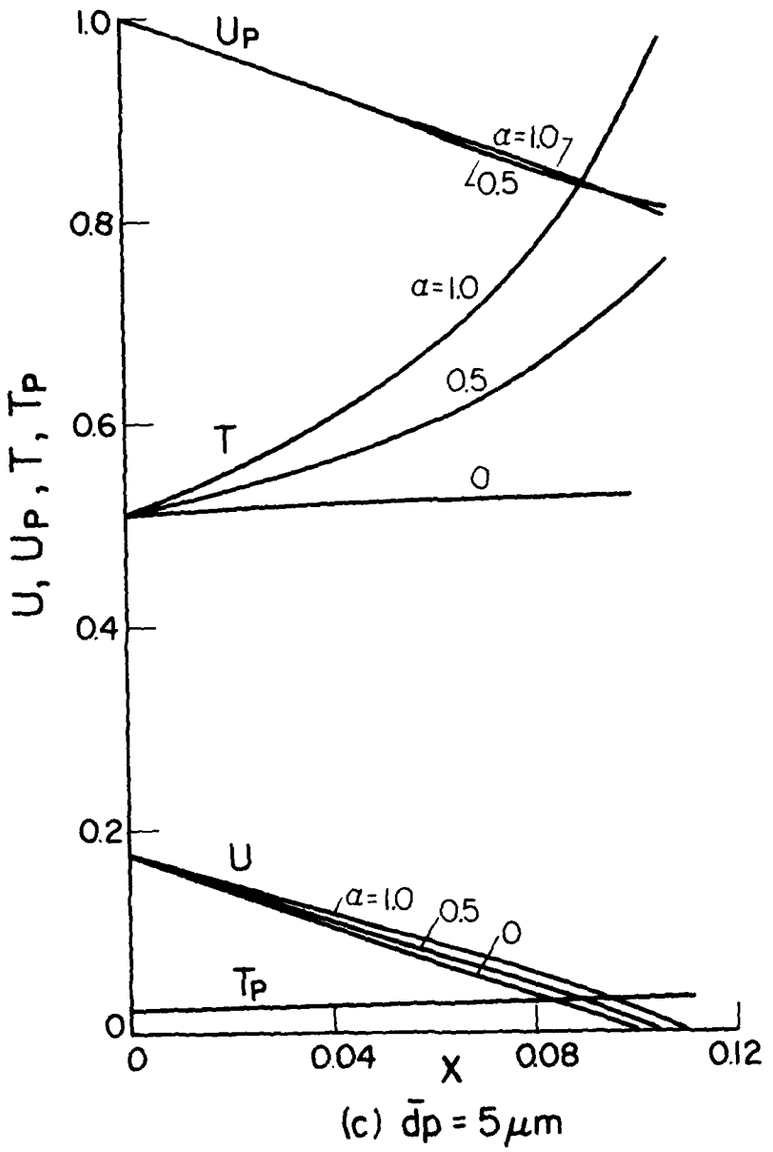

FIG. 7 - CONTINUED
VARIATION OF GAS AND PARTICLE VELOCITY AND TEMPERATURE WITH LOADING RATIO α ALONG STAGNATION STREAMLINES FOR $M_\infty = 10$, $\bar{T}_\infty = 300$ K, $\bar{p}_\infty = 101.3$ KPa AND $\bar{R}_S = 1$ CM.

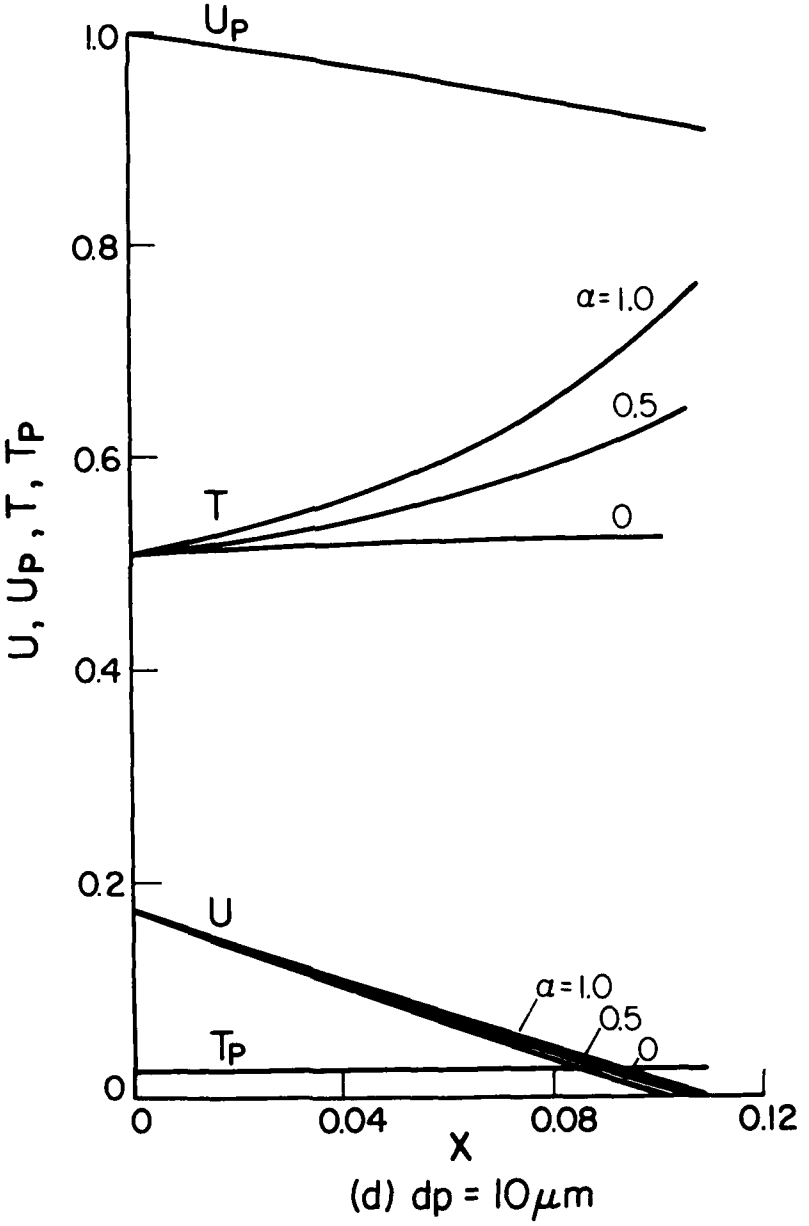

FIG. 7 - CONCLUDED
VARIATION OF GAS AND PARTICLE VELOCITY AND TEMPERATURE WITH LOADING RATIO α ALONG STAGNATION STREAMLINES FOR M_∞ = 10, $\bar{T}_\infty$ = 300 K, $\bar{p}_\infty$ = 101.3 KPa AND $\bar{R}_S$ = 1 CM.

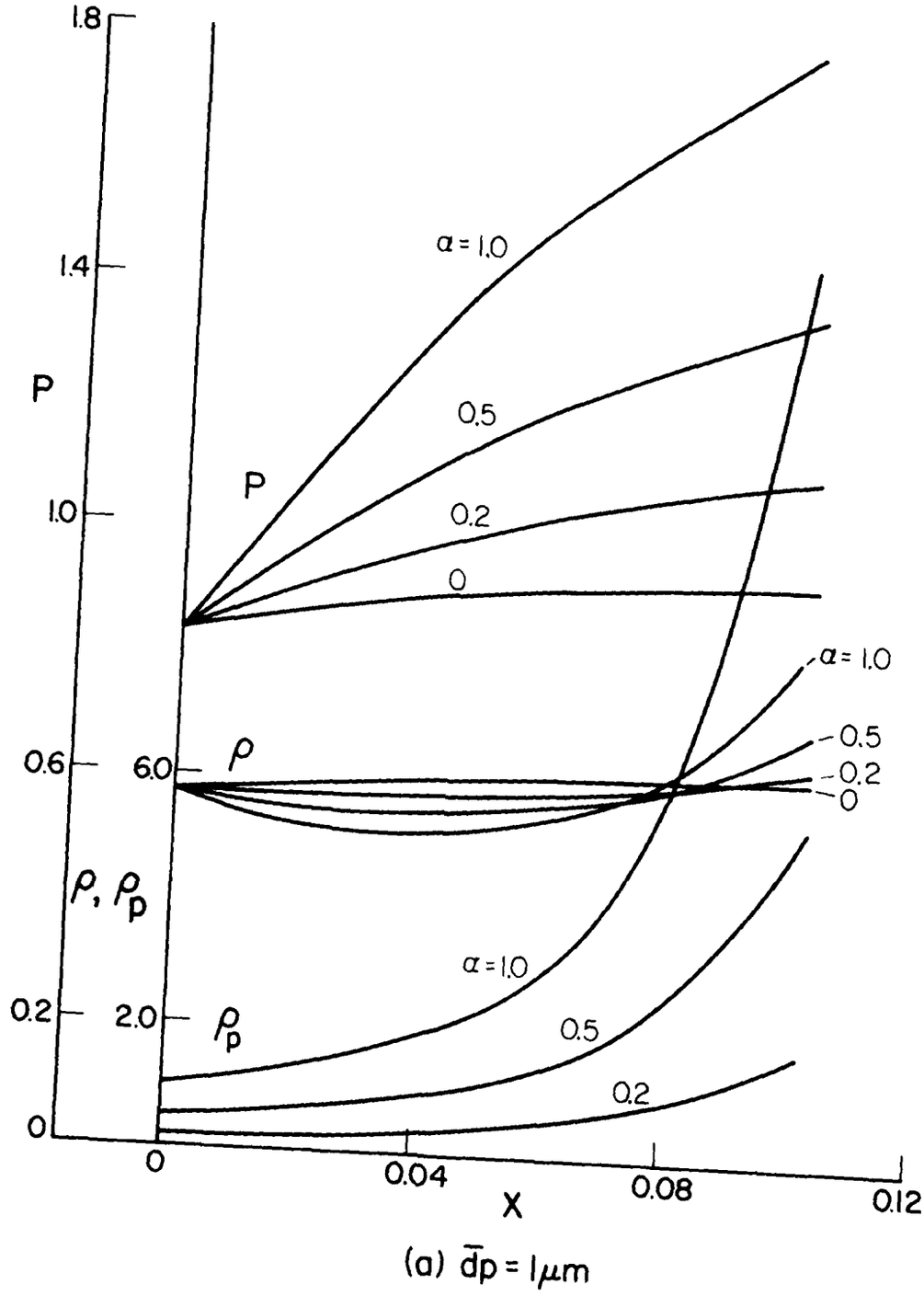

(a) $\bar{d}p = 1\mu m$

FIG. 8 VARIATION OF GAS AND PARTICLE DENSITIES, AND GAS PRESSURE ALONG STAGNATION STREAMLINES FOR $M_\infty = 10$, $\bar{T}_\infty = 300$ K, $\bar{p}_\infty = 101.3$ KPa AND $\bar{R}_S = 1$ CM.

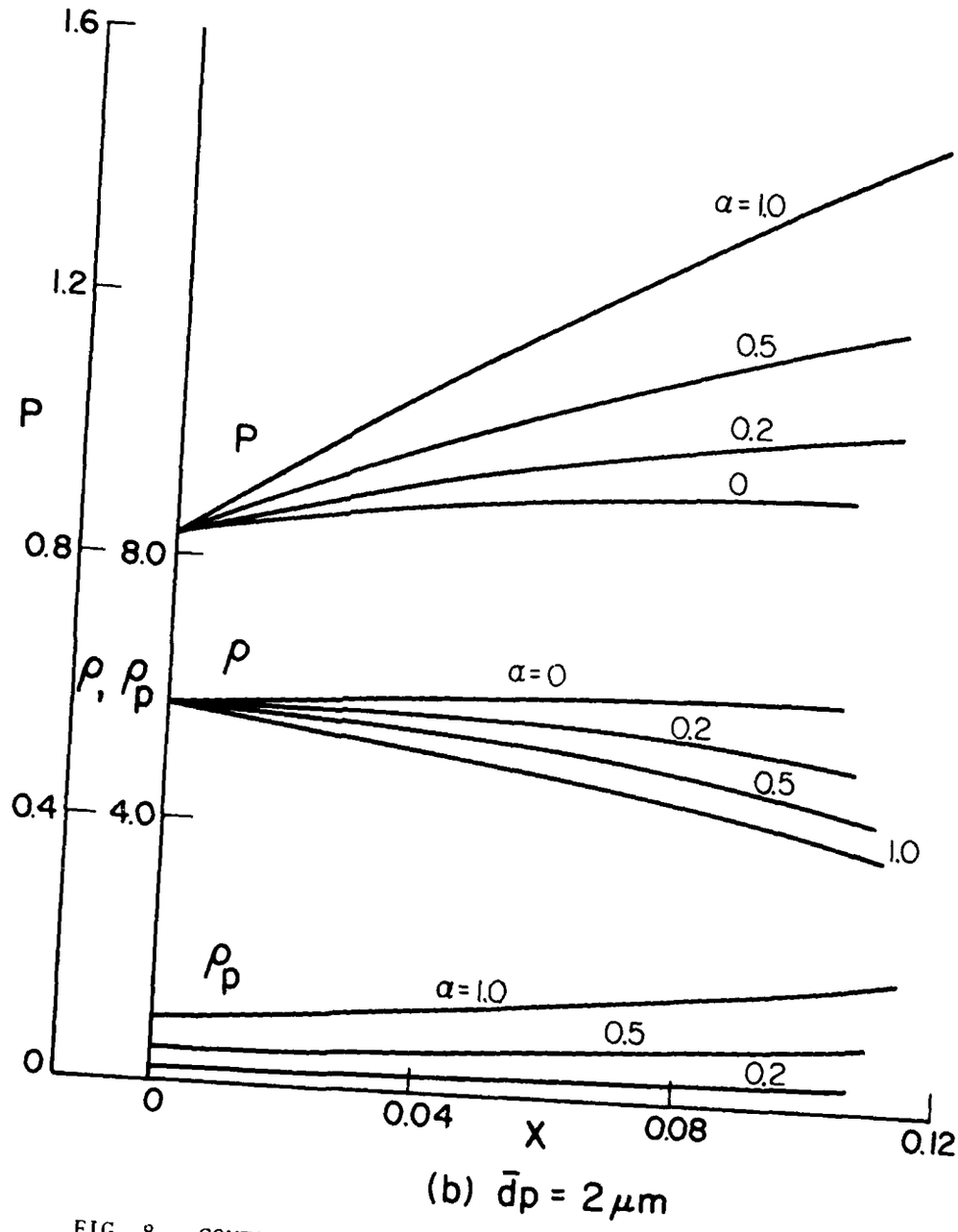

FIG. 8 - CONTINUED
VARIATION OF GAS AND PARTICLE DENSITIES, AND GAS PRESSURE ALONG STAGNATION STREAMLINES FOR M_∞ = 10, $\bar{T}_\infty$ = 300 K, P_∞ = 101.3 KPa AND $\bar{R}_s$ = 1 CM.

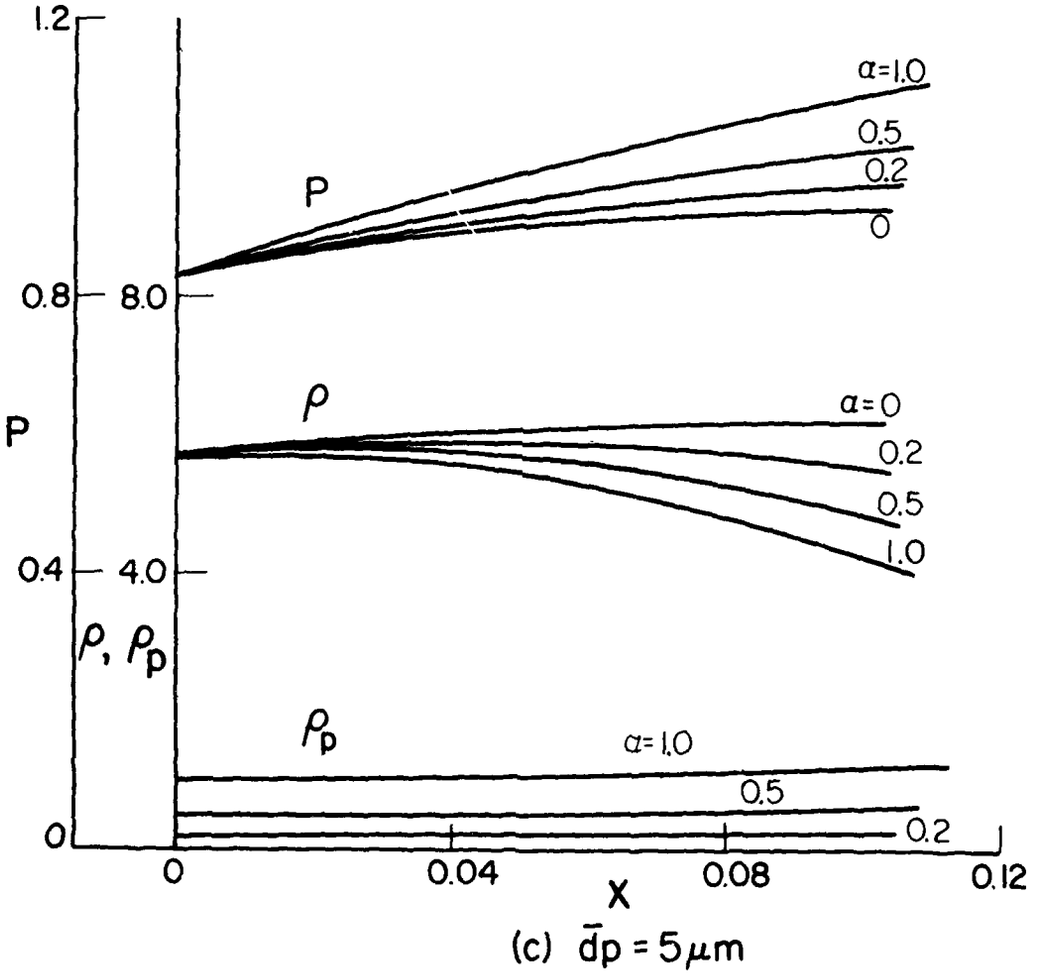

FIG. 8 - CONTINUED
VARIATION OF GAS AND PARTICLE DENSITIES, AND GAS PRESSURE ALONG STAGNATION STREAMLINES FOR M_∞ = 10, $\tilde{T}_\infty$ = 300 K, $\tilde{p}_\infty$ = 101.3 KPa AND $\tilde{R}s$ = 1 CM.

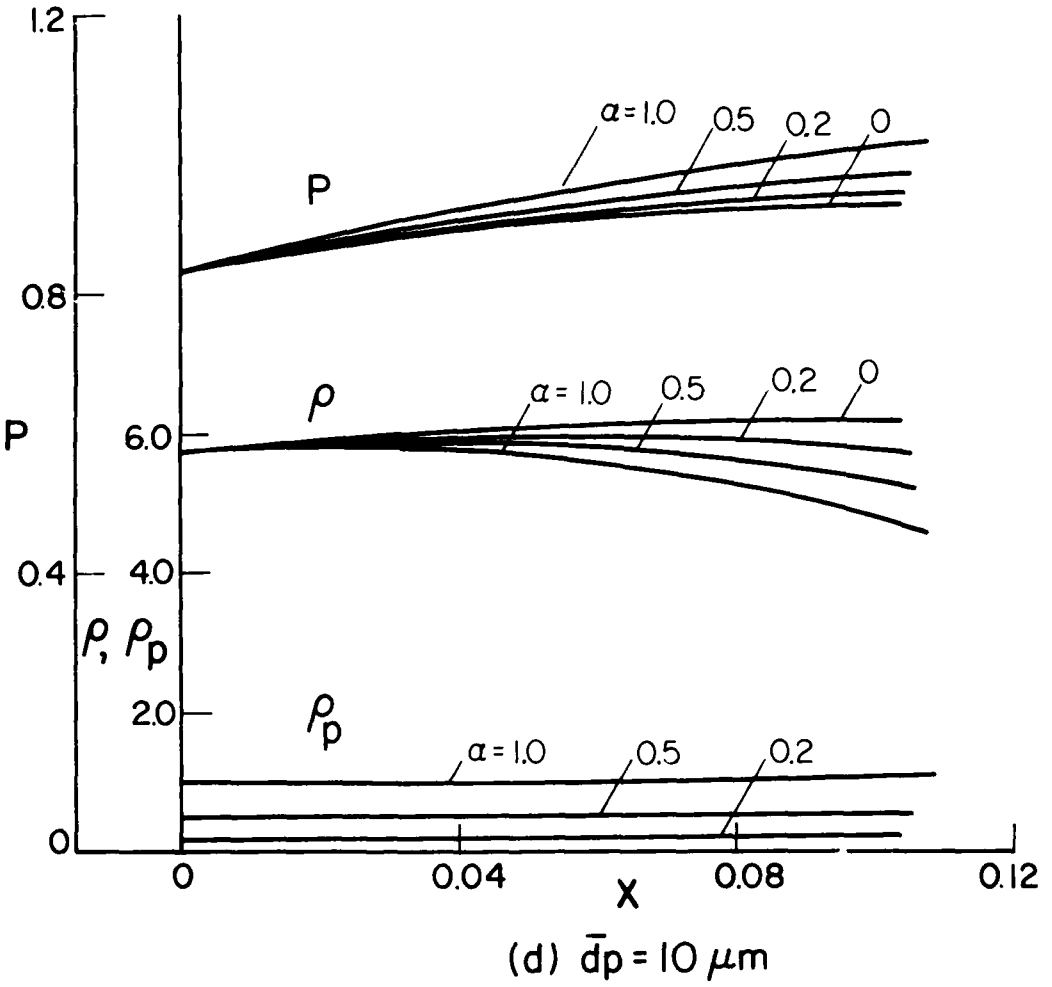

FIG. 8 - CONCLUDED
VARIATION OF GAS AND PARTICLE DENSITIES, AND GAS PRESSURE ALONG STAGNATION STREAMLINES FOR M_∞ = 10, $\bar{T}_\infty$ = 300 K, $\bar{p}_\infty$ = 101.3 KPa AND $\bar{R}_S$ = 1 CM.

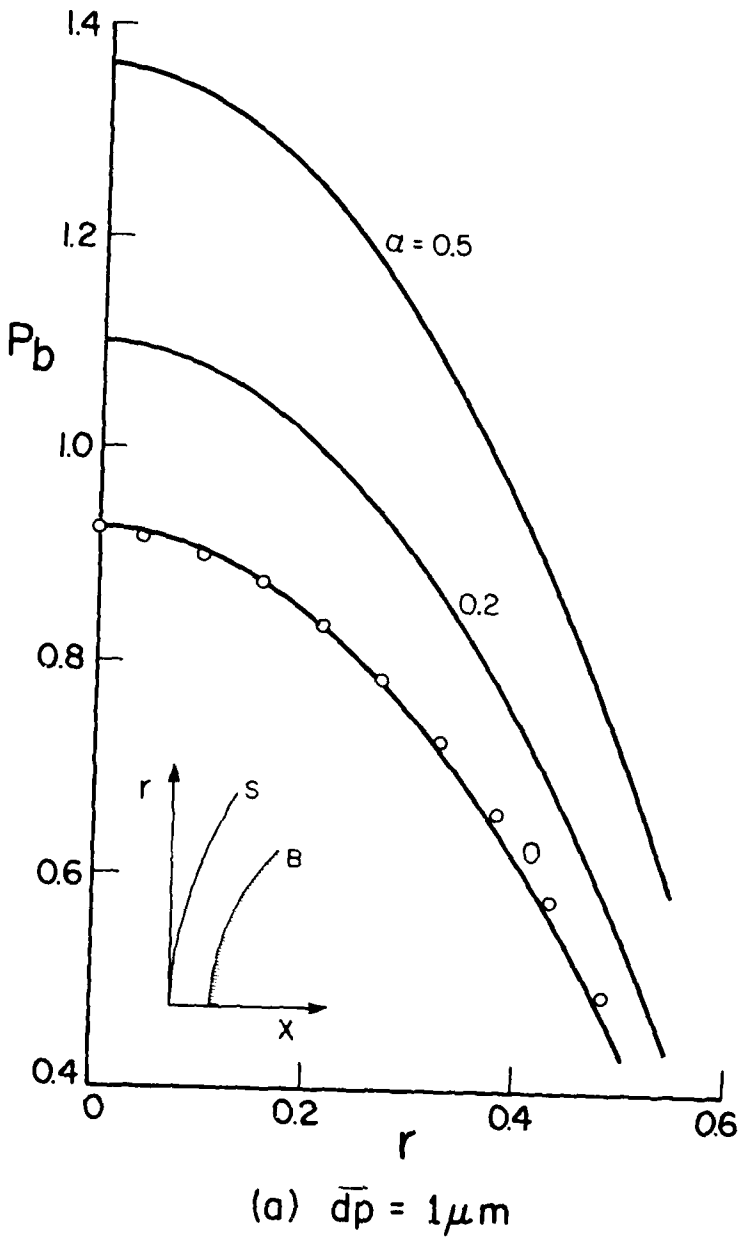

FIG. 9 PRESSURE DISTRIBUTIONS ON BODY SURFACE FOR $M_\infty = 10$, $\bar{T}_\infty = 300$ K, $\bar{p}_\infty = 101.3$ KPa AND $\bar{R}_S = 1$ CM. o VAN DYKE & GORDON [REF. 16].

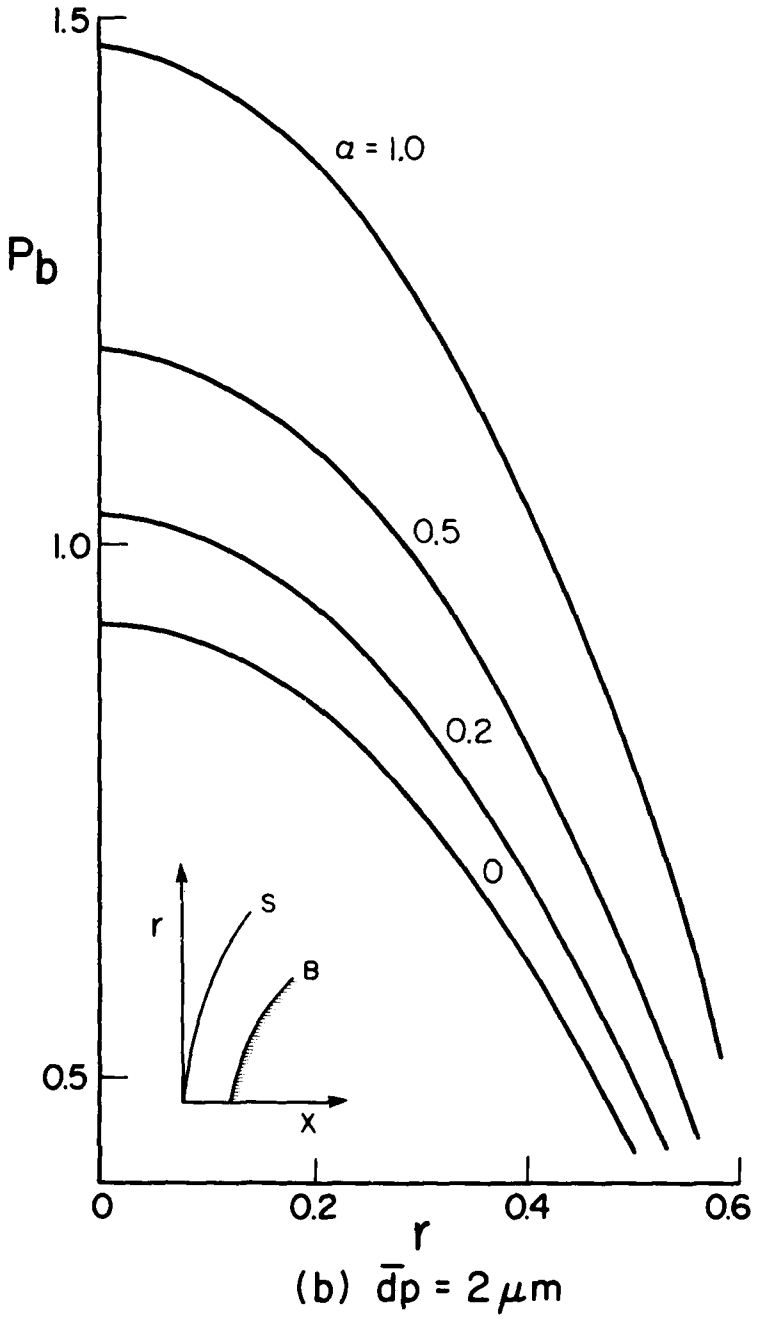

FIG. 9 - CONTINUED
PRESSURE DISTRIBUTIONS ON BODY SURFACE FOR M_∞ = 10, $\bar{T}_\infty$ = 300 K, $\bar{p}_\infty$ = 101.3 KPa AND $\bar{R}_S$ = 1 CM.

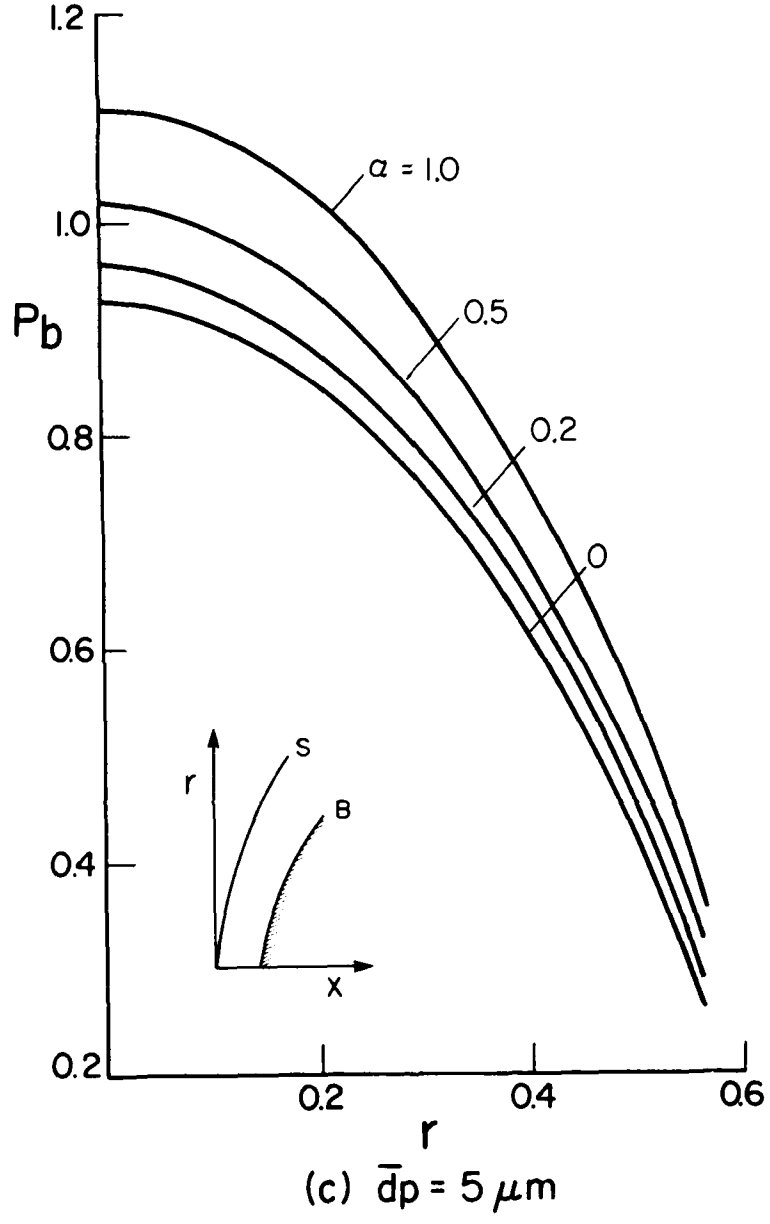

(c) $\bar{d}p = 5\,\mu m$

FIG. 9 - CONTINUED
PRESSURE DISTRIBUTIONS ON BODY SURFACE FOR $M_\infty = 10$, $\bar{T}_\infty = 300$ K, $\bar{p}_\infty = 101.3$ KPa AND $\bar{R}_S = 1$ CM.

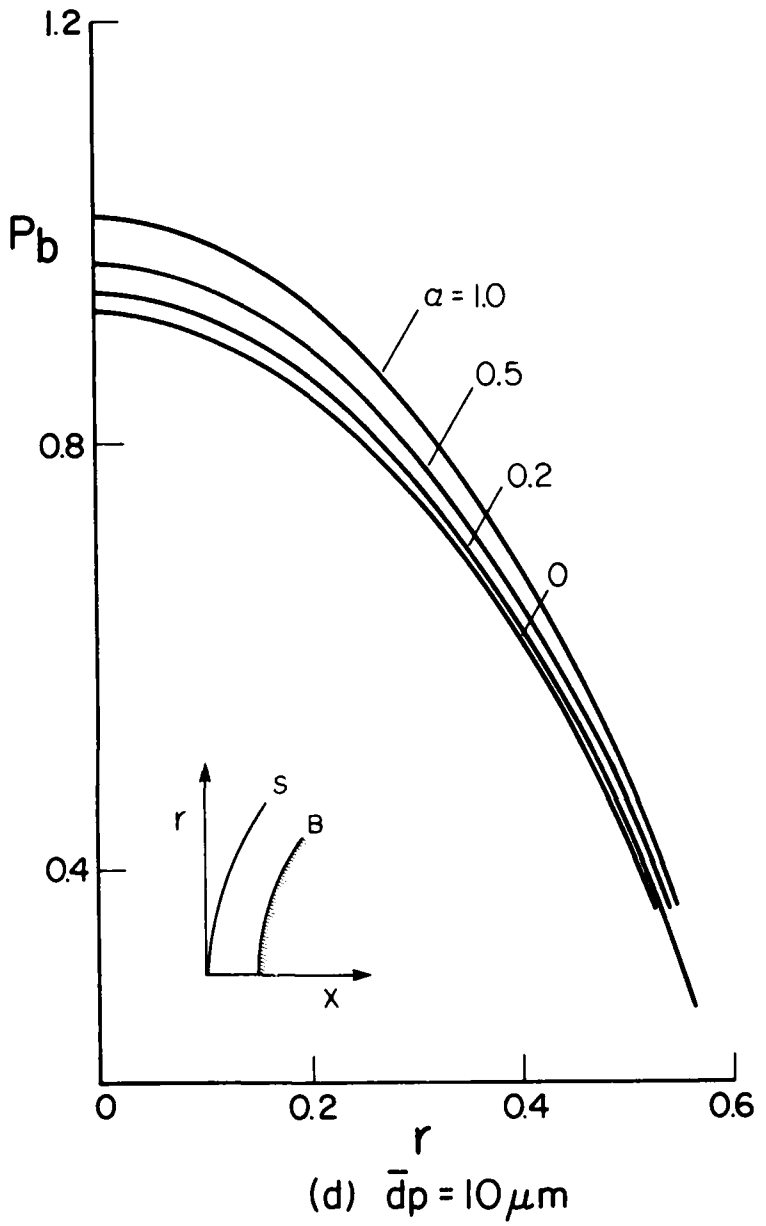

FIG. 9 - CONCLUDED
PRESSURE DISTRIBUTIONS ON BODY SURFACE FOR $M_\infty = 10$, $\bar{T}_\infty = 300$ K, $\bar{p}_\infty = 101.3$ KPa AND $\bar{R}_S = 1$ CM.

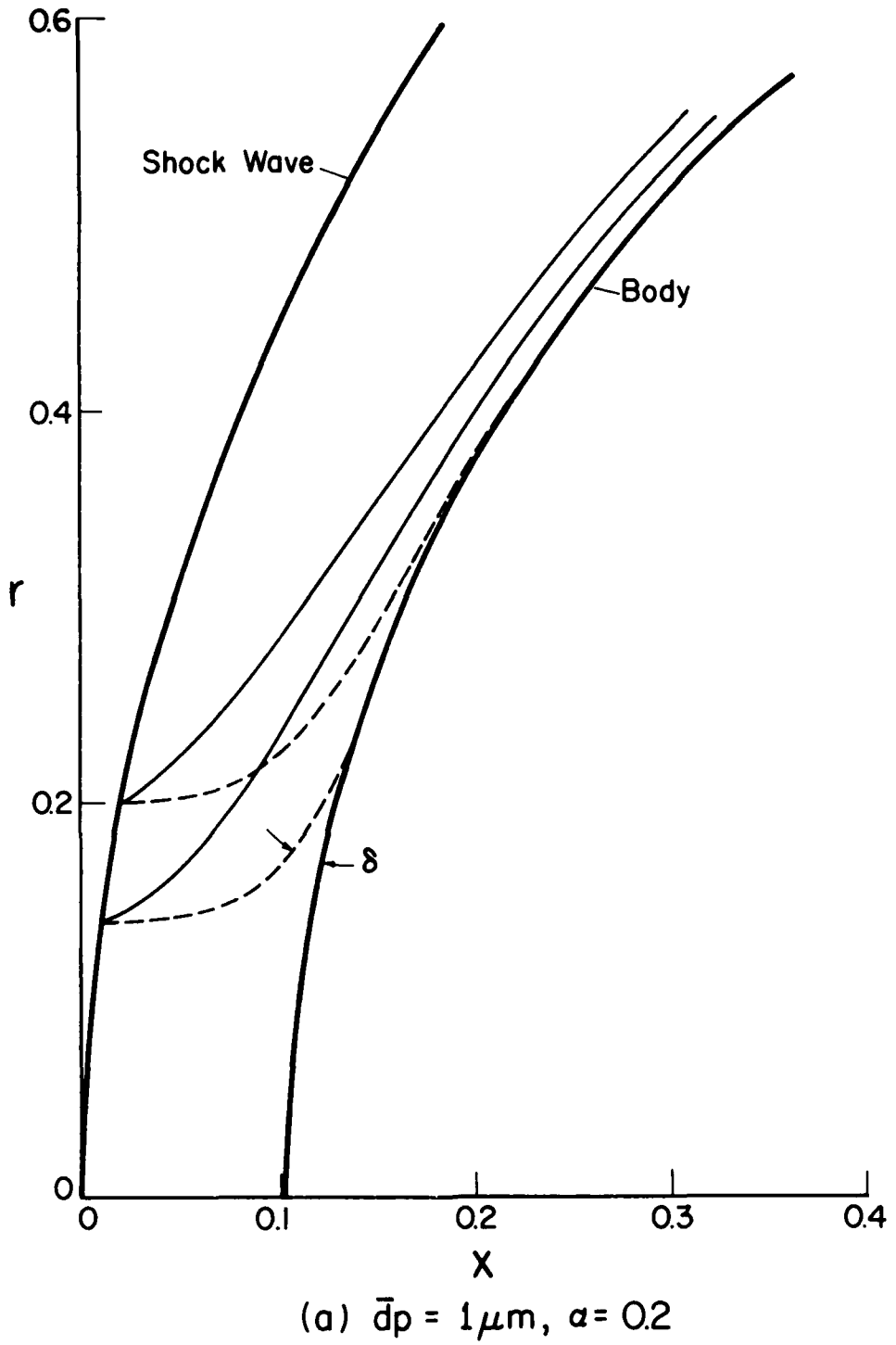

FIG. 10 GAS AND PARTICLE STREAMLINES AROUND BLUNT BODY FOR $M_\infty = 10$, $\bar{T}_\infty = 300$ K, $\bar{p}_\infty = 101.3$ KPa, $\bar{R}_S = 1$ CM.

——— GAS STREAMLINE, ------ PARTICLE STREAMLINE, IMPACT ANGLE δ.

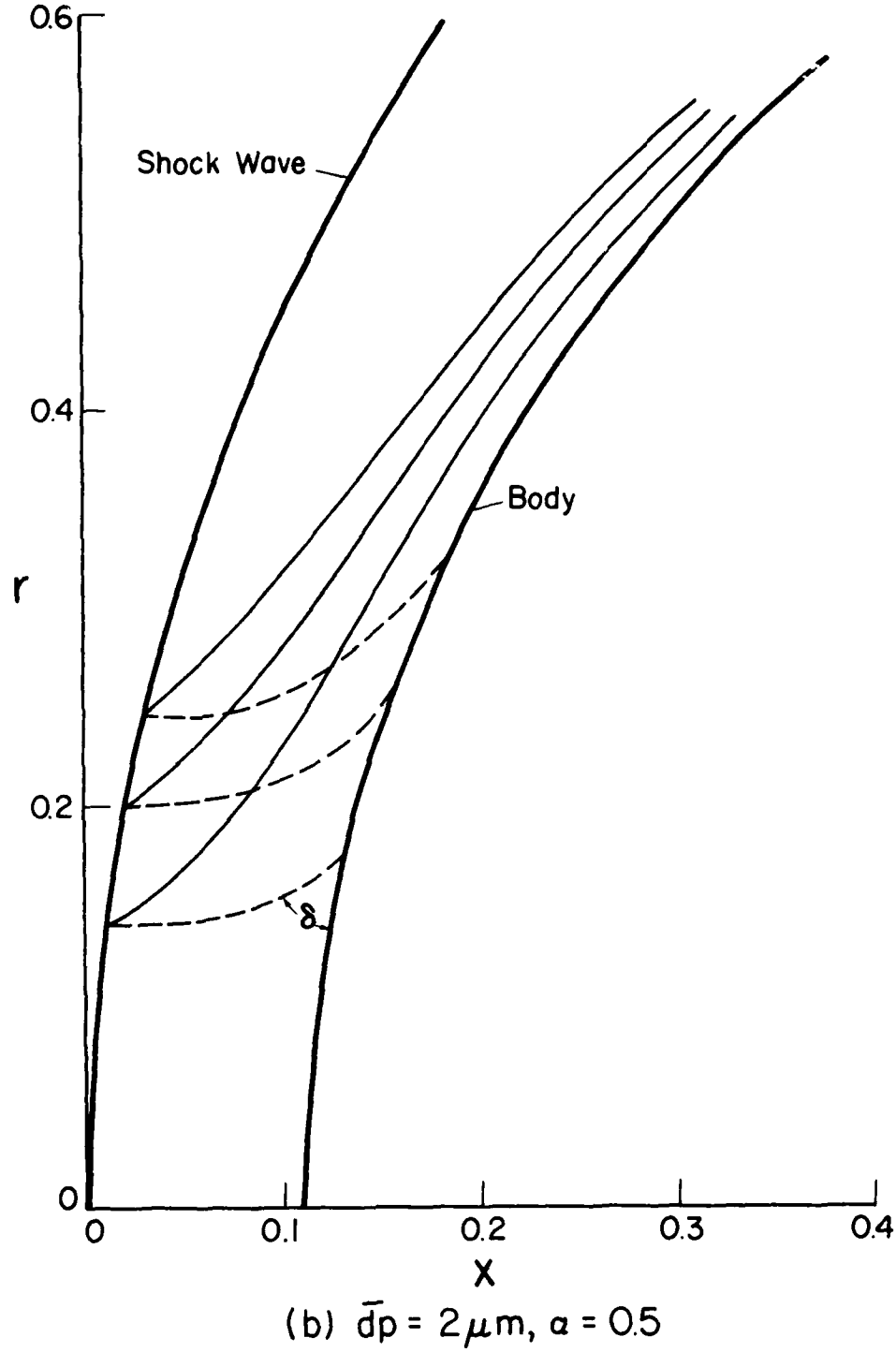

FIG. 10 - CONTINUED
GAS AND PARTICLE STREAMLINES AROUND BLUNT BODY FOR $M_\infty = 10$, $\bar{T}_\infty = 300$ K, $\bar{p}_\infty = 101.3$ KPa, $\bar{R}_S = 1$ CM.
——— GAS STREAMLINE, ------ PARTICLE STREAMLINE, IMPACT ANGLE δ.

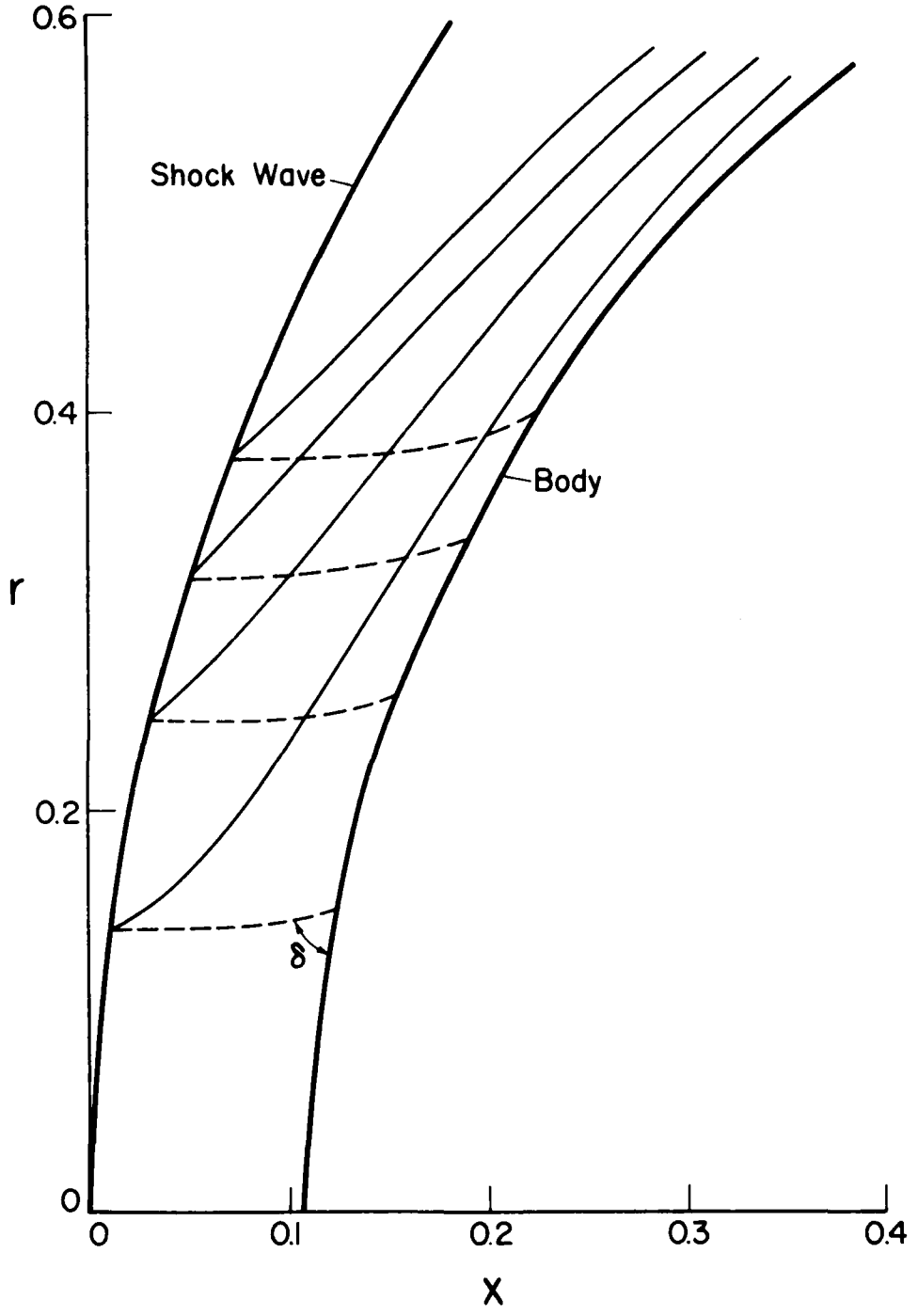

(c) $\bar{d}p = 5\mu m$, $\alpha = 0.5$

FIG. 10 - CONTINUED
GAS AND PARTICLE STREAMLINES AROUND BLUNT BODY FOR $M_\infty = 10$, $\bar{T}_\infty = 300$ K, $\bar{p}_\infty = 101.3$ KPa, $\bar{R}_S = 1$ CM.
——— GAS STREAMLINE, ------ PARTICLE STREAMLINE, IMPACT ANGLE δ.

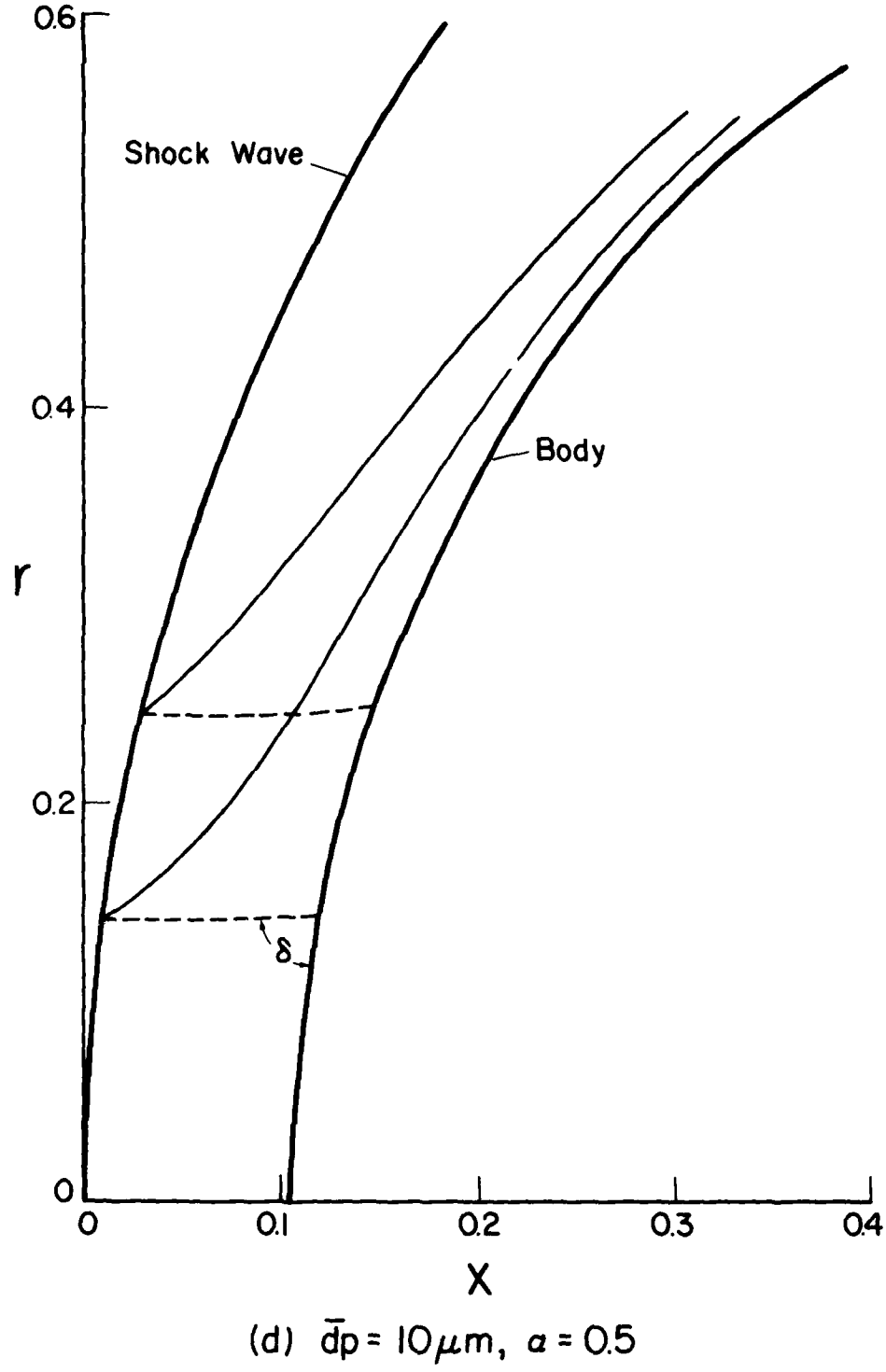

(d) $\bar{d}p = 10\mu m$, $\alpha = 0.5$

FIG. 10 - CONCLUDED
GAS AND PARTICLE STREAMLINES AROUND BLUNT BODY FOR $M_\infty = 10$, $\bar{T}_\infty = 300$ K, $\bar{p}_\infty = 101.3$ KPa, $\bar{R}_S = 1$ CM.
——— GAS STREAMLINE, ------ PARTICLE STREAMLINE, IMPACT ANGLE δ.

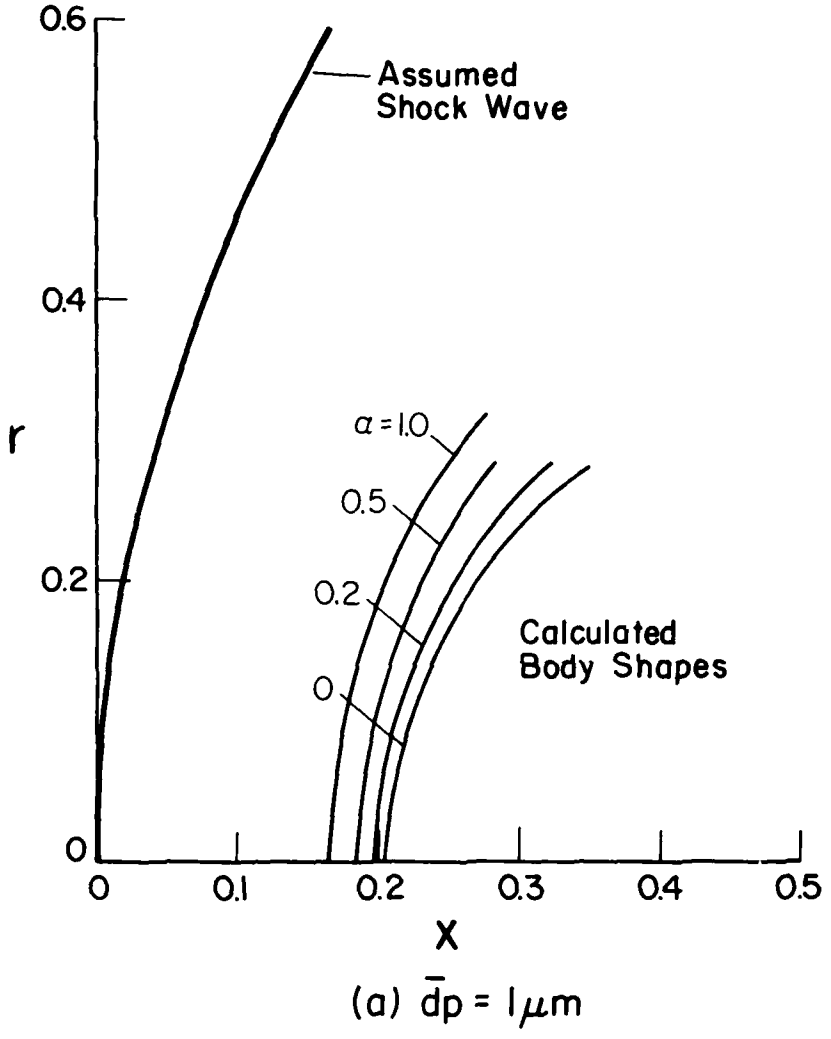

FIG. 11 ASSUMED SHOCK WAVE AND CALCULATED BODY SHAPES.
$M_\infty = 1.5$, $\bar{T}_\infty = 300$ K, $\bar{p}_\infty = 101.3$ KPa, $\bar{R}_S = 1$ CM.

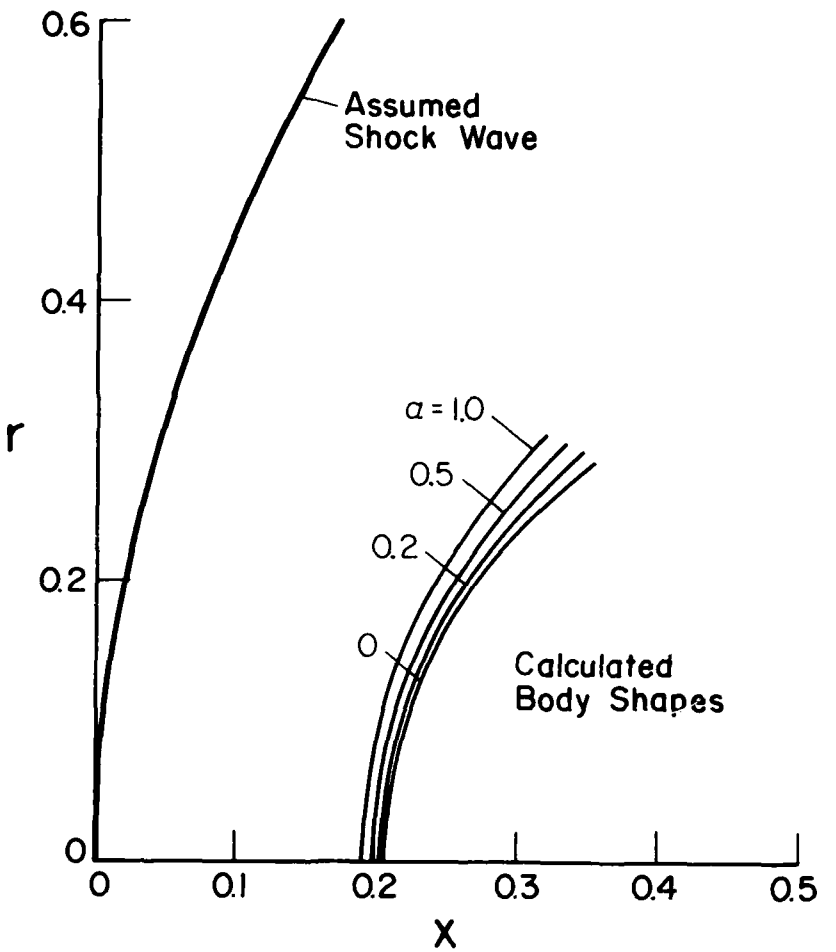

(b) $\bar{d}p = 2\mu m$

FIG. 11 - CONTINUED
ASSUMED SHOCK WAVE AND CALCULATED BODY SHAPES.
$M_\infty = 1.5$, $T_\infty = 300$ K, $\bar{P}_\infty = 101.3$ KPa, $\bar{R}_S = 1$ CM.

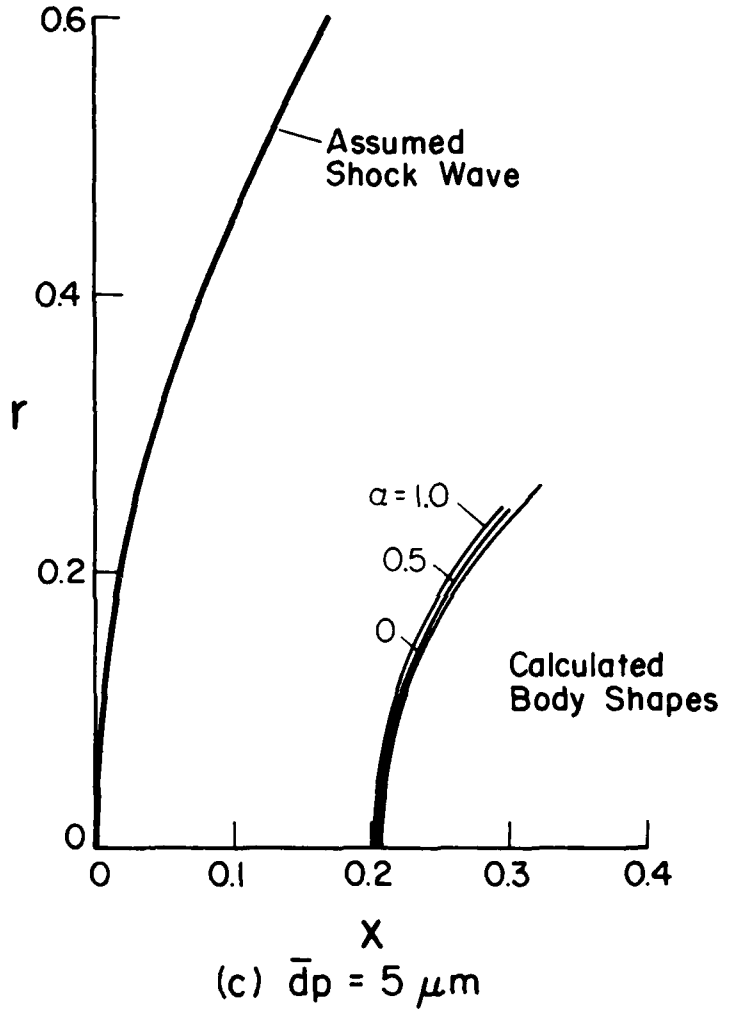

FIG. 11 - CONTINUED
ASSUMED SHOCK WAVE AND CALCULATED BODY SHAPES.
$M_\infty = 1.5$, $T_\infty = 300$ K, $\bar{p}_\infty = 101.3$ KPa, $\bar{R}_S = 1$ CM.

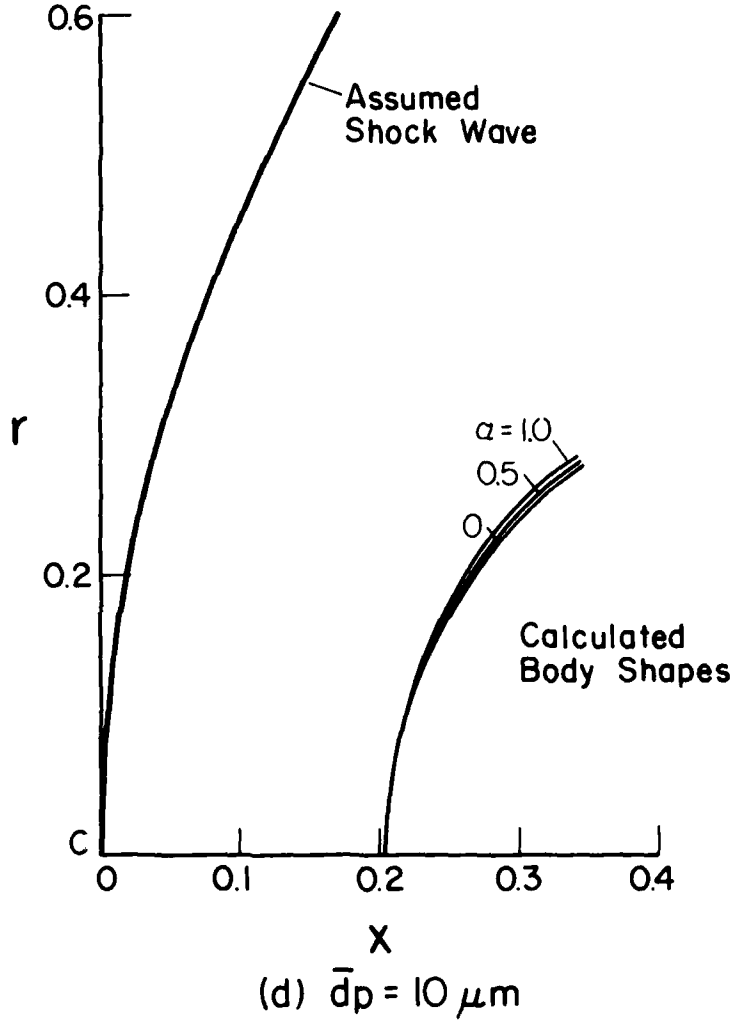

FIG. 11 - CONCLUDED
ASSUMED SHOCK WAVE AND CALCULATED BODY SHAPES.
$M_\infty = 1.5$, $T_\infty = 300$ K, $\bar{p}_\infty = 101.3$ KPa, $\bar{R}_S = 1$ CM.

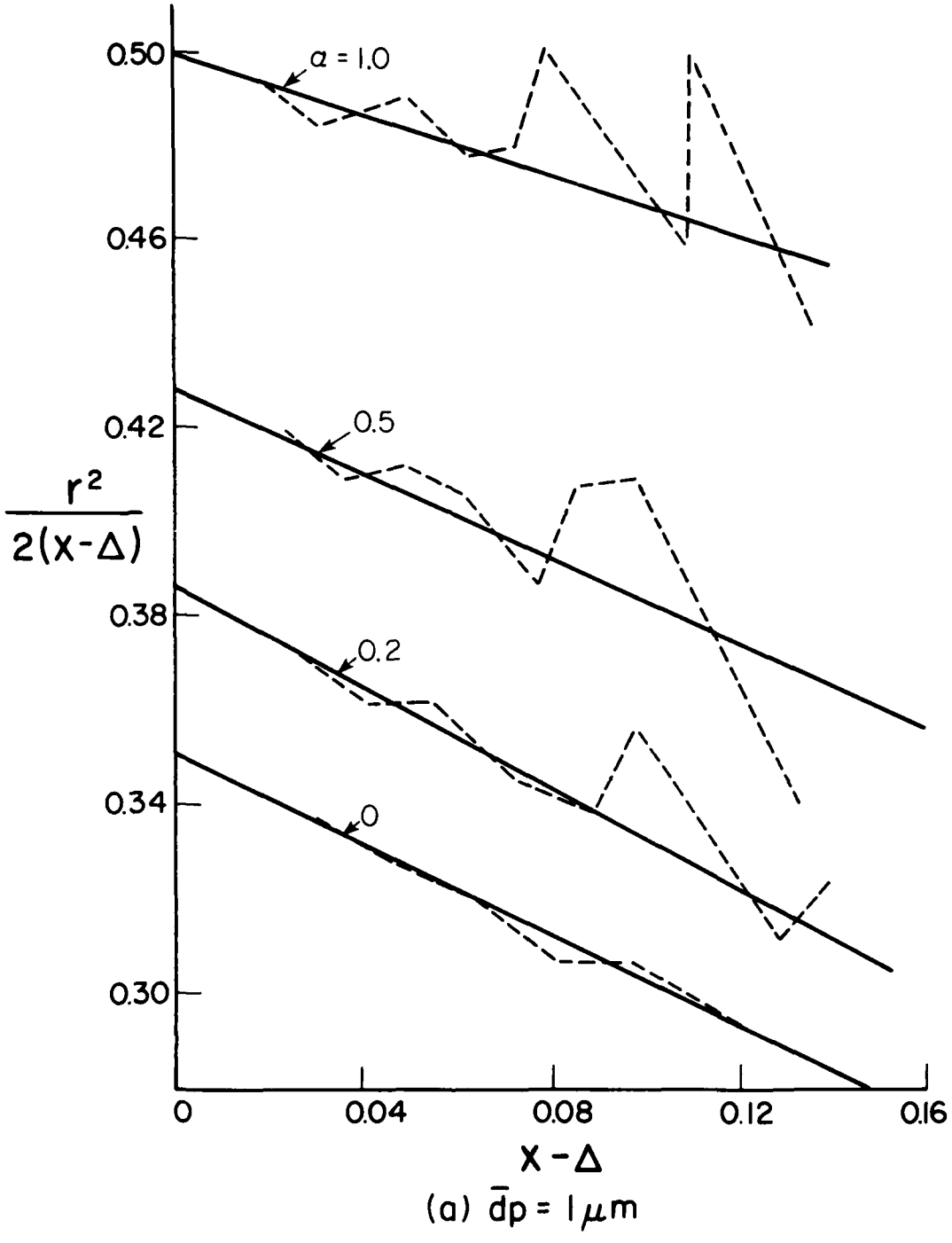

FIG. 12 RELATION BETWEEN $r^2/2(x-\Delta)$ AND $(x-\Delta)$ FOR CALCULATED BODIES. $M_\infty = 1.5$, $\bar{T}_\infty = 300$ K, $\bar{p}_\infty = 101.3$ KPa, $\bar{R}_S = 1$ CM.

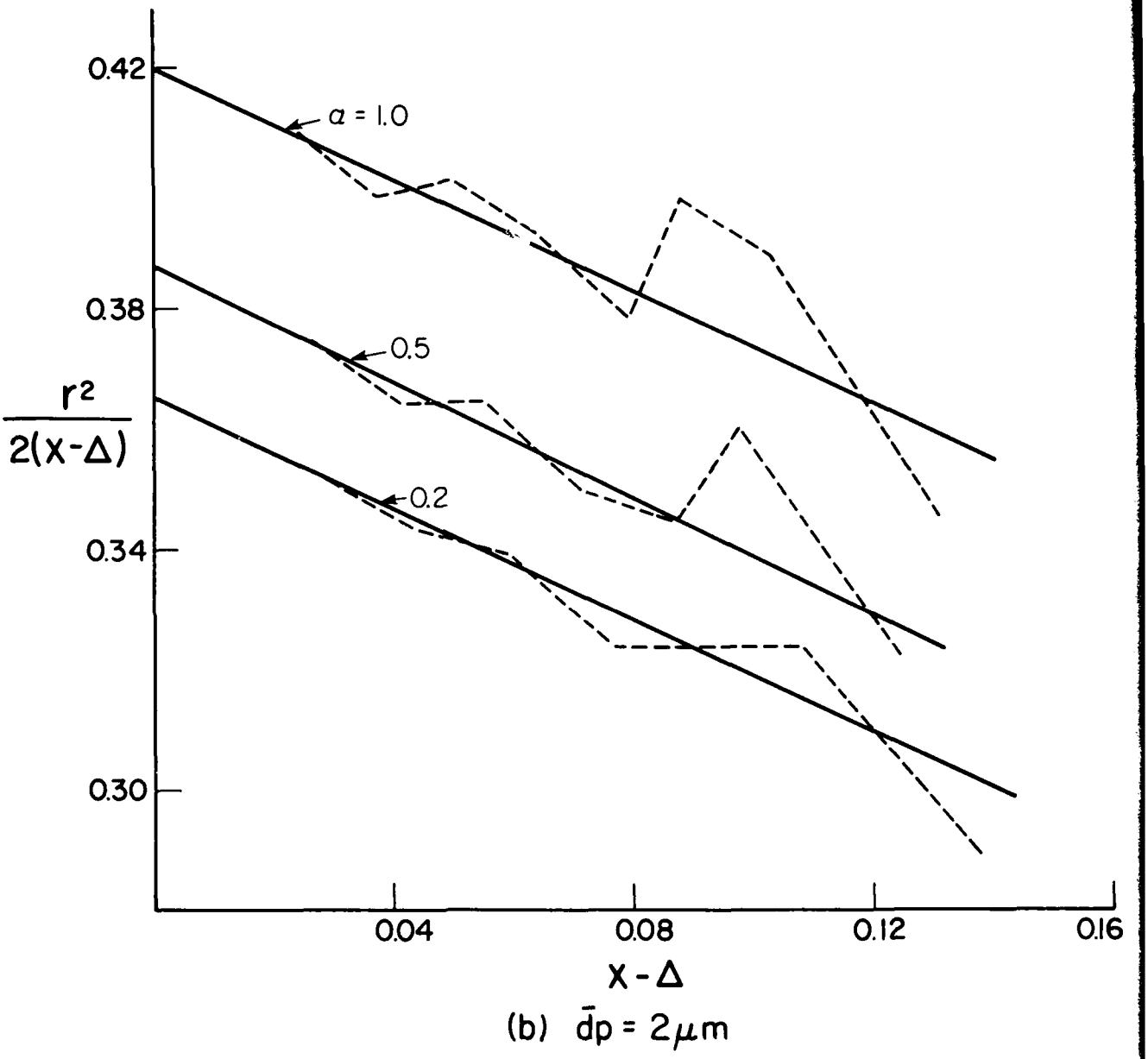

FIG. 12 - CONTINUED
RELATION BETWEEN $r^2/2(x-\Lambda)$ AND $(x-\Lambda)$ FOR CALCULATED BODIES.
$M_\infty = 1.5$, $\bar{T}_\infty = 300$ K, $\bar{p}_\infty = 101.3$ KPa, $\bar{R}_S = 1$ CM.

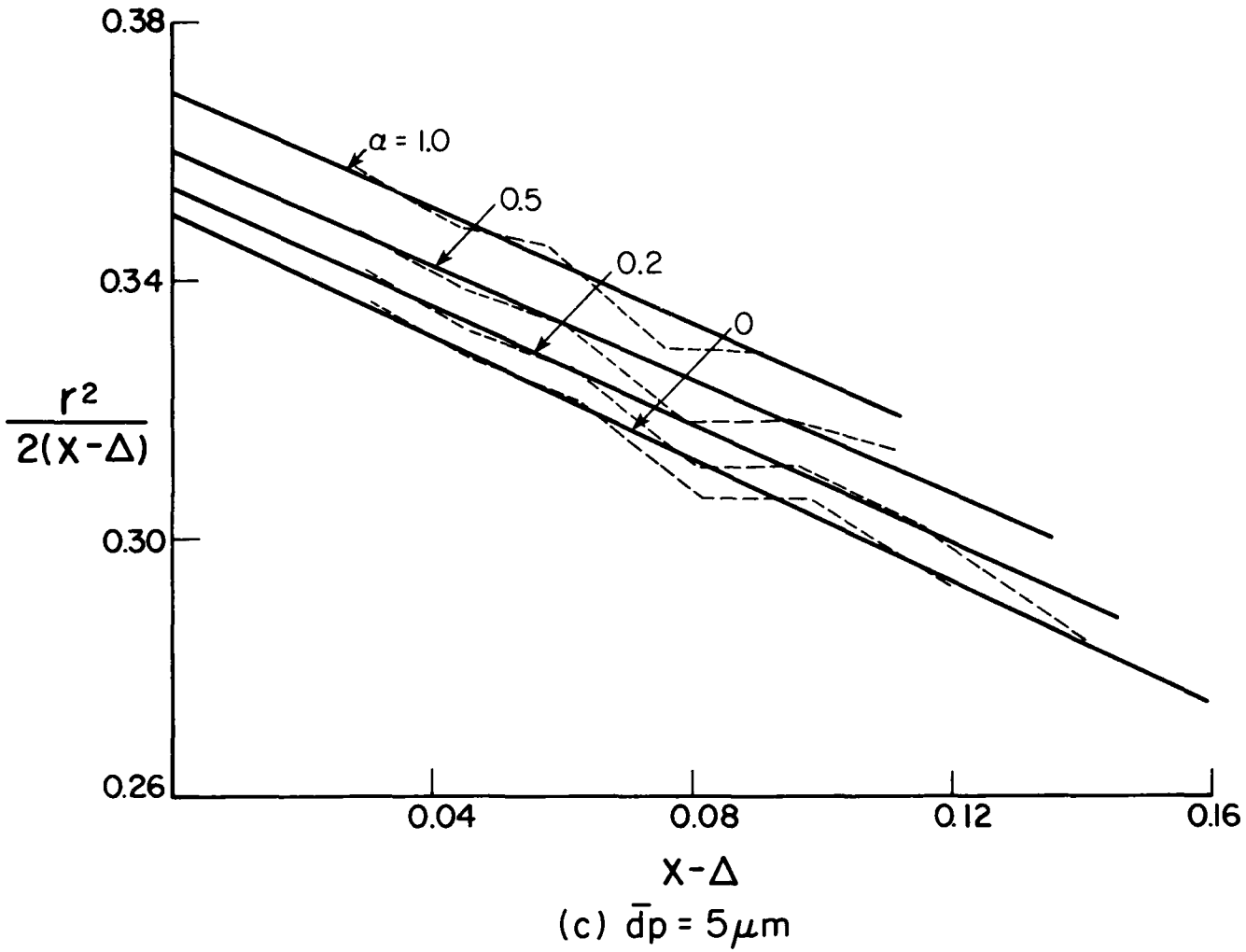

FIG. 12 - CONTINUED
RELATION BETWEEN $r^2/2(x-\Delta)$ AND $(x-\Delta)$ FOR CALCULATED BODIES.
M_∞ = 1.5, $\bar{T}_\infty$ = 300 K, $\bar{p}_\infty$ = 101.3 KPa, $\bar{R}_S$ = 1 CM.

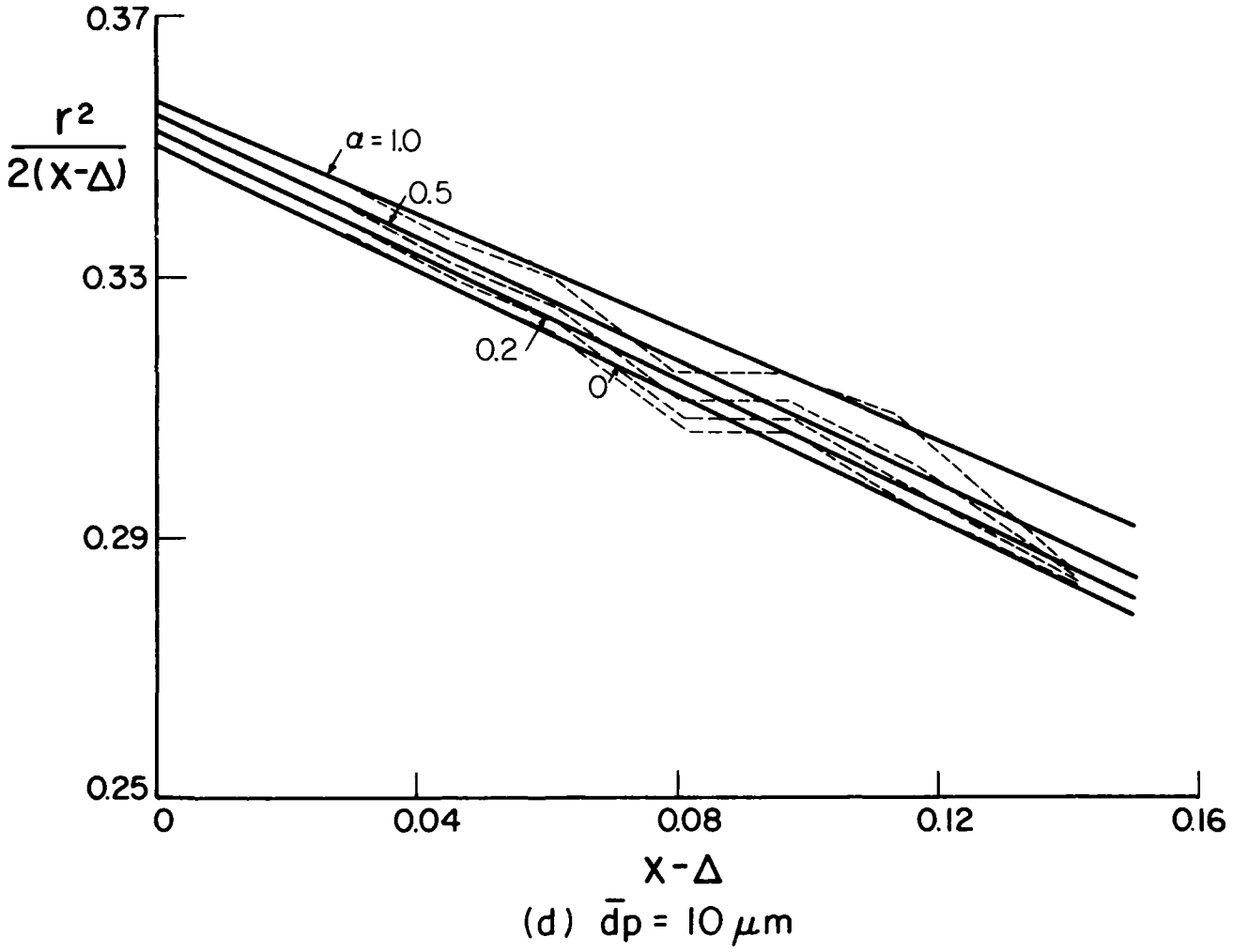

FIG. 12 - CONCLUDED
RELATION BETWEEN $r^2/2(x-\Delta)$ AND $(x-\Delta)$ FOR CALCUALTED BODIES.
$M_\infty = 1.5$, $\bar{T}_\infty = 300$ K, $\bar{p}_\infty = 101.3$ KPa, $\bar{R}_S = 1$ CM.

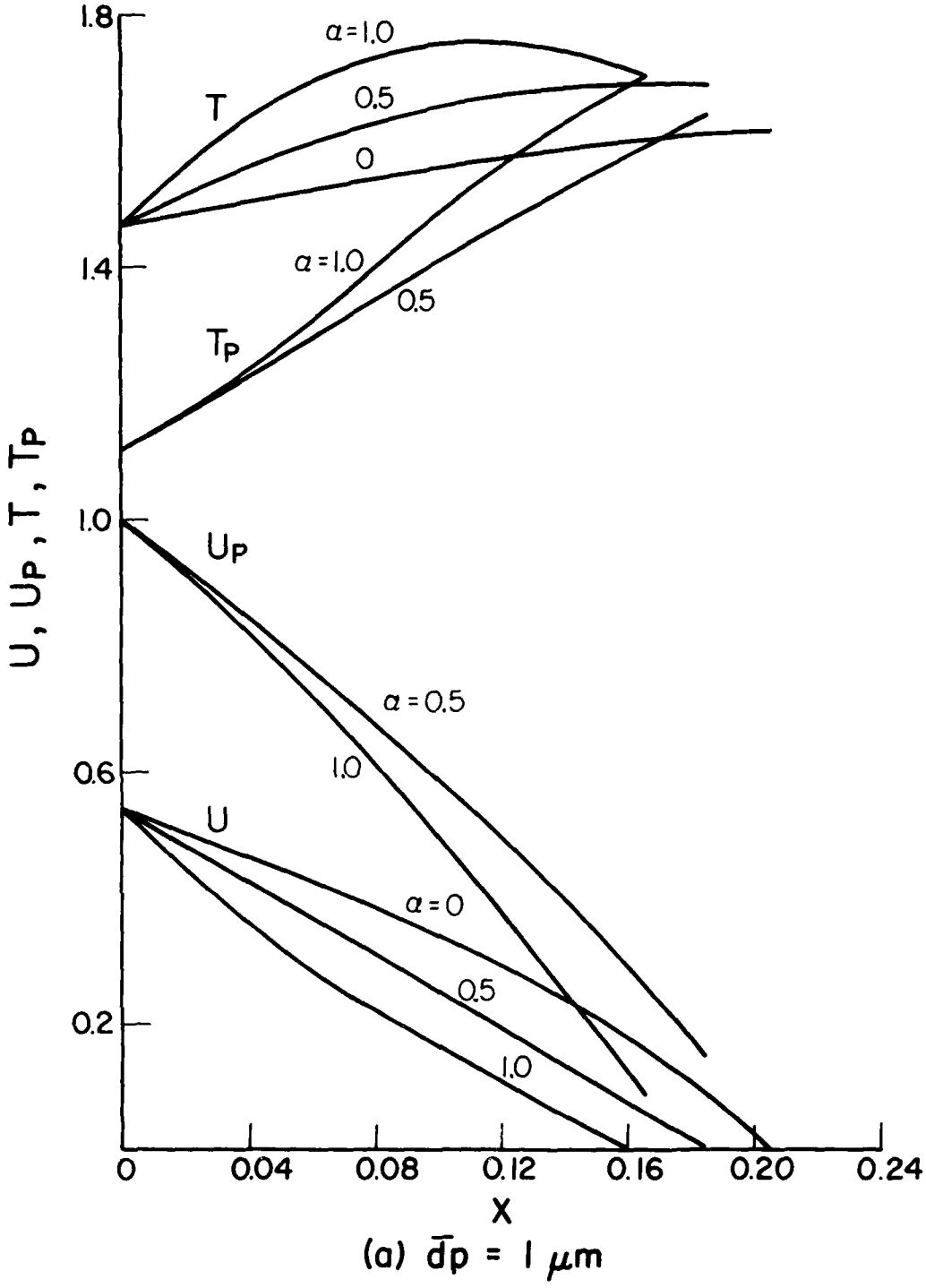

FIG. 13 VARIATION OF GAS AND PARTICLE VELOCITIES AND TEMPERATURE ALONG STAGNATION STREAMLINES. M_∞ = 1.5, $\bar{T}_\infty$ = 300 K, $\bar{p}_\infty$ = 101.3 KPa, $\bar{R}_S$ = 1 CM.

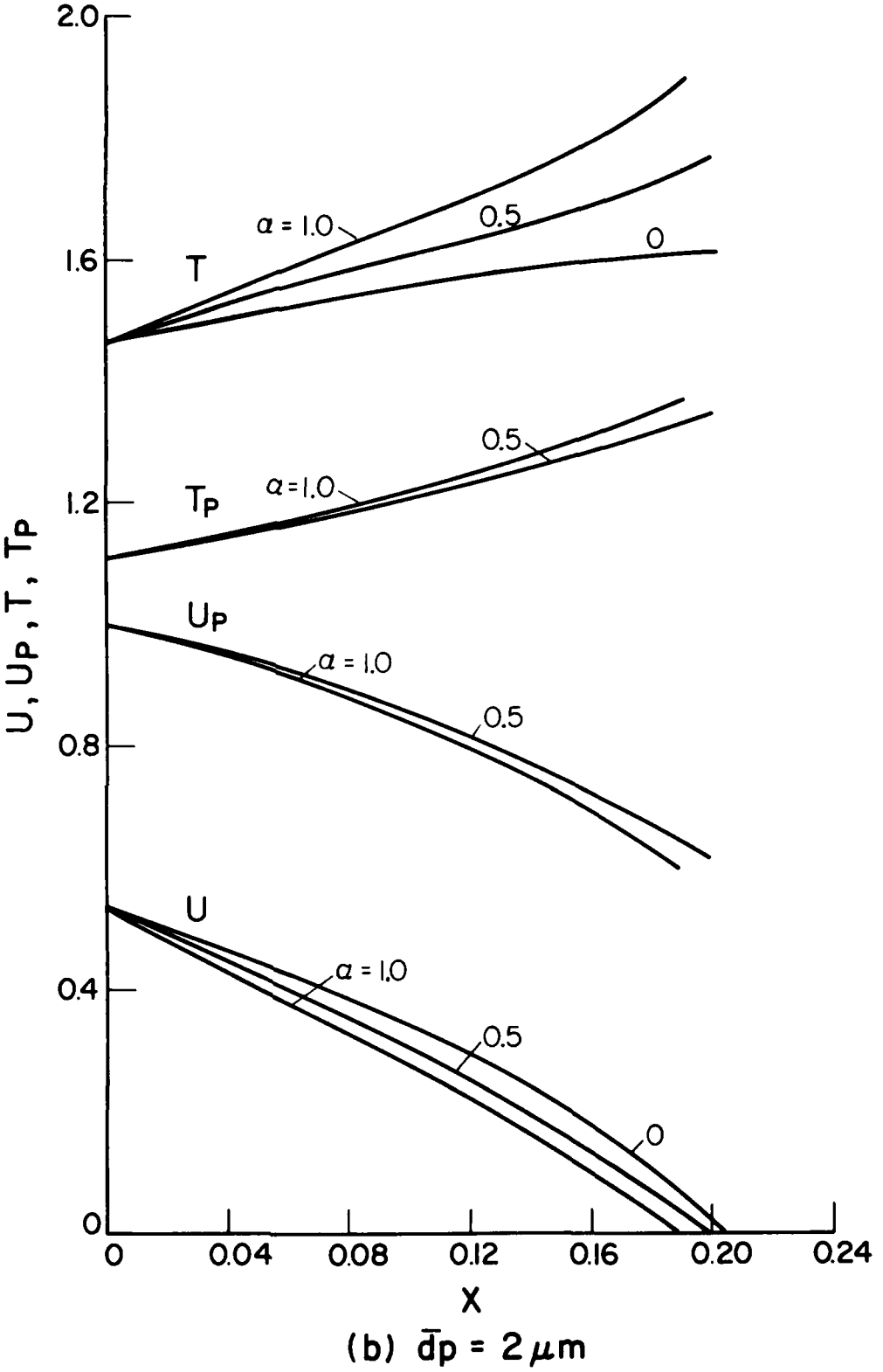

FIG. 13 - CONTINUED
VARIATION OF GAS AND PARTICLE VELOCITIES AND TEMPERATURE ALONG STAGNATION STREAMLINES. M_∞ = 1.5, $\bar{T}_\infty$ = 300 K, $\bar{p}_\infty$ = 101.3 KPa, $\bar{R}_S$ = 1 CM.

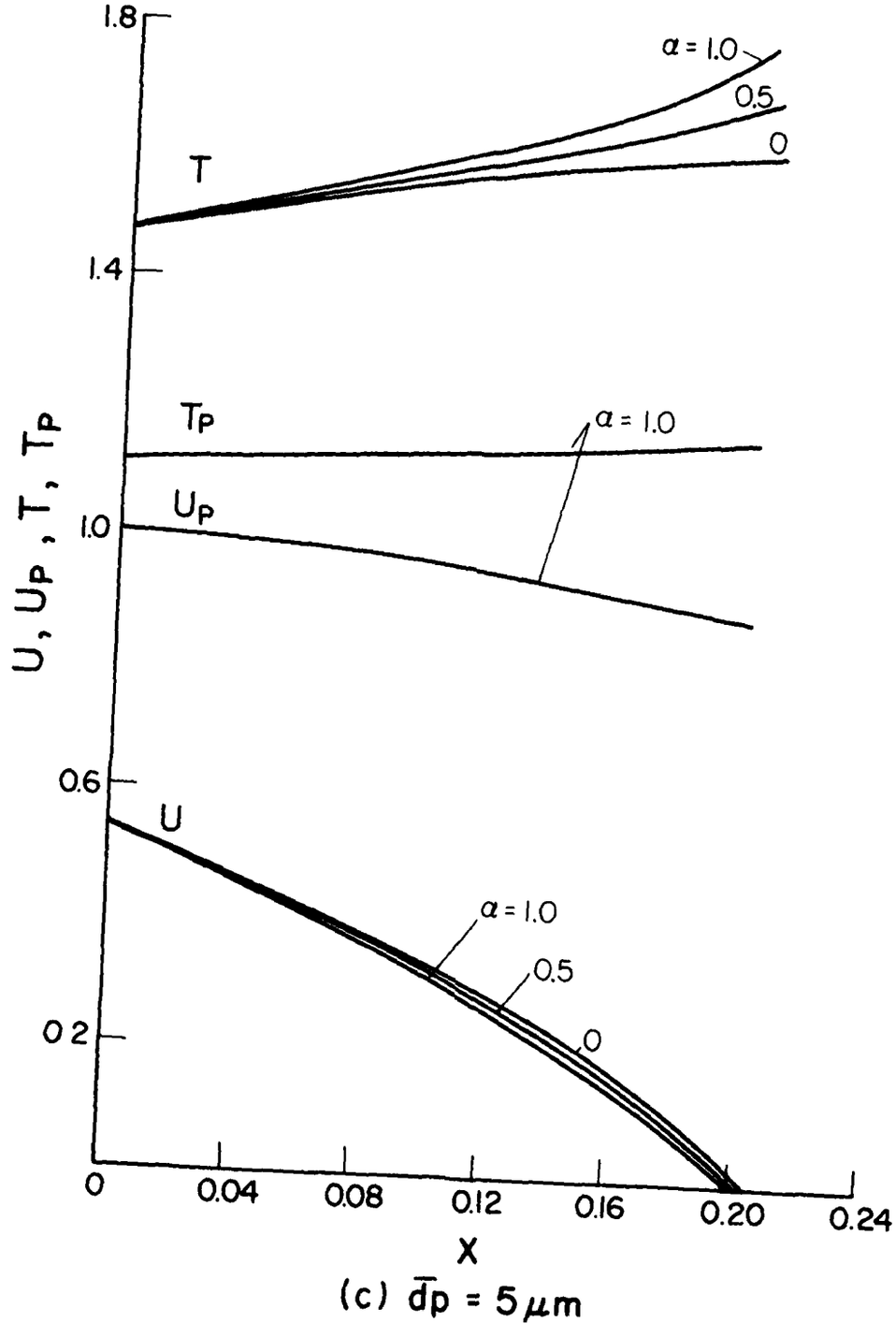

FIG. 13 - CONTINUED
VARIATION OF GAS AND PARTICLE VELOCITIES AND TEMPERATURE ALONG STAGNATION STREAMLINES. $M_\infty = 1.5$, $\bar{T}_\infty = 300$ K, $\bar{P}_\infty = 101.3$ KPa, $\bar{R}_S = 1$ CM.

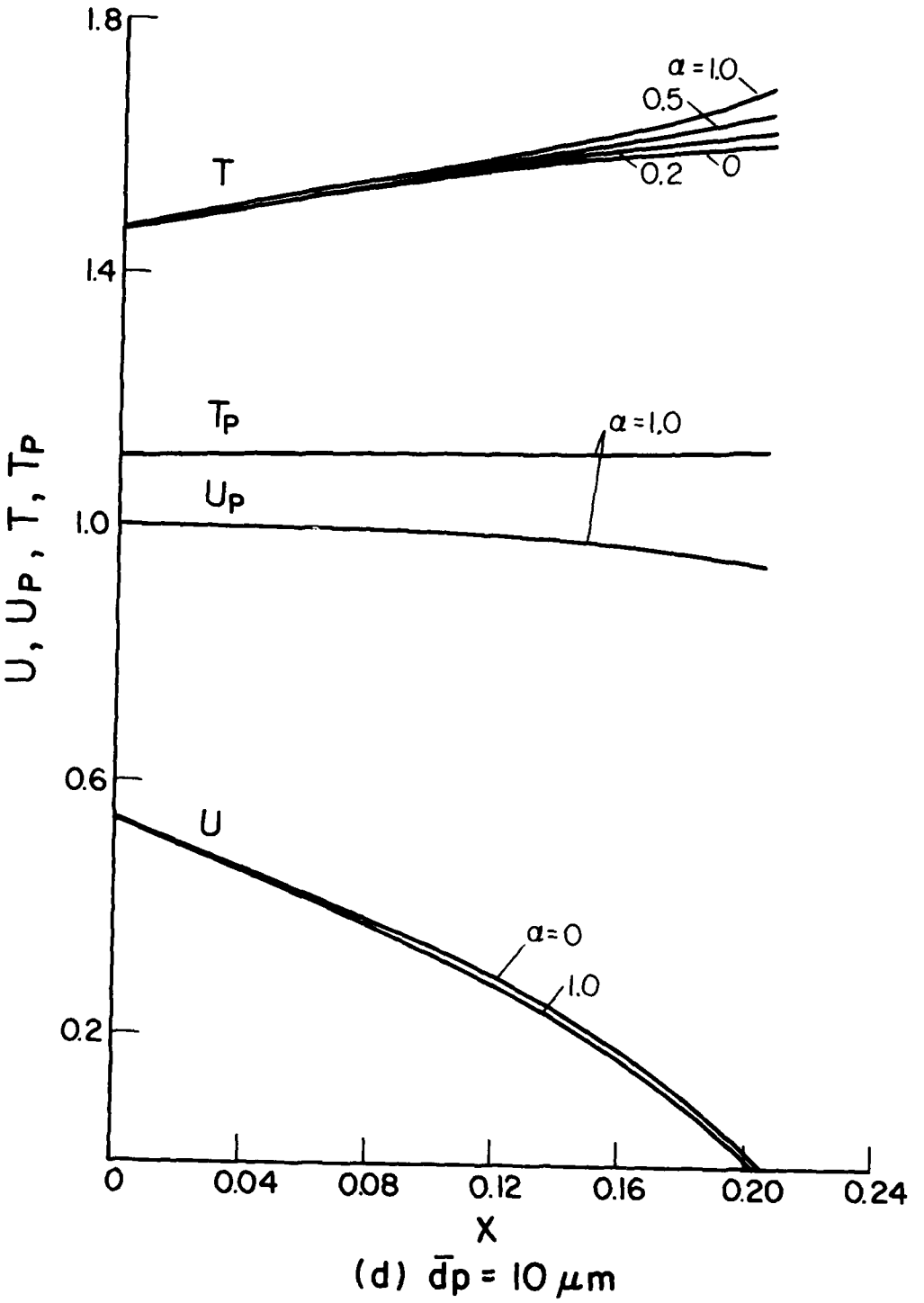

FIG. 13 - CONCLUDED
VARIATION OF GAS AND PARTICLE VELOCITIES AND TEMPERATURE ALONG STAGNATION STREAMLINES. M_∞ = 1.5, $\bar{T}_\infty$ = 300 K, $\bar{p}_\infty$ = 101.3 KPa, $\bar{R}_S$ = 1 CM.

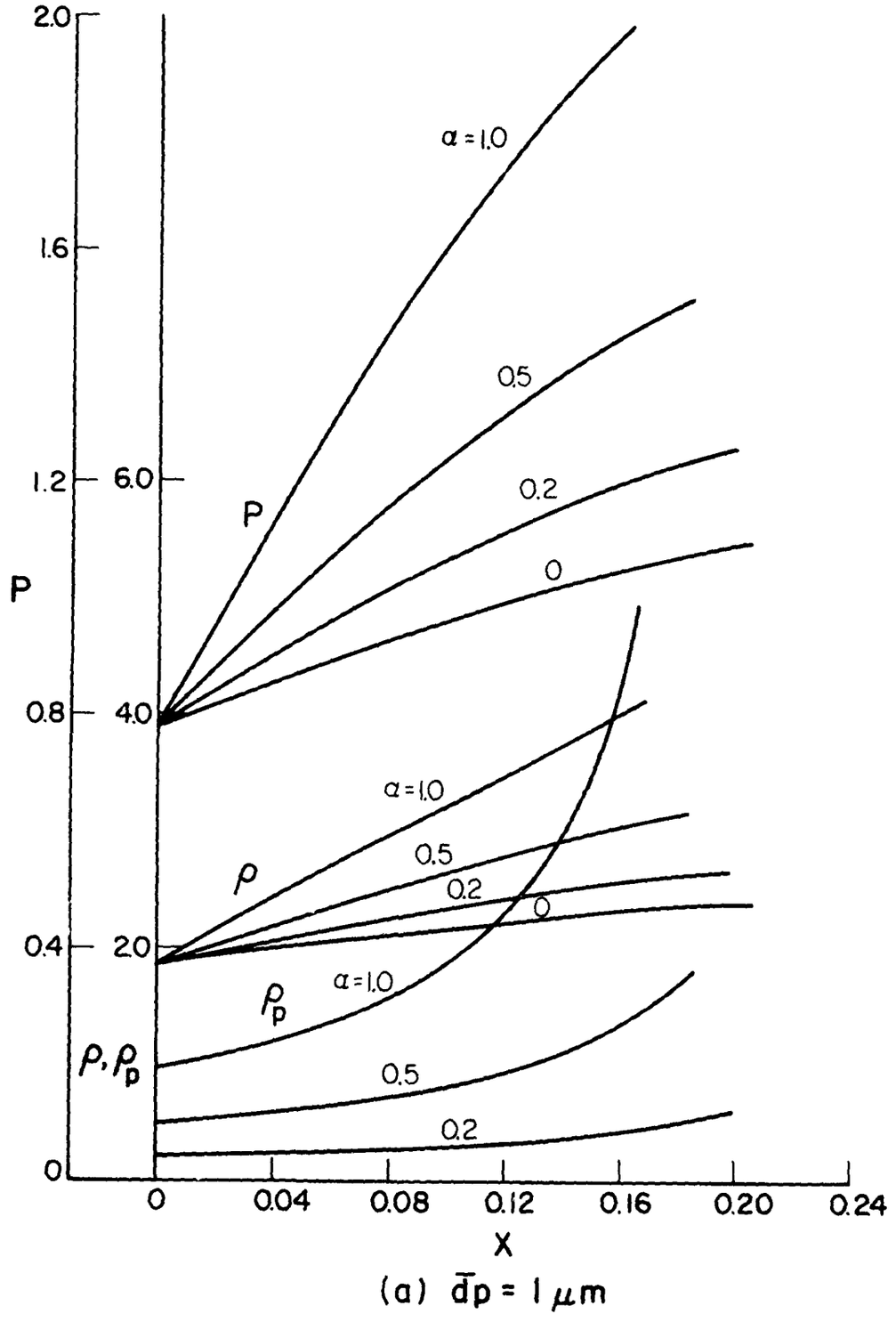

FIG. 14 VARIATION OF GAS AND PARTICLE PHASE DENSITIES AND GAS PRESSURE ALONG STAGNATION STREAMLINES. M_∞ = 1.5, $\bar{T}_\infty$ = 300 K, $\bar{p}_\infty$ = 101.3 KPa, $\bar{R}_S$ = 1 CM.

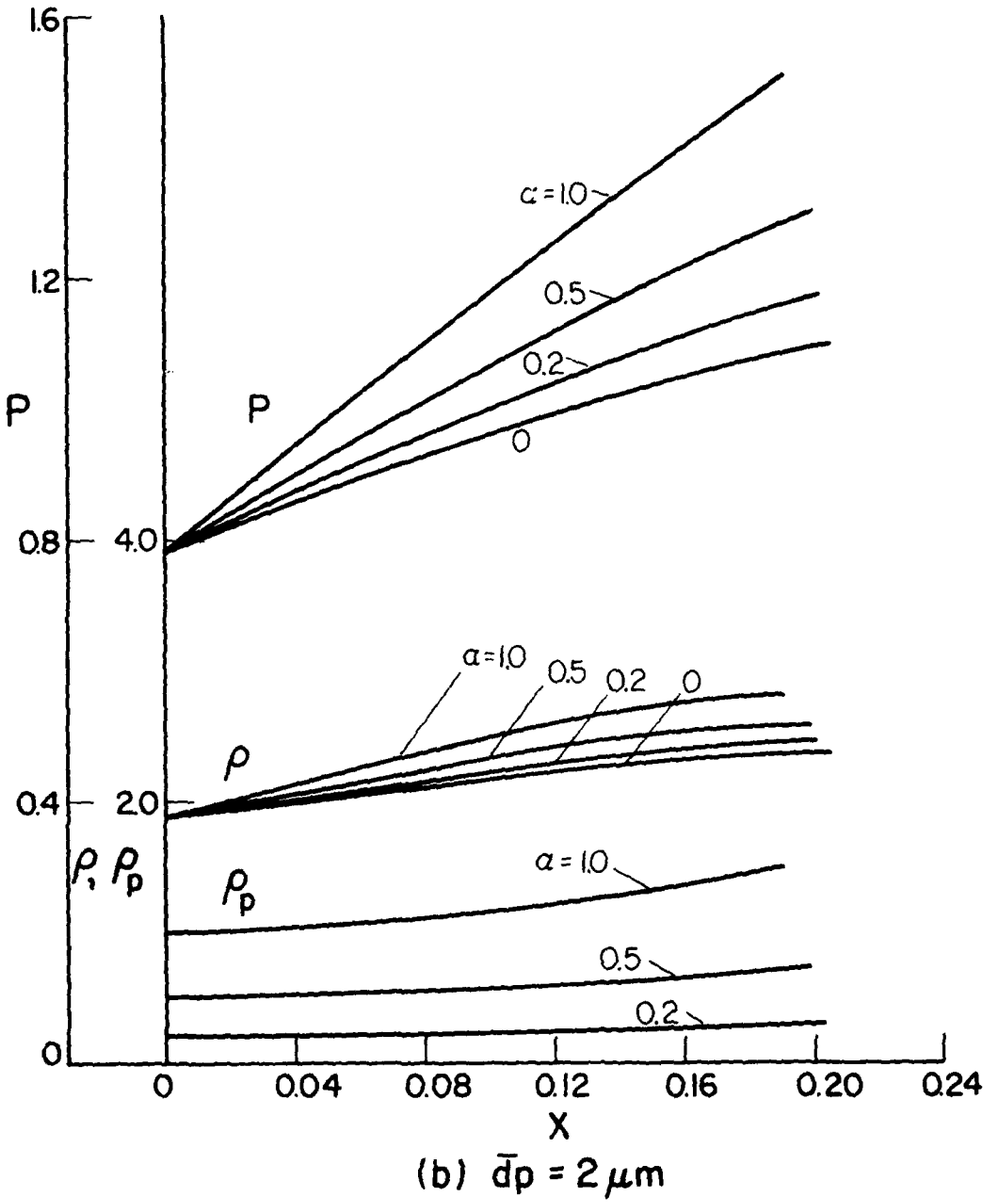

FIG. 14 - CONTINUED
VARIATION OF GAS AND PARTICLE PHASE DENSITIES AND GAS PRESSURE ALONG STAGNATION STREAMLINES. M_∞ = 1.5, $\bar{T}_\infty$ = 300 K, $\bar{p}_\infty$ = 101.3 KPa, $\bar{R}_S$ = 1 CM.

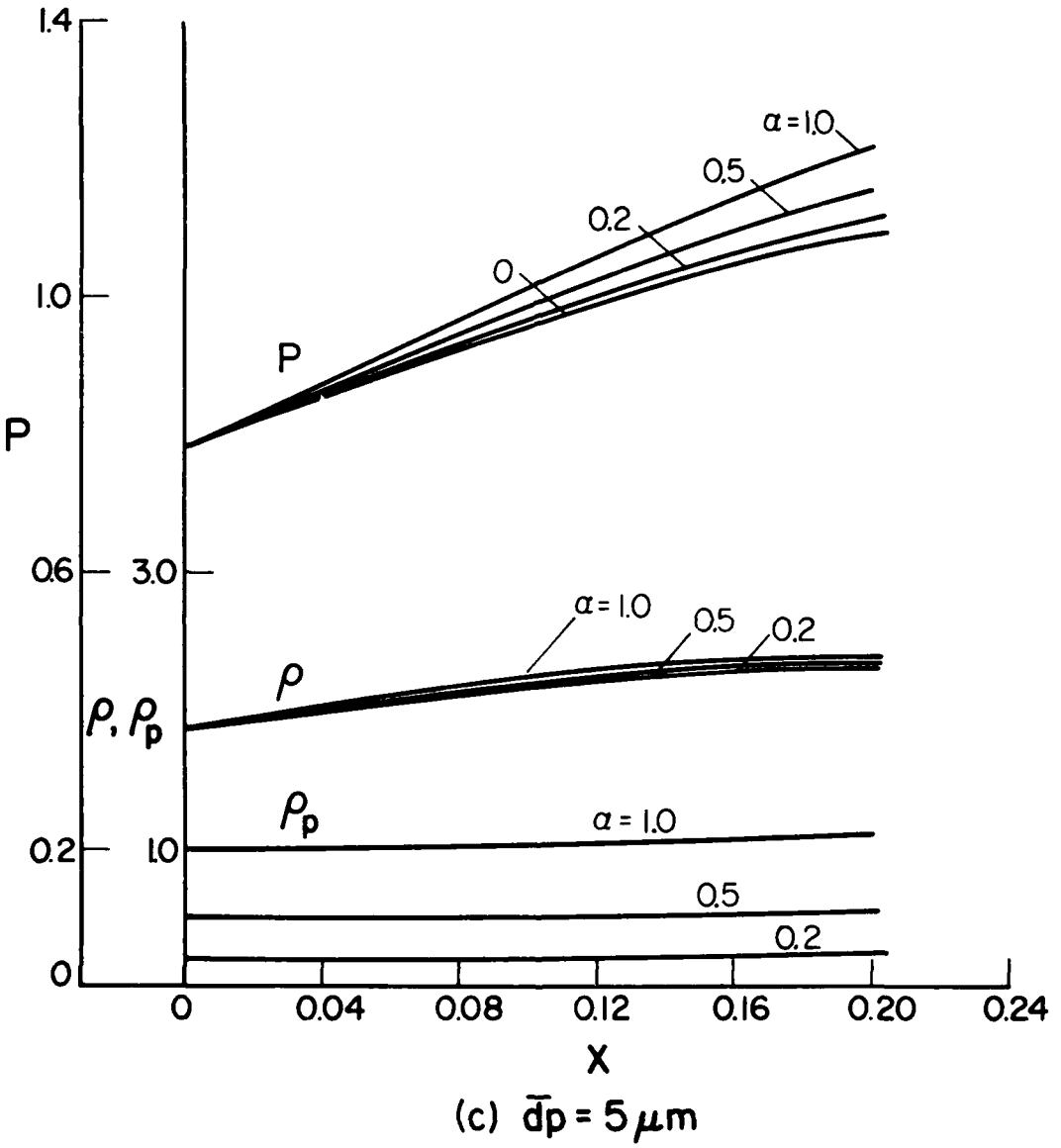

FIG. 14 - CONTINUED
VARIATION OF GAS AND PARTICLE PHASE DENSITIES AND GAS PRESSURE ALONG STAGNATION STREAMLINES. M_∞ = 1.5, $\bar{T}_\infty$ = 300 K, $\bar{p}_\infty$ = 101.3 KPa, $\bar{R}_S$ = 1 CM.

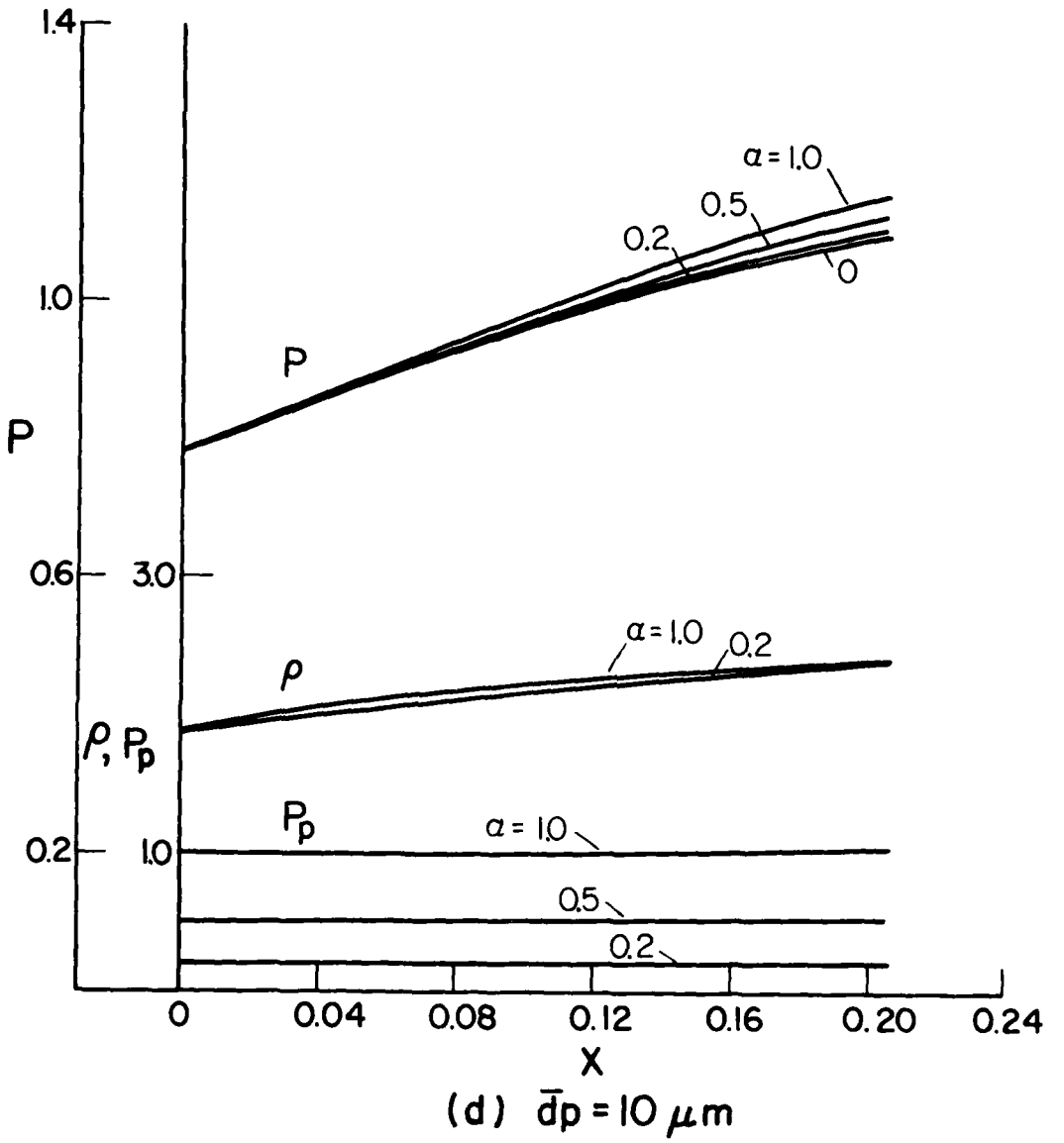

FIG. 14 - CONCLUDED
VARIATION OF GAS AND PARTICLE PHASE DENSITIES AND GAS PRESSURE ALONG STAGNATION STREAMLINES. M_∞ = 1.5, $\bar{T}_\infty$ = 300 K, $\bar{p}_\infty$ = 101.3 KPa, $\bar{R}_s$ = 1 CM.

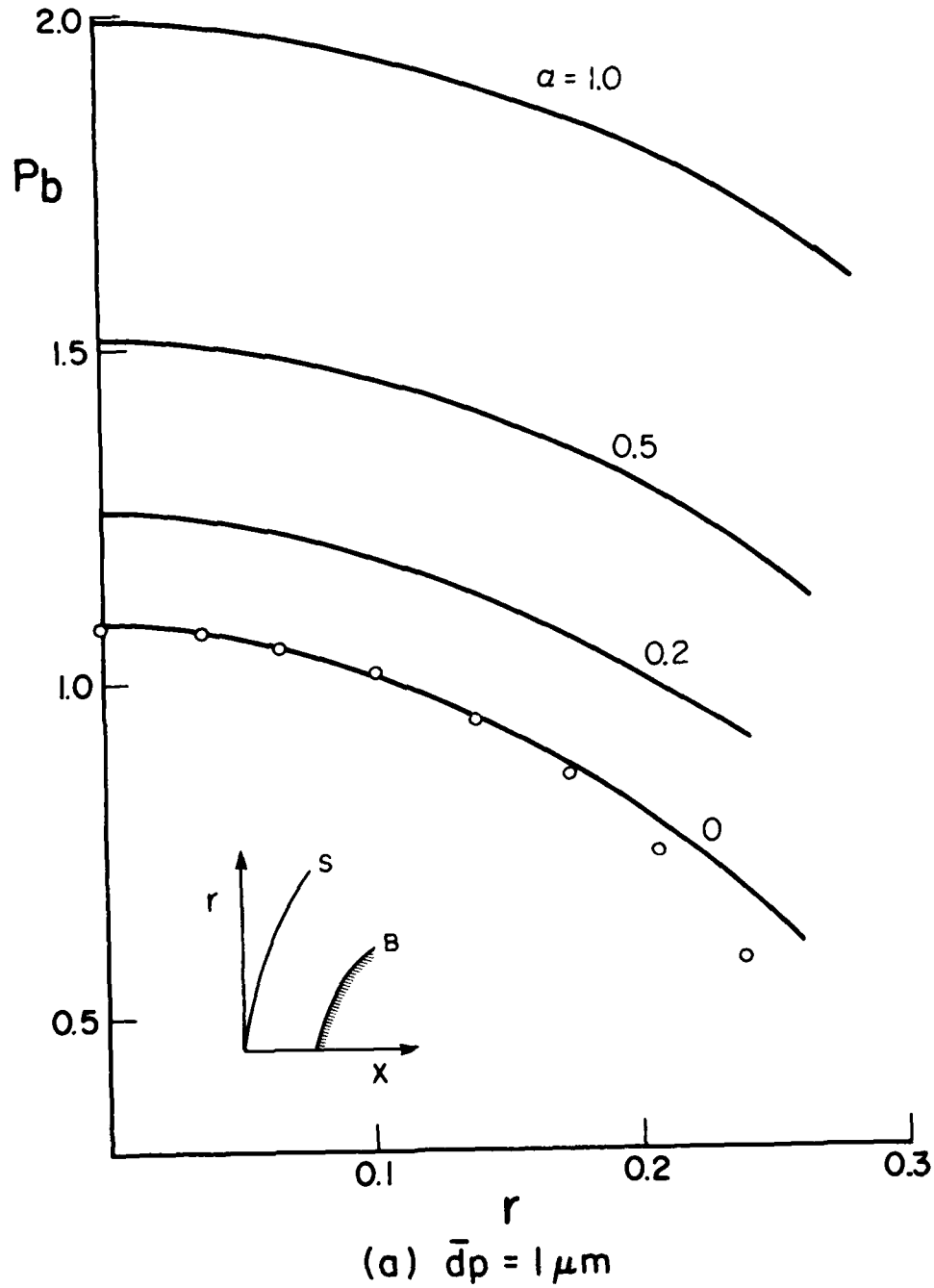

FIG. 15 PRESSURE DISTRIBUTION ON BODY SURFACES. $M_\infty = 1.5$, $\bar{T}_\infty = 300$ K, $\bar{p}_\infty = 101.3$ KPa, $\bar{R}_S = 1$ CM. ^{o} VAN DYKE & GORDON [REF. 16].

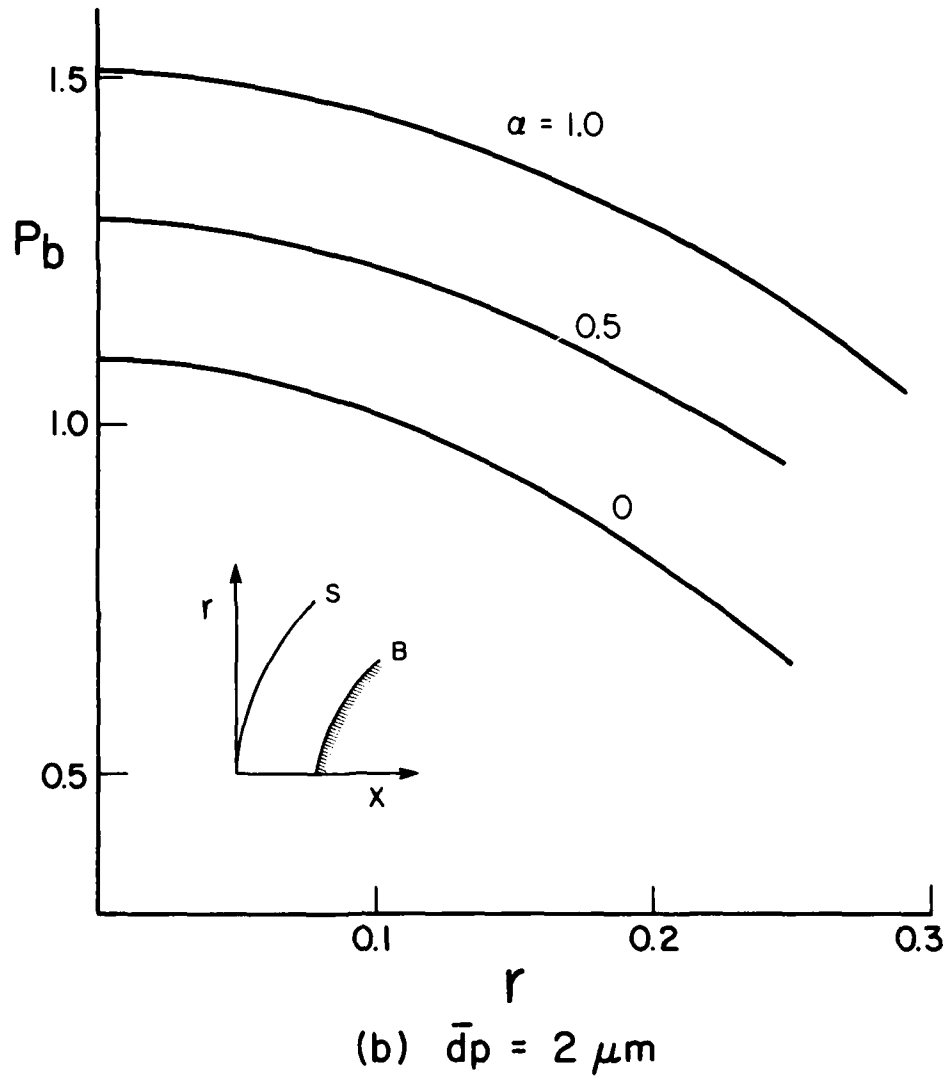

FIG. 15 - CONTINUED
PRESSURE DISTRIBUTION ON BODY SURFACES. M_∞ = 1.5, $\bar{T}_\infty$ = 300 K, $\bar{p}_\infty$ = 101.3 KPa, $\bar{R}_S$ = 1 CM.

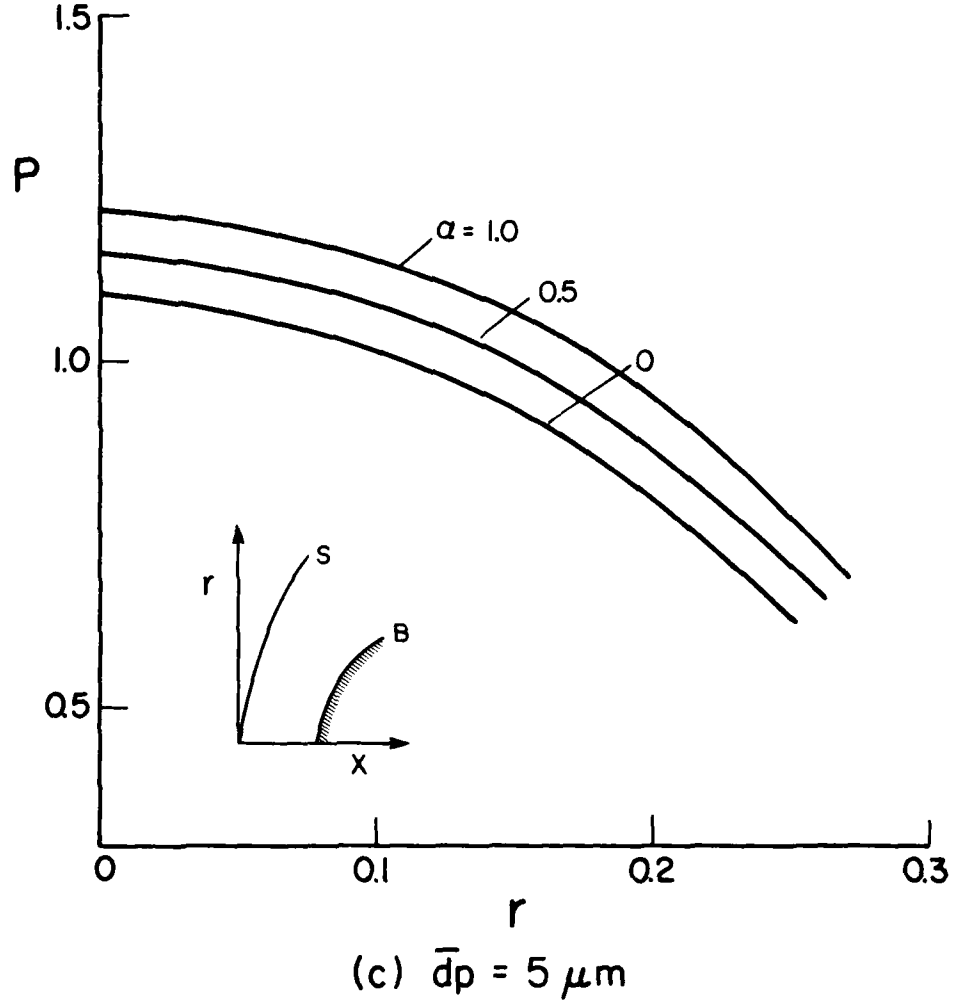

(c) $\bar{dp} = 5\ \mu m$

FIG. 15 - CONTINUED
PRESSURE DISTRIBUTION ON BODY SURFACES. $M_\infty = 1.5$, $\bar{T}_\infty = 300$ K, $\bar{p}_\infty = 101.3$ KPa, $\bar{R}_S = 1$ CM.

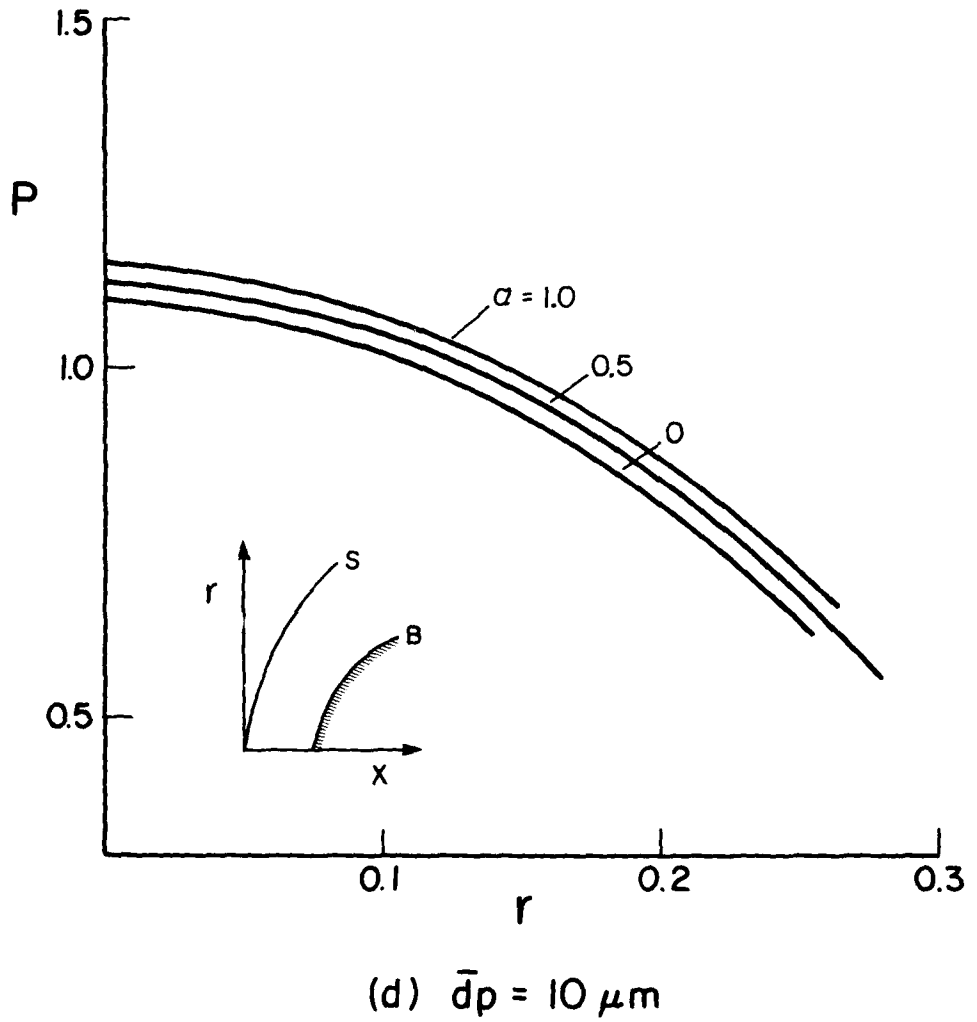

(d) $\bar{d}p = 10\ \mu m$

FIG. 15 - CONCLUDED
PRESSURE DISTRIBUTION ON BODY SURFACES. $M_\infty = 1.5$, $\bar{T}_\infty = 300$ K, $\bar{p}_\infty = 101.3$ KPa, $\bar{R}_S = 1$ CM.

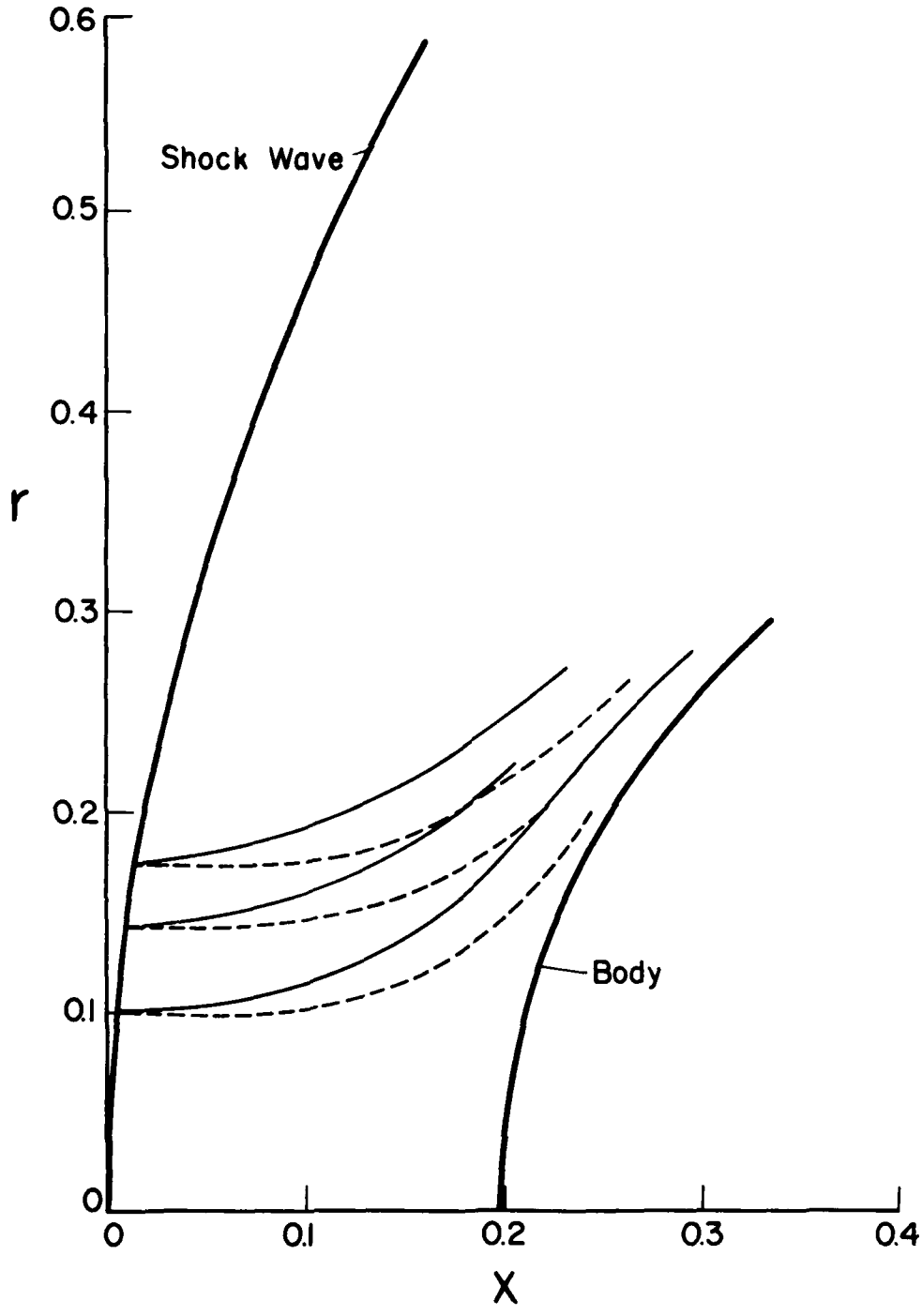

(a) $\bar{d}p = 1\,\mu m$, $\alpha = 0.2$

FIG. 16 GAS AND PARTICLE STREAMLINES AROUND BLUNT BODY.
$M_\infty = 1.5$, $\bar{T}_\infty = 300$ K, $\bar{p}_\infty = 101.3$ KPa, $\bar{R}_S = 1$ CM.
——— GAS STREAMLINE, ------ PARTICLE STREAMLINE.

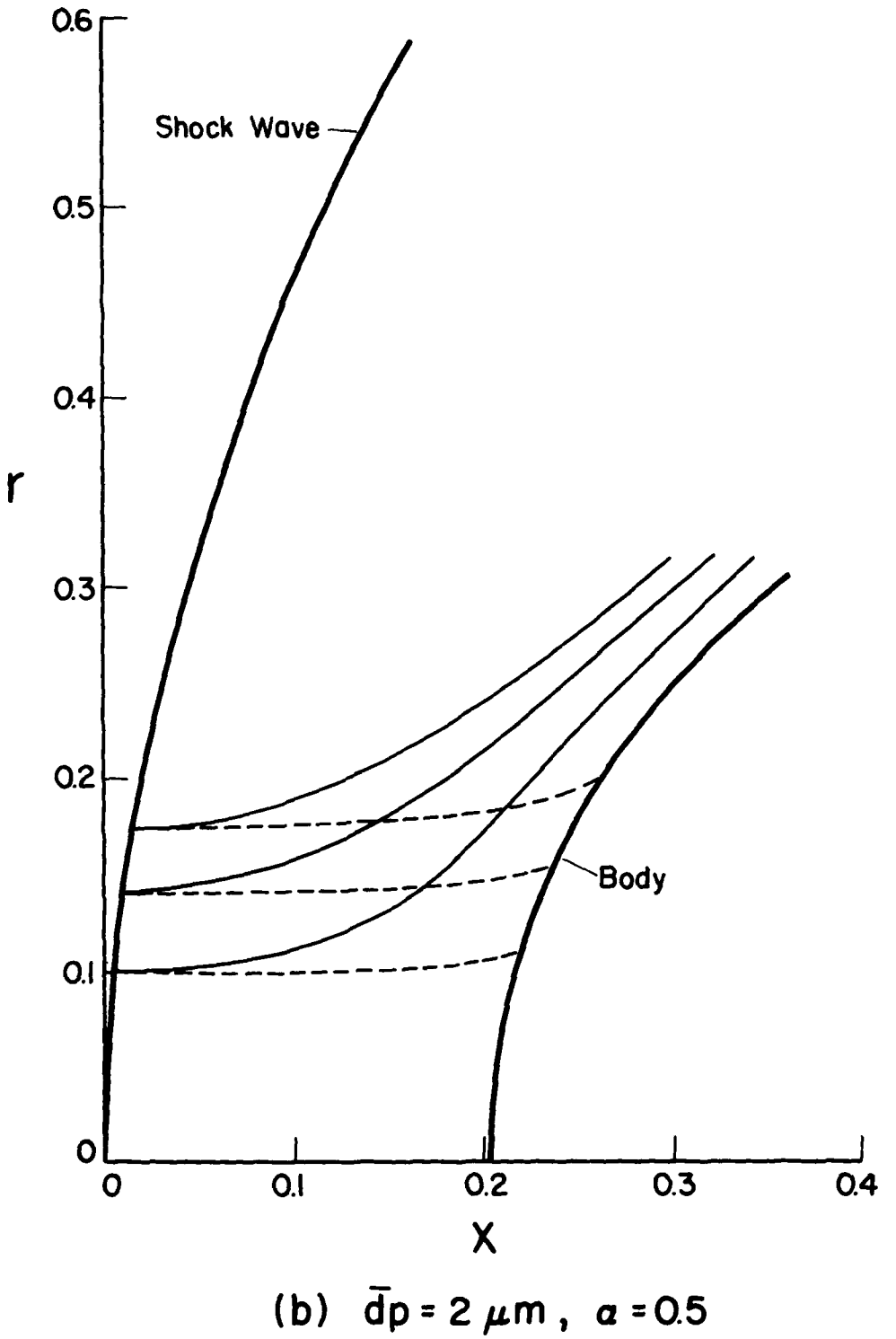

(b) $\bar{d}p = 2\ \mu m$, $\alpha = 0.5$

FIG. 16 - CONTINUED
GAS AND PARTICLE STREAMLINES AROUND BLUNT BODY.
$M_\infty = 1.5$, $\bar{T}_\infty = 300$ K, $\bar{p}_\infty = 101.3$ KPa, $\bar{R}_S = 1$ CM.

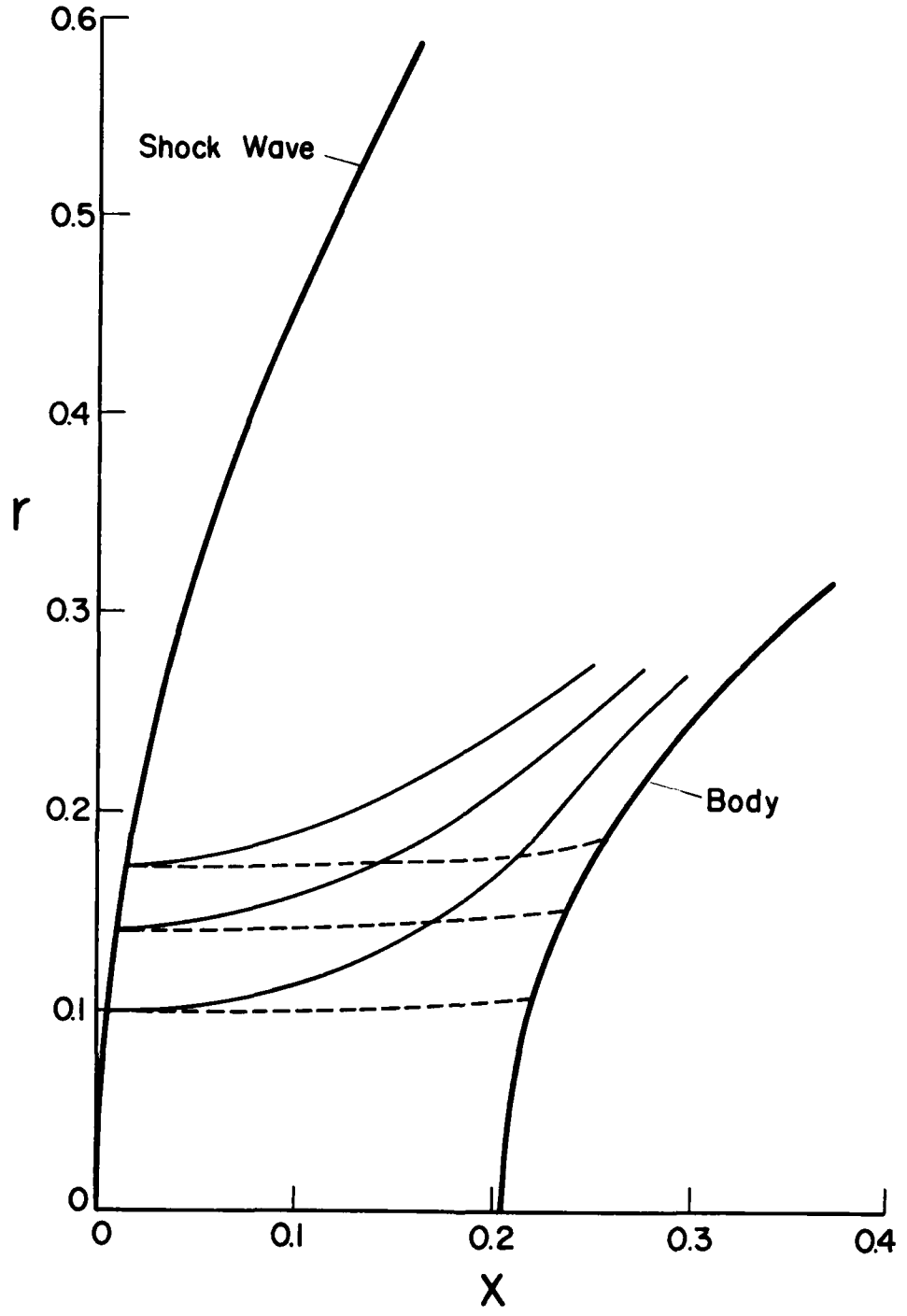

(c) $\bar{d}p = 5\,\mu m$, $\alpha = 0.5$

FIG. 16 - CONTINUED
GAS AND PARTICLE STREAMLINES AROUND BLUNT BODY.
$M_\infty = 1.5$, $\bar{T}_\infty = 300$ K, $\bar{p}_\infty = 101.3$ KPa, $\bar{R}_S = 1$ CM.

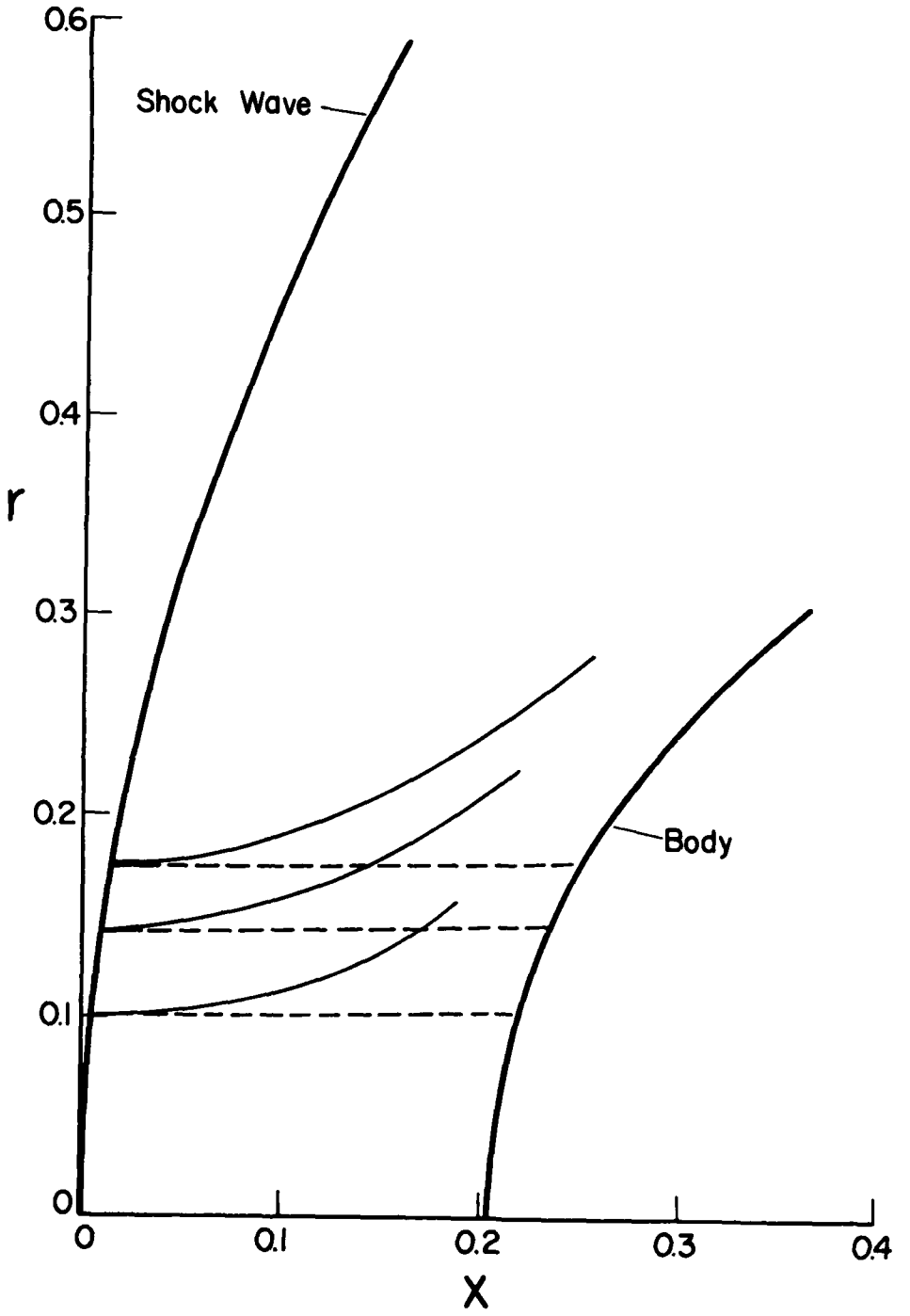

(d) $\bar{d}p = 10\ \mu m$

FIG. 16 - CONCLUDED
GAS AND PARTICLE STREAMLINES AROUND BLUNT BODY.
$M_\infty = 1.5$, $\bar{T}_\infty = 300$ K, $\bar{p}_\infty = 101.3$ KPa, $\bar{R}_S = 1$ CM.

UTIAS Report No. 267

Institute for Aerospace Studies, University of Toronto (UTIAS)
4925 Dufferin Street, Downsview, Ontario, Canada, M3H 5T6

NUMERICAL ANALYSIS OF DUSTY SUPERSONIC FLOW PAST BLUNT AXISYMMETRIC BODIES

Sugiyama, H.

1. Dusty-supersonic-hypersonic flow   2. Blunt-body flow
3. Pitot-tube flow   4. Numerical analysis

I. Sugiyama   II. UTIAS Report No. 267

An inverse method was developed for treating gas-particle supersonic flow past axisymmetric blunt bodies. This method is based on two transformations (von Moses and an additional one), which are convenient for determining the shock-layer flow fields and the body shapes.

In using the present method, the pure gas flow fields around spheres were first solved numerically for the freestream Mach numbers M_∞ = 10, 6, 4, 3, 2 and 1.5. These were found to be in very good agreement with the available results of Van Dyke and Gordon. Then the gas-solid-particle flow in the shock layer around blunt bodies (nearly spheres) were solved for the freestream Mach numbers M_∞ = 10 and 1.5, with freestream loading ratios α = 0, 0.2, 0.5 and 1.0 and particle diameters $\bar{d}_p$ = 1, 2, 5 and 10 μm, respectively. The effects of M_∞, $\bar{d}_p$ and α on the shock-layer thickness and the body surface pressures are discussed. The variations of the flow properties along the stagnation and adjacent streamlines are also shown in some detail.

Available copies of this report are limited. Return this card to UTIAS, if you require a copy.

UTIAS Report No. 267

Institute for Aerospace Studies, University of Toronto (UTIAS)
4925 Dufferin Street, Downsview, Ontario, Canada, M3H 5T6

NUMERICAL ANALYSIS OF DUSTY SUPERSONIC FLOW PAST BLUNT AXISYMMETRIC BODIES

Sugiyama, H.

1. Dusty-supersonic-hypersonic flow   2. Blunt-body flow
3. Pitot-tube flow   4. Numerical analysis

I. Sugiyama   II. UTIAS Report No. 267

An inverse method was developed for treating gas-particle supersonic flow past axisymmetric blunt bodies. This method is based on two transformations (von Moses and an additional one), which are convenient for determining the shock-layer flow fields and the body shapes.

In using the present method, the pure gas flow fields around spheres were first solved numerically for the freestream Mach numbers M_∞ = 10, 6, 4, 3, 2 and 1.5. These were found to be in very good agreement with the available results of Van Dyke and Gordon. Then the gas-solid-particle flow in the shock layer around blunt bodies (nearly spheres) were solved for the freestream Mach numbers M_∞ = 10 and 1.5, with freestream loading ratios α = 0, 0.2, 0.5 and 1.0 and particle diameters $\bar{d}_p$ = 1, 2, 5 and 10 μm, respectively. The effects of M_∞, $\bar{d}_p$ and α on the shock-layer thickness and the body surface pressures are discussed. The variations of the flow properties along the stagnation and adjacent streamlines are also shown in some detail.

Available copies of this report are limited. Return this card to UTIAS, if you require a copy.

UTIAS Report No. 267

Institute for Aerospace Studies, University of Toronto (UTIAS)
4925 Dufferin Street, Downsview, Ontario, Canada, M3H 5T6

NUMERICAL ANALYSIS OF DUSTY SUPERSONIC FLOW PAST BLUNT AXISYMMETRIC BODIES

Sugiyama, H.

1. Dusty-supersonic-hypersonic flow   2. Blunt-body flow
3. Pitot-tube flow   4. Numerical analysis

I. Sugiyama   II. UTIAS Report No. 267

An inverse method was developed for treating gas-particle supersonic flow past axisymmetric blunt bodies. This method is based on two transformations (von Moses and an additional one), which are convenient for determining the shock-layer flow fields and the body shapes.

In using the present method, the pure gas flow fields around spheres were first solved numerically for the freestream Mach numbers M_∞ = 10, 6, 4, 3, 2 and 1.5. These were found to be in very good agreement with the available results of Van Dyke and Gordon. Then the gas-solid-particle flow in the shock layer around blunt bodies (nearly spheres) were solved for the freestream Mach numbers M_∞ = 10 and 1.5, with freestream loading ratios α = 0, 0.2, 0.5 and 1.0 and particle diameters $\bar{d}_p$ = 1, 2, 5 and 10 μm, respectively. The effects of M_∞, $\bar{d}_p$ and α on the shock-layer thickness and the body surface pressures are discussed. The variations of the flow properties along the stagnation and adjacent streamlines are also shown in some detail.

Available copies of this report are limited. Return this card to UTIAS, if you require a copy.

UTIAS Report No. 267

Institute for Aerospace Studies, University of Toronto (UTIAS)
4925 Dufferin Street, Downsview, Ontario, Canada, M3H 5T6

NUMERICAL ANALYSIS OF DUSTY SUPERSONIC FLOW PAST BLUNT AXISYMMETRIC BODIES

Sugiyama, H.

1. Dusty-supersonic-hypersonic flow   2. Blunt-body flow
3. Pitot-tube flow   4. Numerical analysis

I. Sugiyama   II. UTIAS Report No. 267

An inverse method was developed for treating gas-particle supersonic flow past axisymmetric blunt bodies. This method is based on two transformations (von Moses and an additional one), which are convenient for determining the shock-layer flow fields and the body shapes.

In using the present method, the pure gas flow fields around spheres were first solved numerically for the freestream Mach numbers M_∞ = 10, 6, 4, 3, 2 and 1.5. These were found to be in very good agreement with the available results of Van Dyke and Gordon. Then the gas-solid-particle flow in the shock layer around blunt bodies (nearly spheres) were solved for the freestream Mach numbers M_∞ = 10 and 1.5, with freestream loading ratios α = 0, 0.2, 0.5 and 1.0 and particle diameters $\bar{d}_p$ = 1, 2, 5 and 10 μm, respectively. The effects of M_∞, $\bar{d}_p$ and α on the shock-layer thickness and the body surface pressures are discussed. The variations of the flow properties along the stagnation and adjacent streamlines are also shown in some detail.

Available copies of this report are limited. Return this card to UTIAS, if you require a copy.

UTIAS Report No. 267

Institute for Aerospace Studies, University of Toronto (UTIAS)
4925 Dufferin Street, Downsview, Ontario, Canada, M3H 5T6

NUMERICAL ANALYSIS OF DUSTY SUPERSONIC FLOW PAST BLUNT AXISYMMETRIC BODIES

Sugiyama, H.

1. Dusty-supersonic-hypersonic flow   2. Blunt-body flow
3. Pitot-tube flow   4. Numerical analysis

I. Sugiyama   II. UTIAS Report No. 267

An inverse method was developed for treating gas-particle supersonic flow past axisymmetric blunt bodies. This method is based on two transformations (von Moses and an additional one), which are convenient for determining the shock-layer flow fields and the body shapes.

In using the present method, the pure gas flow fields around spheres were first solved numerically for the freestream Mach numbers M_∞ = 10, 6, 4, 3, 2 and 1.5. These were found to be in very good agreement with the available results of Van Dyke and Gordon. Then the gas-solid-particle flow in the shock layer around blunt bodies (nearly spheres) were solved for the freestream Mach numbers M_∞ = 10 and 1.5, with freestream loading ratios α = 0, 0.2, 0.5 and 1.0 and particle diameters d_p = 1, 2, 5 and 10 μm, respectively. The effects of M_∞, d_p and α on the shock-layer thickness and the body surface pressures are discussed. The variations of the flow properties along the stagnation and adjacent streamlines are also shown in some detail.

Available copies of this report are limited. Return this card to UTIAS, if you require a copy.

UTIAS Report No. 267

Institute for Aerospace Studies, University of Toronto (UTIAS)
4925 Dufferin Street, Downsview, Ontario, Canada, M3H 5T6

NUMERICAL ANALYSIS OF DUSTY SUPERSONIC FLOW PAST BLUNT AXISYMMETRIC BODIES

Sugiyama, H.

1. Dusty-supersonic-hypersonic flow   2. Blunt-body flow
3. Pitot-tube flow   4. Numerical analysis

I. Sugiyama   II. UTIAS Report No. 267

An inverse method was developed for treating gas-particle supersonic flow past axisymmetric blunt bodies. This method is based on two transformations (von Moses and an additional one), which are convenient for determining the shock-layer flow fields and the body shapes.

In using the present method, the pure gas flow fields around spheres were first solved numerically for the freestream Mach numbers M_∞ = 10, 6, 4, 3, 2 and 1.5. These were found to be in very good agreement with the available results of Van Dyke and Gordon. Then the gas-solid-particle flow in the shock layer around blunt bodies (nearly spheres) were solved for the freestream Mach numbers M_∞ = 10 and 1.5, with freestream loading ratios α = 0, 0.2, 0.5 and 1.0 and particle diameters d_p = 1, 2, 5 and 10 μm, respectively. The effects of M_∞, d_p and α on the shock-layer thickness and the body surface pressures are discussed. The variations of the flow properties along the stagnation and adjacent streamlines are also shown in some detail.

Available copies of this report are limited. Return this card to UTIAS, if you require a copy.

UTIAS Report No. 267

Institute for Aerospace Studies, University of Toronto (UTIAS)
4925 Dufferin Street, Downsview, Ontario, Canada, M3H 5T6

NUMERICAL ANALYSIS OF DUSTY SUPERSONIC FLOW PAST BLUNT AXISYMMETRIC BODIES

Sugiyama, H.

1. Dusty-supersonic-hypersonic flow   2. Blunt-body flow
3. Pitot-tube flow   4. Numerical analysis

I. Sugiyama   II. UTIAS Report No. 267

An inverse method was developed for treating gas-particle supersonic flow past axisymmetric blunt bodies. This method is based on two transformations (von Moses and an additional one), which are convenient for determining the shock-layer flow fields and the body shapes.

In using the present method, the pure gas flow fields around spheres were first solved numerically for the freestream Mach numbers M_∞ = 10, 6, 4, 3, 2 and 1.5. These were found to be in very good agreement with the available results of Van Dyke and Gordon. Then the gas-solid-particle flow in the shock layer around blunt bodies (nearly spheres) were solved for the freestream Mach numbers M_∞ = 10 and 1.5, with freestream loading ratios α = 0, 0.2, 0.5 and 1.0 and particle diameters d_p = 1, 2, 5 and 10 μm, respectively. The effects of M_∞, d_p and α on the shock-layer thickness and the body surface pressures are discussed. The variations of the flow properties along the stagnation and adjacent streamlines are also shown in some detail.

Available copies of this report are limited. Return this card to UTIAS, if you require a copy.

UTIAS Report No. 267

Institute for Aerospace Studies, University of Toronto (UTIAS)
4925 Dufferin Street, Downsview, Ontario, Canada, M3H 5T6

NUMERICAL ANALYSIS OF DUSTY SUPERSONIC FLOW PAST BLUNT AXISYMMETRIC BODIES

Sugiyama, H.

1. Dusty-supersonic-hypersonic flow   2. Blunt-body flow
3. Pitot-tube flow   4. Numerical analysis

I. Sugiyama   II. UTIAS Report No. 267

An inverse method was developed for treating gas-particle supersonic flow past axisymmetric blunt bodies. This method is based on two transformations (von Moses and an additional one), which are convenient for determining the shock-layer flow fields and the body shapes.

In using the present method, the pure gas flow fields around spheres were first solved numerically for the freestream Mach numbers M_∞ = 10, 6, 4, 3, 2 and 1.5. These were found to be in very good agreement with the available results of Van Dyke and Gordon. Then the gas-solid-particle flow in the shock layer around blunt bodies (nearly spheres) were solved for the freestream Mach numbers M_∞ = 10 and 1.5, with freestream loading ratios α = 0, 0.2, 0.5 and 1.0 and particle diameters d_p = 1, 2, 5 and 10 μm, respectively. The effects of M_∞, d_p and α on the shock-layer thickness and the body surface pressures are discussed. The variations of the flow properties along the stagnation and adjacent streamlines are also shown in some detail.

Available copies of this report are limited. Return this card to UTIAS, if you require a copy.

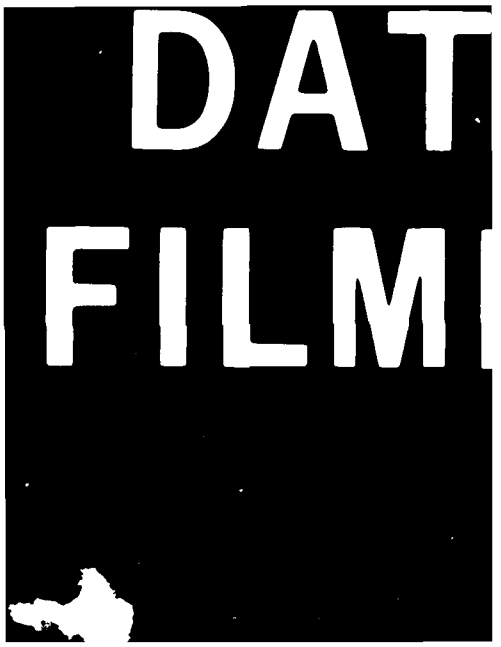
DAT
FILM